# SYNTHESIS AND CHARACTERIZATION OF $H_5$DECAPA AND RELATED LIGANDS

by

KAREN ARANE

Hons. B.Sc. McGill University, 2013

A THESIS SUBMITTED IN PARTIAL FULFILLMENT OF

THE REQUIREMENTS FOR THE DEGREE OF

MASTER OF SCIENCE

in

THE FACULTY OF GRADUATE AND POSTDOCTORAL STUDIES

(Chemistry)

THE UNIVERSITY OF BRITISH COLUMBIA

(Vancouver)

July 2015

# ABSTRACT

Radiopharmaceuticals have provided a great breakthrough in tumor imaging and treatment, and the continued exploration in the field is required to make their use widespread. This vast potential lies in the variety of the radioisotopes, due to the different emission profiles and half-lives, and it is the chemist's job to harness these isotopes into functional pharmaceuticals. Bifunctional chelators (BFC), that incorporate a radiometal into a ligand scaffold that is functionalized to target a specific biological site, provide a mode to access many of these isotopes: $\alpha$, $\beta^-$, or auger electron emitters for therapy, $\beta^+$ emitters for positron emission tomography (PET) imaging, and $\gamma$ emitting isotopes for single photon emission computed tomography (SPECT) imaging. The first requirement of a BFC is the thermodynamic stability and kinetically inert complex it forms with the isotope, especially *in vivo*. The Orvig group has discovered the promise of the ligands $H_2$dedpa for $^{67/68}$Ga and $H_4$octapa for $^{111}$In, and has thus led to the idea of expanding this scaffold for larger radioisotopes. An improved synthetic scheme for $H_5$decapa, a decadentate ligand, allowed for thermodynamic testing and radiolabeling experiments to be performed with $^{86/90}$Y, $^{177}$Lu and $^{89}$Zr. $H_5$decapa showed promising serum stability over 5 days with $^{177}$Lu, and was able to quantitatively bind $^{89}$Zr after 30 minutes at room temperature. A bifunctional version of $H_5$decapa was synthesised, coupling para-nitroethylbenzene to the central nitrogen, for future conjugation to biomolecules. As well, preliminary investigation into creating a version of $H_5$decapa with hydroxamate groups catered to binding $Zr^{4+}$was undertaken.

# PREFACE

This dissertation is original, unpublished work by the author, K. Arane. Chapter 2, Section 2.2.2 was done in collaboration with Dr. Eric Price at the Memorial Sloan Kettering Cancer Center in New York; and Section 2.2.4 was done in collaboration with Dr. Jacqueline Cawthray who performed the computational fittings.

# TABLE OF CONTENTS

# LIST OF TABLES

# LIST OF FIGURES

# LIST OF SCHEMES

# LIST OF ABBREVIATIONS

| | |
|---|---|
| ~ | approximate |
| 2D | two dimensional |
| 3D | three dimensional |
| α | alpha particle |
| Å | Angstrom, 10 x $10^{-10}$ m |
| $\beta^-$ | beta particle |
| $\beta^+$ | positron |
| γ | gamma ray |
| δ | delta or chemical shift in parts per million (NMR) |
| Δ | heat |
| µ | micro ($10^{-6}$) |
| µM | micromolar ($10^{-6}$ M) |
| AAS | atomic absorption spectroscopy |
| Ab | antibody |
| BF | bifunctional |
| BFC | bifunctional chelate, also means bifunctional ligand |
| biomolecule | vector, biovector, targeting vector, (e.g. antibody, peptide) |
| Bn | benzyl |
| br | broad (NMR) |
| Bq | Becquerel |
| °C | degrees Celsius |
| calcd. | calculated |
| CD | circular dichroism |
| *CHX* | cyclohexane/cyclohexyl |
| Ci | Curie |
| $cm^{-1}$ | wavenumber |
| CN | coordination number |
| COSY | correlation spectroscopy ($^1$H-$^1$H NMR) |
| CT | computed tomography |
| d | doublet (NMR) |
| Da | Dalton |
| DCM | dichloromethane |
| DFO | desferrioxamine B |
| DFT | density functional theory (in silico calculations) |
| Dien | diethylenetriamine |
| DGA | N,N,N',N',-tetra-n-octyl-diglycolamide |
| DIPEA | diisopropylethylamine |
| DMF | dimethylformamide |
| DMSO | dimethyl sulfoxide |
| DOTA | 1,4,7,10-tetraazacyclododecane -N,N',N'',N'''-tetraacetic acid |
| DTPA | diethylenetetraaminepentaacetic acid |
| EA | elemental analysis |
| EDTA | ethylenediaminetetraacetic acid |
| equiv. | equivalent(s) |
| ESI-MS | electrospray ionization mass spectrometry |
| EtOAc | ethyl acetate |
| eV | electronvolt(s) |
| FDA | Food and Drug Administration (USA) |

| | |
|---|---|
| g | gram |
| h | hours |
| $H_2$dedpa | 1,2-[[6-carboxy-pyridin-2-yl]-methylamino]ethane |
| $H_4$octapa | N,N'-bis(6-carboxy-2-pyridylmethyl)-ethylenediamine-N,N'-diacetic acid |
| $H_5$dedpa | 6,6'-(((((carboxymethyl)azanediyl)bis(ethane-2,1-diyl))bis((carboxymethyl)azanediyl))bis(methylene))dipicolinic acid |
| HPLC | high performance liquid chromatography |
| HR | high resolution |
| HSQC | heteronuclear single bond correlation/coherence ($^1$H-$^{13}$C NMR) |
| Hz | hertz |
| iTLC | instant thin layer chromatography (typically radioactive) |
| Ig | immunoglobulin |
| IR | infrared |
| *J* | coupling constant (NMR) |
| k | kilo |
| $K_{ML}$ | thermodynamic complex stability constant |
| L | litre or ligand |
| LET | linear energy transfer |
| m | milli- or multiplet (NMR) or meters |
| M | molar (moles/ litre) or mega ($10^6$) or metal |
| MeOH | methanol |
| min | minute(s) |
| mol | mole |
| MRI | magnetic resonance imaging |
| MS | mass spectrometry |
| n | nano ($10^{-9}$), neutron |
| NBS | *N*-bromosuccinimide |
| NMR | nuclear magnetic resonance |
| nM | nanomolar ($10^{-9}$ M) |
| Nosyl | 2-nitrobenzenesulfonamide (protecting group) |
| p | proton or pico ($10^{-12}$) |
| *p* | para substituent |
| PBS | phosphate buffered saline |
| Pd/C | palladium on carbon (10% by weight) |
| PET | positron emission tomography |
| pH | -log[$H_3O$]+ |
| p$K_a$ | protonation constant |
| pM | -log[free metal], or picomolar ($10^{-12}$ M) |
| ppm | parts per million |
| q | quartet (NMR) |
| quin | quintet (NMR) |
| ® | trademark |
| RCY | radiochemical yield |
| $R_f$ | retention factor |
| RGD | Arg-Gly-Asp cyclic peptide |
| RP | reverse phase (column chromatography) |
| rpm | rotations per minute |
| RT | room temperature |
| $R_t$ | retention time |
| s | singlet (NMR) or second (s) |
| SPECT | single photon emission computed tomography |

| | |
|---|---|
| t | triplet (NMR) |
| $t_R$ | retention time (HPLC) |
| $t_{1/2}$ | half-life |
| TEA | triethylamine |
| TFA | trifluoroacetic acid |
| THF | tetrahydrofuran |
| TLC | thin layer chromatography |
| trastuzumab | HER2/*neu* targeting antibody |
| TRF | time resolved fluorescence |
| UV | ultraviolet |
| Vis | visible |
| VT-NMR | variable temperature NMR |

# ACKNOWLEDGEMENTS

First and foremost I would like to thank my supervisor Professor Chris Orvig for his guidance and support throughout my degree. I would also like to thank all of the wonderful people I have had the chance to work with in the Orvig group over the past 2 years. In particular, I would like to thank Eric for the introduction into the 'decapa' project and making my transition into grad school a breeze, always being available for help and support, even since moving away for his post-doc. I would also like to thank Caterina for her constant support in a variety of realms including chemistry, social and physical endeavors. Thank you to Jacquie for her tireless efforts towards the physical and computational analysis included herein. And special thanks to Christina and Dorothee, for their contributions, as well as to Madeleine for her positive energy and stress relief in the lab. I would also like to thank the shops and services at UBC for their assistance, specifically Maria for her NMR expertise and Marshall for his MS knowledge, along with the staff in Bioservices and the SIF for the use of their facilities and training. The staff and researchers at TRIUMF provided great skills and assistance throughout my degree. I would like to thank my friends and family for their support and encouragement throughout the past 2 years. Finally, a special thanks to Kyle for his countless hours spent towards helping in chemistry, editing and overall support.

# Chapter 1 : INTRODUCTION

## 1.1 SPECT/PET NUCLEAR IMAGING

Computerized tomography (CT) scans and magnetic resonance imaging (MRI) both provide critical structural and anatomical information, and are the main detection methods for oncological tumours. While significant research has greatly improved the detection limits of both these methods, there is still a major limit to the molecular and biochemical information accessible, which is needed for improved accuracy as well as early detection. Molecular imaging is the measurement and visualization of biological activities at the cellular and subcellular levels and provides a mode to characterize and phenotype diseases based on their biological information, to supplement the anatomical data.[4] Nuclear imaging, a form of molecular imaging, relies on the radioactive emission of a nuclear agent (radiotracer) that specifically targets the area of interest. The radiative emissions of the nuclide are recorded by detector cameras which can convert the collected data into a 3D image visualising the accumulation of radioactivity in the body. In order to obtain high resolution and sensitive images, only very small amounts of radioactivity and minimal amounts of agent are needed (low mass technique), meaning the injected

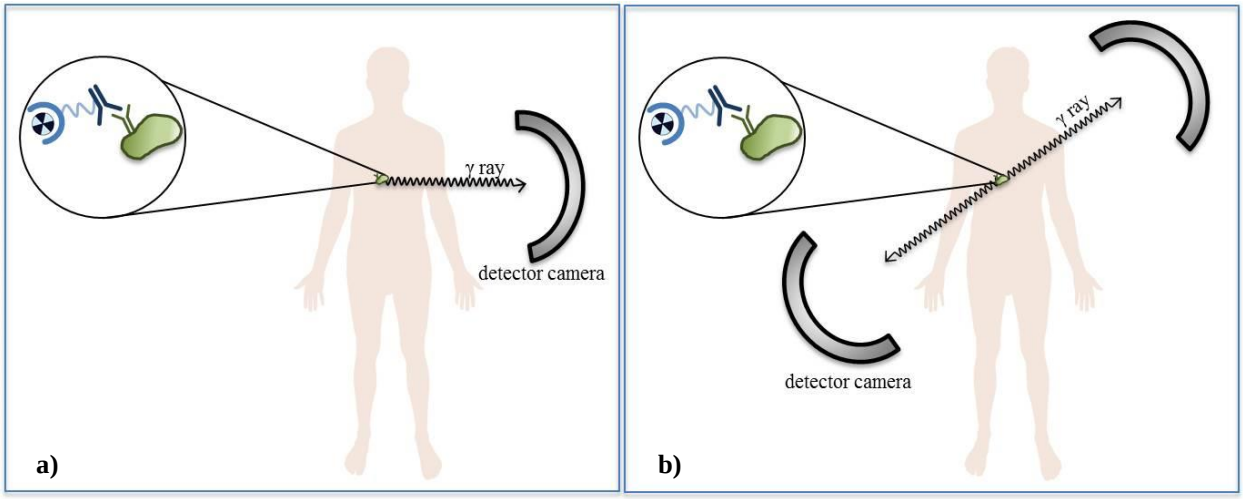


**Figure 1.1. Depiction of clinically employed nuclear imaging techniques a) SPECT imaging and b) PET imaging, using the bifunctional chelate (BFC) method to specifically deliver the radioactive dose to the area of interest *in vivo*.**

agent causes no physiological disturbance (tracer levels). The two clinical nuclear imaging techniques are SPECT (single-photon emission computed tomography) and PET (positron-emission tomography). SPECT (Figure 1.1 a) relies on the radionuclide to emit γ-rays that are then recorded by the detector cameras, allowing for resolution between 6-8 mm with a radiotracer concentration of ~$10^{-6}$ M *in vivo*.[5] Over 80% of diagnostic nuclear imaging scans today use SPECT due to the ease of production, wide-spread availability of SPECT cameras in hospitals and use of the γ-emitting radioisotope $^{99m}$Tc. Recent disruptions to the production and supply of the parent isotope, $^{99}$Mo, have spurred research into other potential isotopes, such as $^{67}$Ga, $^{111}$In, and $^{177}$Lu, that could potentially help fill this void.[6]

PET (Figure 1.1 b) involves the injected radiopharmaceutical emitting a positron ($\beta^+$). When the radionuclide decays, it releases a $\beta^+$ that collides with an electron, releasing two 511 keV γ-rays that are 180° apart.[5,7] The PET scanner then detects these coincident γ-rays with detector cameras. PET is a more expensive method than SPECT, but provides higher resolution images (2-4 mm), and is much more sensitive (tracer concentrations on the order of $10^{-12}$ M) compared to SPECT imaging. The main reason for the large difference in sensitivity is the use of lead-collimators in SPECT cameras, which filter out a large percentage of emitted gamma rays. PET imaging agents are dominated by organic radioisotopes, particularly $^{18}$F, but also $^{15}$O, $^{13}$N and $^{11}$C, all of which have short half-lives (under 2 hours) and often involve multistep synthetic protocols to incorporate the radionuclide into the pharmaceutical.[8] These drawbacks have limited the use of PET to effectively image biological processes that occur on the order of minutes. Recent efforts have simultaneously been made to expand this library to include radiometals, such as $^{68}$Ga, $^{64}$Cu, $^{86}$Y and $^{89}$Zr, which possess varying half-lives and would normally require a less time-consuming synthetic protocol to prepare the radiopharmaceutical. These metals also provide the opportunity for different delivery methods to a known biological target using vectors such as peptides and antibodies that have longer biological half-lives and do not match well with the traditional short half-life non-metals.

## 1.2 RADIOTHERAPY

A large array of radiometals may be found in the periodic table with varying emission profiles, allowing for a wide spectrum of uses. Nuclear imaging, either via SPECT or PET, requires a $\gamma$ or $\beta^+$ emitting nuclide, respectively. While nuclear imaging is crucial for diagnosis, monitoring, and management of many diseases, such as cancerous growths, the use of radioisotopes for therapeutic purposes provides an opportunity to eradicate these cancerous tumours (Table 1.1). Current radiotherapy focuses on beta particle ($\beta^-$) emission, which is best suited for large and poorly vascularised tumours, as its emission is deposited over several milimeters.[9,10] Conversely, α-particles have a path length ranging only over a few cell diameters, which translates to a strong linear energy transfer (LET) efficiency that makes α-emitters ideal for treating small tumors, if very well targeted.[10] The challenge with incorporating an α-emitting radionuclide into a radiopharmaceutical is accounting for the daughter isotopes that are created upon decay of the parent isotope, and usually are radioactive themselves. This leads to new radioisotopes being formed that do not necessarily conform with the desired radiopharmaceutical treatment, and most importantly are typically ejected from the radiopharmaceutical/chelator upon decay due to the high recoil energy of alpha emission.[11] Auger electrons also emit radiation that can be used for therapeutic purposes; however, as the emitted electrons are of low energy, it is necessary for them to be located within the cell nucleus to be effective.[9,12]

**Table 1.1. Types of radiative emissions employed in radiotherapy (α, β and Auger) with corresponding linear energy transfer (LET), range in tissue, and selected example radiometals.**[12,13,14]

| Emission | Energy | LET | Range | Tumour size | Isotopes |
|---|---|---|---|---|---|
| α-particle | high<br>5-8 MeV | high<br>100 keV/μm | 40-100 μm<br>~1-3 cell diameters | small | $^{212/213}$Bi, $^{225}$Ac |
| $\beta^-$ particles | high-medium<br>0.1-2.2 MeV | low<br>0.2 keV/μm | 0.5-10 mm<br>50-1000 cell diameters | large | $^{177}$Lu, $^{90}$Y |
| Auger electron | low<br>~1-10 keV | high | 1-20 μm<br><1 cell diameter<br>(subcellular) | small | $^{67}$Ga, $^{111}$In, |

## 1.3 RADIOMETAL-BASED RADIOPHARMACEUTICALS

Central to the basic design principle for radiometal-based radiopharmaceuticals is the concept of a bifunctional chelator (BFC). The BFC is designed to have binding properties catered towards a specific metal whilst also possessing a functional moiety that can be covalently coupled to a targeting vector (Figure 1.2).[15]

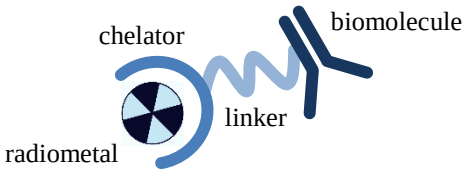


**Figure 1.2 Bifunctional chelator (BFC)**

These targeting vectors range from peptides and nucleotides to antibodies and nanoparticles (Table 1.2), all of which allow for site-specific delivery of the radioisotope via the BFC. The linker connects the metal-chelate complex to the biovector, and usually takes advantage of the many primary amine sites located on the biomolecule. This can be done via thiourea bond formation, which couples an isothiocynate (NCS) moiety on the chelator, to a primary amine.

**Table 1.2. Biomolecules used in BFCs and their corresponding half-lives in humans.**

| Biomolecule | Biological Half-life |
|---|---|
| Antibody (Ab)/ Immunoglobulin (Ig) | 3-4 weeks |
| Peptide | ~30-60 mins |
| Antibody Fragment | >10 hours |
| Nanoparticle | Variable |

What gives the BFC radiopharmaceutical design so much specificity is that both the biomolecule and radiometal can be tuned such that the construct can be catered to treat or image a specific disease or tumour site. There has been tremendous progress recently in identifying an array of over-expressed receptors (antigens) and their corresponding native binding ligands (biomolecules) that play a role in a variety of oncological tumours.[16] Depending on the physicochemical characteristics of specific

biomolecules they will have different circulation times in the body; for example, large molecular weight antibodies often take several days to circulate the blood stream and localize at the tumor site, compared to smaller molecular weight peptides that have a very rapid clearance profile from blood and non-target tissue. Consequently, this requires matching of the radiometal to the biomolecule, in order for the physical half-life of the radioisotope to match the biological half-life of the biovector. This ensures high uptake of the radiometal at the tumour source, along with clearance of any unbound agent, in the time frame of the radioactive emission, to yield a good signal-to-noise ratio (also called tumor to background ratio).

When designing a new chelator for a specific radiometal, many factors must be accounted for: good thermodynamic stability, kinetic inertness, and quick labeling kinetics at ambient temperatures. All of these factors are essential to create a viable radiopharmaceutical, which possesses a very strong metal-chelate affinity and therefore does not allow the release of radiometal *in vivo*. These properties can be assessed through experiments that are used to predict the effectiveness of the radiopharmaceutical metal-chelate complex. To assess the thermodynamic stability, potentiometric or spectrophotometric titrations can be performed to calculate log $K_{ML}$ ($K_{ML}$ = [ML]/[M][L]) and pM (-log$[M]_{free}$), which quantify the binding affinity of the chelator to the specific metal. Acceptable kinetic inertness can be accessed via *in vitro* competition assays with endogenous proteins and chelators that are found in the body and known to complex metals (eg. *apo*-transferrin, albumin). While both of these methods attempt to mimic *in vivo* scenaria, in reality it is much more complicated to predict how a radiopharmaceutical complex will behave; hence, *in vivo* experiments and biodistribution studies tend to provide the most clear-cut results of the metal-ligand complex's thermodynamic stability and kinetic inertness.

## 1.4 Radioisotopes $^{86/90}$Y, $^{177}$Lu, and $^{89}$Zr

Lutetium-177 emits $\beta^-$ particles that can be used for radiotherapy and has a half-life ($t_{1/2}$) of 6.6 days. As it decays, $^{177}$Lu also emits two γ-rays that can be used for SPECT imaging, making $^{177}$Lu an

extremely attractive radionuclide as it allows for simultaneous imaging and therapy to occur at the tumor site. Due to its long half-life, $^{177}$Lu is best suited when conjugated to larger biomolecules, used for radionuclide targeting, with comparably longer biological half-lives. $Lu^{3+}$ has an ionic radius ranging between 86-109 pm (CN = 6-9),[17] and commonly exists in an oxidation state of 3+ with a coordination number of 9.[13] $^{177}$Lu can be produced through a few different methods, such as in a medium flux reactor by irradiating $^{176}$Lu($^{176}$Lu($n,\gamma$)$^{177}$Lu). Currently there are late phase-II clinical trials investigating the therapeutic potential of $^{177}$Lu-DOTA-TATE (Lutetium-177 octreotate), a radiolabeled peptide targeting neuroendocrine tumors.[18]

**Table 1.3. Radiometal isotopes and their corresponding half-lives, decay modes and production methods.**[19]

| Isotope | $t_{1/2}$ (h) | Decay mode | Production method |
|---|---|---|---|
| $^{67}$Ga | 78.2 | EC (100%) | cyclotron, $^{68}$Zr($p,2n$)$^{67}$Ga |
| $^{68}$Ga | 1.1 | $\beta^+$ (90%)<br>EC (10%) | $^{68}$Ge/$^{68}$Ga generator |
| $^{86}$Y | 14.7 | $\beta^+$ (33%)<br>EC (66%) | cyclotron, $^{86}$Sr($p,n$)$^{86}$Y |
| $^{90}$Y | 64.1 | $\beta^-$ (100%) | $^{90}$Zr($n,p$)$^{90}$Y |
| $^{89}$Zr | 78.5 | $\beta^+$ (23%)<br>EC (77%) | cyclotron, $^{89}$Y($p,n$)$^{89}$Zr |
| $^{111}$In | 67.2 | EC (100%) | cyclotron, $^{111}$Cd($p,n,$)$^{111m,g}$In |
| $^{177}$Lu | 159.4 | $\beta^-$ (100%) | $^{176}$Lu($n,\gamma$)$^{177}$Lu |
| $^{225}$Ac | 240 | $\alpha$ (100%) | $^{226}$Ra($p,2n$)$^{225}$Ac, $n$-Capture of $^{232}$Th → $^{223}$U →$^{225}$Ac |

EC = electron capture

Yttrium possesses two useful radioisotopes, $^{86}$Y and $^{90}$Y, the first possessing suitable properties for PET imaging and the latter suitable for radiotherapy. $^{86}$Y decays via high-energy $\beta^+$ particle emission and has a half-life of 14.7 hours. It can be produced using a small biomedical cyclotron via the $^{86}$Sr($p,n$)$^{86}$Y nuclear reaction.[5] $^{90}$Y, which decays solely via $\beta^-$ emission, has a half-life of 64 hours and is an ideal radioisotope for $\beta^-$ radiotherapy. The general production of $^{90}$Y is through the use of a $^{90}$Zr($n,p$)$^{90}$Y reaction in a nuclear reactor.[5] Yttrium prefers an oxidation state of 3+ and has an ionic radius between 90-108 pm (CN = 6-9)[12] allowing for coordination numbers ranging from 6 to 9. It is

considered to behave as a hard acidic cation, showing preference for harder donor atoms like oxygen and nitrogen. Because both yttrium isotopes have the same binding preferences, $^{86}Y$ can be used as an imaging surrogate for $^{90}Y$, to perform dosimetry prior to injection of the therapeutic formulation using $^{90}Y$. There is currently an FDA approved $^{90}Y$ labeled monoclonal antibody, Zevalin®, that is targeted for $\beta^-$ therapy towards a form of B-cell non-Hodgkin's lymphoma.[20]

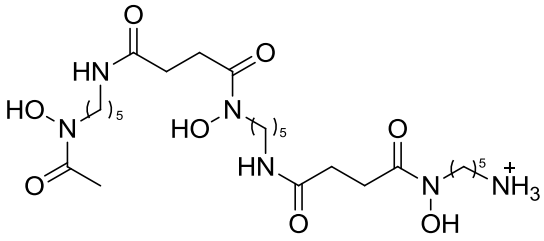


**DFO (desferrioxamine)**

Zirconium-89 is a $\beta^+$ emitter that can be used for PET imaging and has a half-life of 78.4 hours, which makes it a suitable match for antibodies, due to their longer biological half-lives. Zirconium prefers an oxidation state of 4+ which makes it an extremely acidic cation with an ionic radius of 84-89 pm (CN = 8-9)[19] and consequently prefers to form 8-9 coordinate complexes. Because of its very hard nature, it is difficult to radiolabel, as it tends to form insoluble polynuclear species under non-acidic conditions.[21] It preferentially binds with hard donor molecules that are rich in anionic oxygen atoms and functional groups such as hydroxamates, carboxylates, carbonyls and hydroxypyridones.[22] The most suitable chelator to date for Zr(IV) is desferrioxamine (DFO), and $^{89}$Zr-DFO complexes are currently in clinical trials.[23] Presently, radioactive $^{89}Zr$ is produced using the (*p*,*n*) reaction of $^{89}Y$ using a cyclotron.[5] Due to its markedly long half-life in comparison to other $\beta^+$ emitters, there is much interest in using $^{89}Zr$ as a PET imaging nuclide; however, its challenging chemical properties has made finding a suitable stable chelator more difficult. Although DFO is a sufficient chelator for $^{89}Zr$, some $^{89}Zr$ can be observed to leach out of the radiopharmaceutical and into the bone over time.[22] This observation has spurred a recent surge in interest for developing new $^{89}Zr$ chelators with superior *in vivo* stability to DFO.

## 1.5 CURRENT RADIOPHARMACEUTICALS

Macrocyclic chelators form kinetically inert metal complexes and are thermodynamically favourable due to their prearranged structure, known as the macrocycle effect.[24] Conversely, they normally require elevated temperatures and longer reaction times to bind the radiometal in quantitative yields, which is much less desirable. Longer reaction times lead to loss of the radioactive half-life, and once the BFC is conjugated to a biovector, the elevated temperatures that are required for radiolabeling can lead to denaturing of the peptide or antibody. Nevertheless, because they offer such strong metal-chelate complexes, the current 'gold-standards' for many radioisotopes are macrocyclic ligands. DOTA (1,4,7,10-tetra-azacyclododecane-1,4,7,10-tetraacetic acid), an $N_4O_4$ macrocyclic chelator, is the leading chelator for a number of radiometals including $^{111}$In, $^{177}$Lu, $^{86/90}$Y, and $^{225}$Ac. It has a coordination number of 8, and although it has slow radiolabeling kinetics and requires heating, the versatility and thermodynamic stability of its resultant complexes make it the leading chelator candidate. Many BFCs have been designed by using one of the carboxylic acid appendages of DOTA to conjugate to a biovector, or by functionalization of the carbon-skeleton, to create derivatives such as *p*-SCN-Bn-DOTA (C-DOTA).

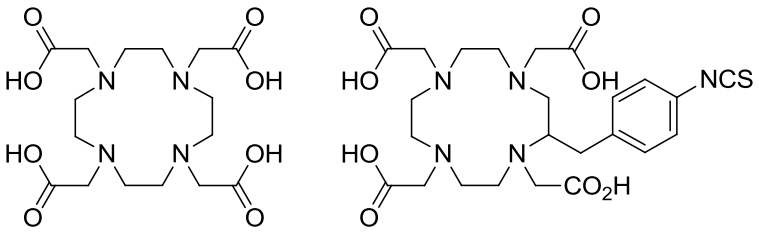


On the other hand, acyclic chelators often provide very fast labeling kinetics with minimal to no heating required, but are overall less thermodynamically favourable due to the loss in entropy ensued by the amount of rearrangement necessary to form a metal-chelate complex. The most widespread used acyclic chelator is DTPA (diethylenetriaminepentaacetic acid), an $N_3O_5$ donor, which also has a coordination number of 8. DTPA can bind many radiometals, such as $^{111}$In, $^{177}$Lu, $^{86/90}$Y, and $^{44/47}$Sc, at

room temperature within minutes. However, further testing has shown DTPA to be unstable *in vivo* with many radioisotopes.[25] The next generation chelator CHX-A"-DTPA, incorporates a cyclohexyl backbone linkage that provides increased rigidity to the ligand and leads to a greater degree of preorganization of the chelate structure, reducing the thermodynamic barrier and improving the kinetic inertness of the resultant metal-complexes.[19] However, this modification also slows the radiolabeling kinetics and CHX-A"-DTPA has failed to demonstrate improved stability over DOTA.[26]

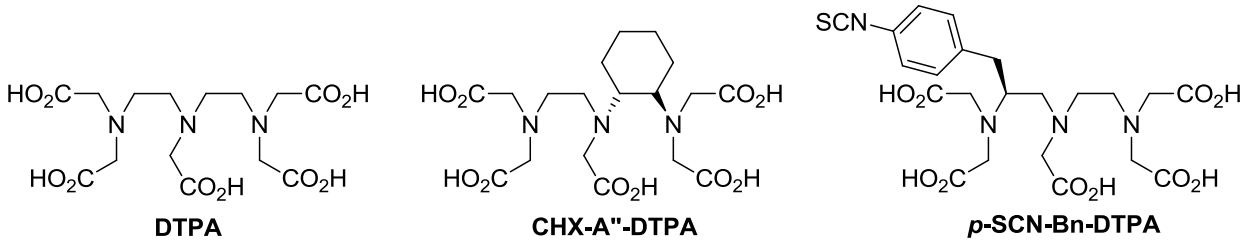


## 1.6 'PA' FAMILY – A VERSATILE ACYCLIC LIGAND SYSTEM FOR RADIOMETALS

The Orvig group has recently investigated a new set of acyclic chelators based on the picolinic acid (pa) moiety for radiolabeling a variety of radiometals, referred to as the 'pa' family. The first member of this family, hexadentate $H_2$dedpa ($N_4O_2$), showed a remarkable ability to complex $^{67/68}Ga/Ga^{3+}$, and exhibited quantitative radiolabeling yields (RCY > 99%) after 10 minutes at room temperature.[27] This ligand was then functionalized to create the BFC *p*-SCN-Bn-$H_2$dedpa that was subsequently conjugated to a cyclic targeting peptide RGD for *in vivo* PET imaging.[28,29] Further work on this specific backbone has included the addition of a cyclohexyl group onto the ethylenediamine backbone to improve rigidity and pre-organization; concurrent modifications through addition of lipophilic moieties to the backbone nitrogen atoms were explored towards use in cardiac perfusion imaging.[28] The 'pa' family was then expanded to include larger ligands, the next being $H_4$octapa ($N_4O_4$), an octadentate chelator. $H_4$octapa shows very promising radiochemistry with both $^{111}In$ and $^{177}Lu$ demonstrating quantitative radiolabeling at room temperature in less than 10 minutes.[1] A bifunctional

derivative of this ligand was synthesized creating the BFC *p*-SCN-Bn-$H_4$octapa that was subsequently conjugated to the Trastuzumab antibody and tested on mice with ovarian cancer.[3] Both the $^{111}$In and $^{177}$Lu $H_4$octapa complexes have shown comparable, if not improved, *in vivo* stability compared to the gold standard DOTA analogues.[3]

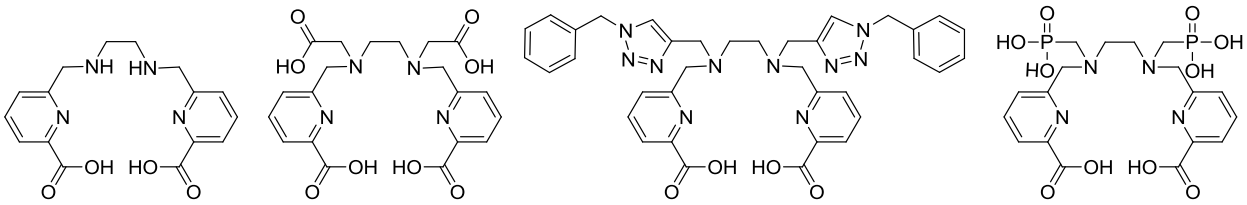


Other derivatives based on this family have also since been synthesized and tested. $H_2$azapa ($N_6O_2$) uses the $H_2$dedpa scaffold with the addition of two triazole rings (containing lipophilic benzyl "place-holders"), which stands as a model for click-based bifunctional chelating agents. $H_2$azapa was radiolabeled with $^{64}$Cu, which showed quantitative labeling at ambient temperature; however *in vivo* testing revealed high uptake of $^{64}$Cu in the liver and the gut, demonstrating that the metal-chelate complex was not stable *in vivo*.[30] $H_6$phospa is a methylene-phosphonate derivative of $H_4$octapa with the bifunctional derivative *p*-SCN-Bn-$H_6$phospa, and was evaluated *in vivo* with radioisotopes $^{111}$In, $^{177}$Lu and $^{89}$Zr when conjugated to the antibody Trastuzumab. Although none of the conjugates achieved quantitative radiochemical yields (90% to 8% respectively), $H_6$phospa demonstrated a scaffold with potential for future $^{89}$Zr chelators as it was the only known chelate to show any binding with $^{89}$Zr after DFO.[31]

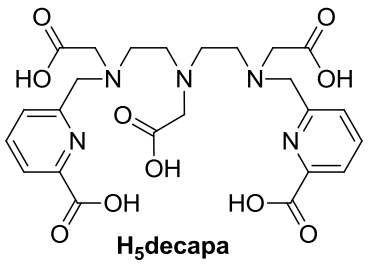

The final ligand in this series is the largest, decadentate, chelator $H_5$decapa ($N_5O_5$). Limited research into its radiolabeling potential has been undertaken, besides the poor labeling demonstrated with $^{111}$In.[1] This is most likely due to the big difference in coordination preference between the metal and the chelator, where $H_5$decapa has 10 potential binding sites, and a large binding cavity, and $In^{3+}$ only has an ionic radius of 62-92 pm (CN of 4-8). The limitations in the synthesis of $H_5$decapa were what had been restricting further testing of this ligand. This was in conjunction with the lack of a synthetic route to create the bifunctional version of the ligand, which is needed for the eventual *in vivo* testing and attachment of a biovector.

## 1.7 THESIS AIMS

Because many of the potentially clinically useful radiometals (such as $^{177}$Lu and $^{89/90}$Y) are relatively large in size and prefer to form complexes of high denticity (CN >7), we hypothesized that the previously studied decadentate chelator $H_5$decapa may be of interest for its coordination properties with these radiometals. The following chapter will discuss a new synthetic scheme that has been developed to synthesize $H_5$decapa, and the initial characterization and radiolabeling studies performed. This ligand was designed with the intended purpose to chelate larger radiometals in a more stable fashion, as the need for an expanded ligand library that can cater to a different variety of radiometals is growing. The complexes of $H_5$decapa with the metals $Lu^{3+}$, $Y^{3+}$ and $Zr^{4+}$ were analysed in both their 'cold' (non-radioactive) chemistry characteristics, via NMR and thermodynamic studies, as well as their 'hot' (radioactive) chemistry labeling efficiency and serum stability.

In order to utilise $H_5$decapa as part of a fully functional radiopharmaceutical, the chelate must bear a reactive linker group which can be used for conjugation to biomolecules (i.e. a BFC version of $H_5$decapa), yet no bifunctional $H_5$decapa analogues have been previously prepared. Herein, a novel synthetic route was developed which resulted in the preparation of a bifunctional $H_5$decapa analogue for the first time, to allow for future *in vivo* testing.

Translating this ligand design to suit the hard radiometal $^{89}Zr$ will also be discussed. New synthetic pathways, based on the 'pa' ligand design, were tested that attempt to cater to the preferences of the $Zr^{4+}$ ion.

# Chapter 2 : $H_5$DECAPA: AN ACYCLIC LIGAND FOR RADIOPHARMACEUTICAL APPLICATIONS

## 2.1 INTRODUCTION

As discussed in Chapter 1, the need to continuously grow and expand the current library of bifunctional chelators is omnipresent, requiring new ligand designs in order to match a wider range of clinically relevant radiometals. The current commercially available ligand standards (such as DOTA and DTPA (*vide supra*)) are used extensively with a wide range of radiometals, despite fundamental differences in the coordination properties of each metal. Consequently, one must often make a compromise between fast and mild radiolabeling conditions, and forming a kinetically inert radiometal-chelate complex. For example, acyclic chelators that can be quantitatively radiolabeled under ambient temperatures provide an advantage that their macrocyclic counter parts cannot match; however, macrocyclic chelators tend to form kinetically inert complexes, due to their prearranged structure, that prevent the radioisotope from being released from the chelate *in vivo*. Therefore, expansion of the ligand library to amalgamate the fast, labile chelation with very strong, stable binding, into new and improved ligands for radiopharmaceuticals is required.

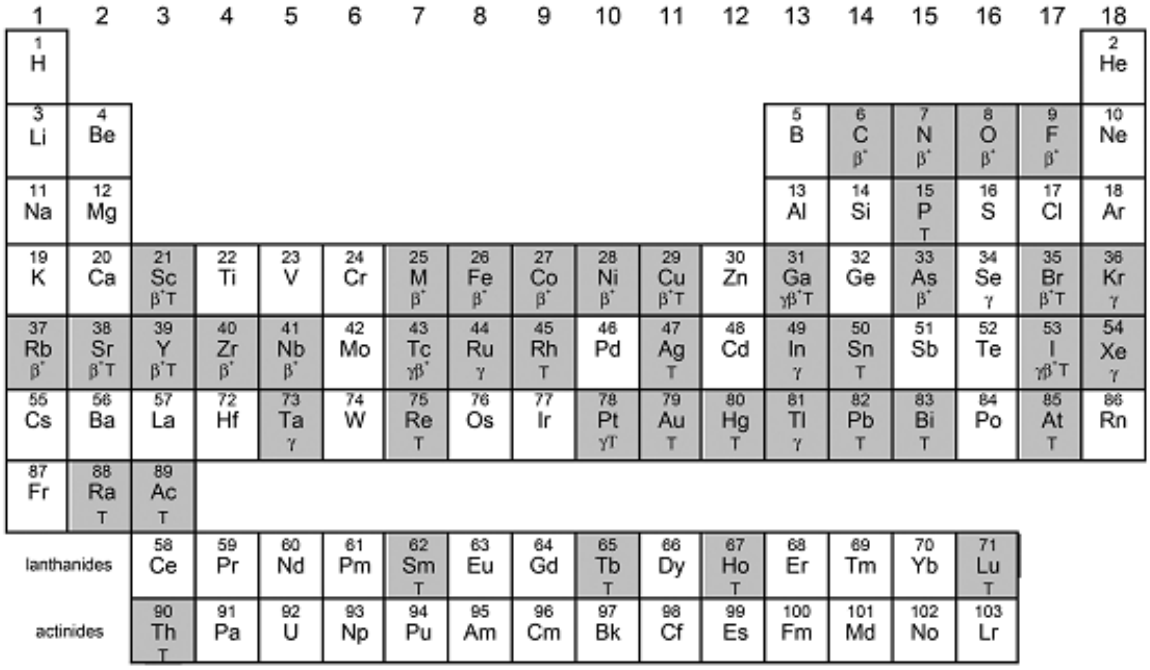


**Figure 2.1. Periodic table of accessible radionuclides; γ – SPECT imaging, $\beta^+$ - PET imaging, T – therapy (either α, $\beta^-$, Auger electrons).**[32]

As seen in Figure 2.1, metals that have potentially attractive decay properties for imaging, therapy, or both span the length of the periodic table. Each of the radiometal isotopes exhibits different decay profiles while possessing dissimilar coordination chemistry. Many of these radiometals contain large ionic radii and reside with higher oxidation states of 3-4, meaning they prefer to form complexes of high denticity (CN 8-10) in order to form a stable complex. Consequently there is need for new chelators that can accommodate these larger radiometals. Due to the great potential of the isotopes $Y^{3+}$ and $Lu^{3+}$, coupled with their similar coordination chemistry and ionic radii (as discussed in Chapter 1), a ligand scaffold that can form kinetically inert complexes while also retaining the ability to facilitate fast and efficient radiolabeling chemistries would be very attractive.

Based on the previous success of the ligands $H_2$dedpa and $H_4$octapa, which form stable complexes with $Ga^{3+}$ and $In^{3+}$ respectively, the synthesis and metal complexation properties of the largest ligand in the 'pa' family $H_5$decapa was explored herein. It was hypothesized that the decadentate $N_5O_5$ chelating ligand would satisfactorily saturate the coordination sphere of larger radiometals (i.e. $Y^{3+}$, $Lu^{3+}$)

due to its elongated dien (diethylenetriamine) backbone and larger binding cavity. In this chapter, an improved synthesis of the chelator was designed, followed by the derivatization to create a bifunctional version of the ligand. The unfunctionalized ligand was analysed for its thermodynamic stability via potentiometric titrations and serum stability assays to help predict the metal-chelates' *in vivo* kinetic inertness. UV-vis spectroscopy and circular dichroism were used as an alternative method for predicting the *in vivo* stability of the M-decapa complexes.

## 2.2 Results and Discussion

### 2.2.1 Synthesis and Characterization

Although the synthesis and characterization of $H_5$decapa has been previously reported,[1] herein an upgraded synthetic approach has been developed, improving the previous 5-step synthetic yield of ~2.5% to a yield of ~16.7% (Scheme 2.1). $H_5$decapa was synthesized from dien beginning with *N*-nosyl (nosyl = 2-nitrobenzene sulfonamide) protection to yield **2.1**, followed by selective *N*-alkylation using 2 equivalents of bromo-methyl picolinate to give **2.2**. Nosyl deprotection was accomplished via addition of thiophenol to yield **2.3**, followed by a second *N*-alkylation reaction using *t*-butyl bromoacetate to give the fully protected pro-ligand **2.4.** Complete methyl ester and butyl ester deprotection was accomplished in a two-step one-pot reaction, whereby LiOH was added to remove the methyl esters and refluxing HCl removed the remaining *t*-butyl ester protecting groups.

**Scheme 2.1. Improved synthetic scheme of $H_5$decapa (2.1 – 2.5).**

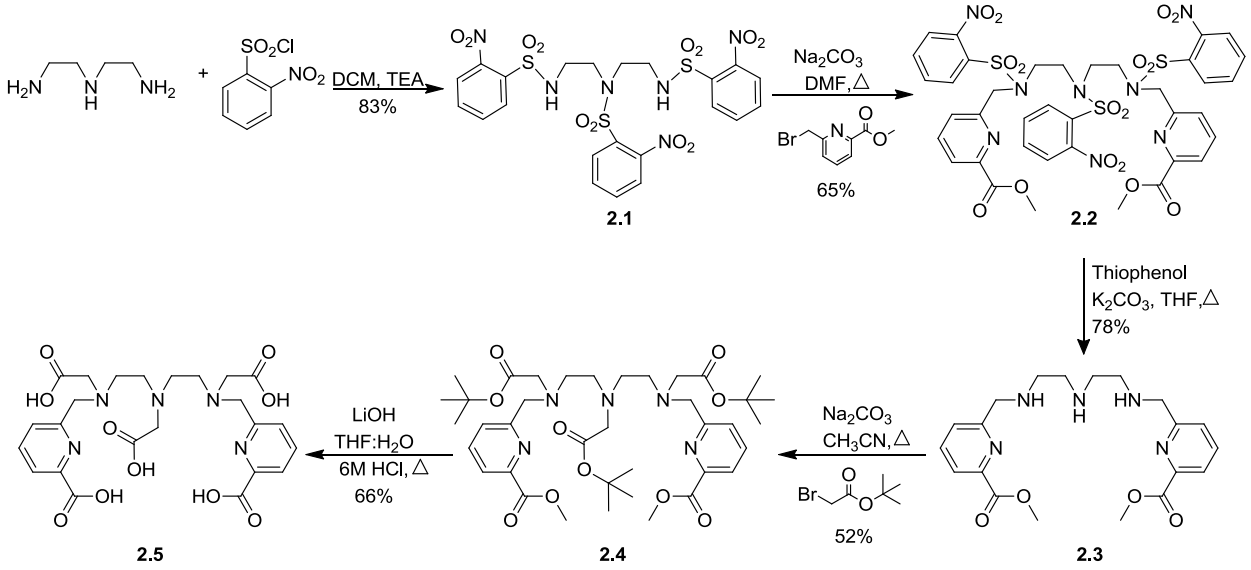


Previous methods to synthesize $H_5$decapa involved *N*-benzyl protection, where the vigorous hydrogenation conditions required for deprotection consequently resulted in a major loss of yield (Scheme 2.2). Furthermore, the previous scheme involved the addition of *tert*-butylacetate prior to *N*-alkylation of the bromopicolinates, as deprotection of the benzyl protecting group with the picolinate moieties resulted in an unwanted cleavage. The hydrogenation of the benzyl protecting group also resulted in cleavage of the backbone, drastically reducing the overall yield, an unexpected result that was not observed using analogous benzyl-protection schemes during the synthesis of $H_4$octapa.[1] The above synthetic pathway alleviates the aforementioned synthetic pitfalls, also observed with $H_4$octapa,[3] as the nosyl protecting group's deprotection is carried out using milder conditions that do not affect the surrounding functional groups.[33]

**Scheme 2.2. Previous synthetic scheme of $H_5$decapa,[1] highlighting the low yielding deprotection step.**

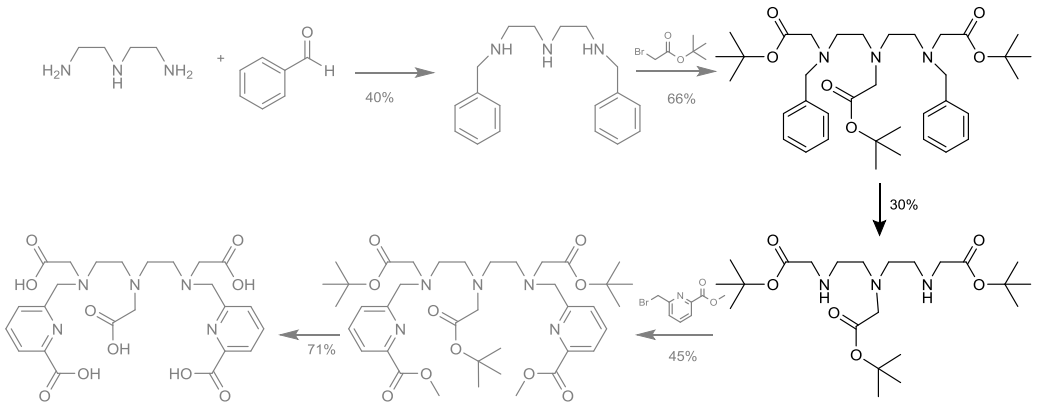


Following the successful preparation of the ligand $H_5$decapa, metal complexation experiments with 'cold' non-radioactive metal solutions were performed to assess the coordination chemistry of decapa with $Y^{3+}$ and $Lu^{3+}$. The $Y^{3+}$ complex of $H_5$decapa, $[Y(decapa)]^{2-}$ was synthesized by mixing $H_5$decapa with a small excess of $YCl_3 \cdot 6H_2O$ in deionized water to ensure quantitative complexation. The pH of the solution was adjusted using NaOH (0.1 M) to ~4-5 and stirred at ambient temperature for 1 hour. The formation of the expected coordination complex was confirmed by both low and high resolution mass spectroscopy and by NMR techniques (Figure 2.2).

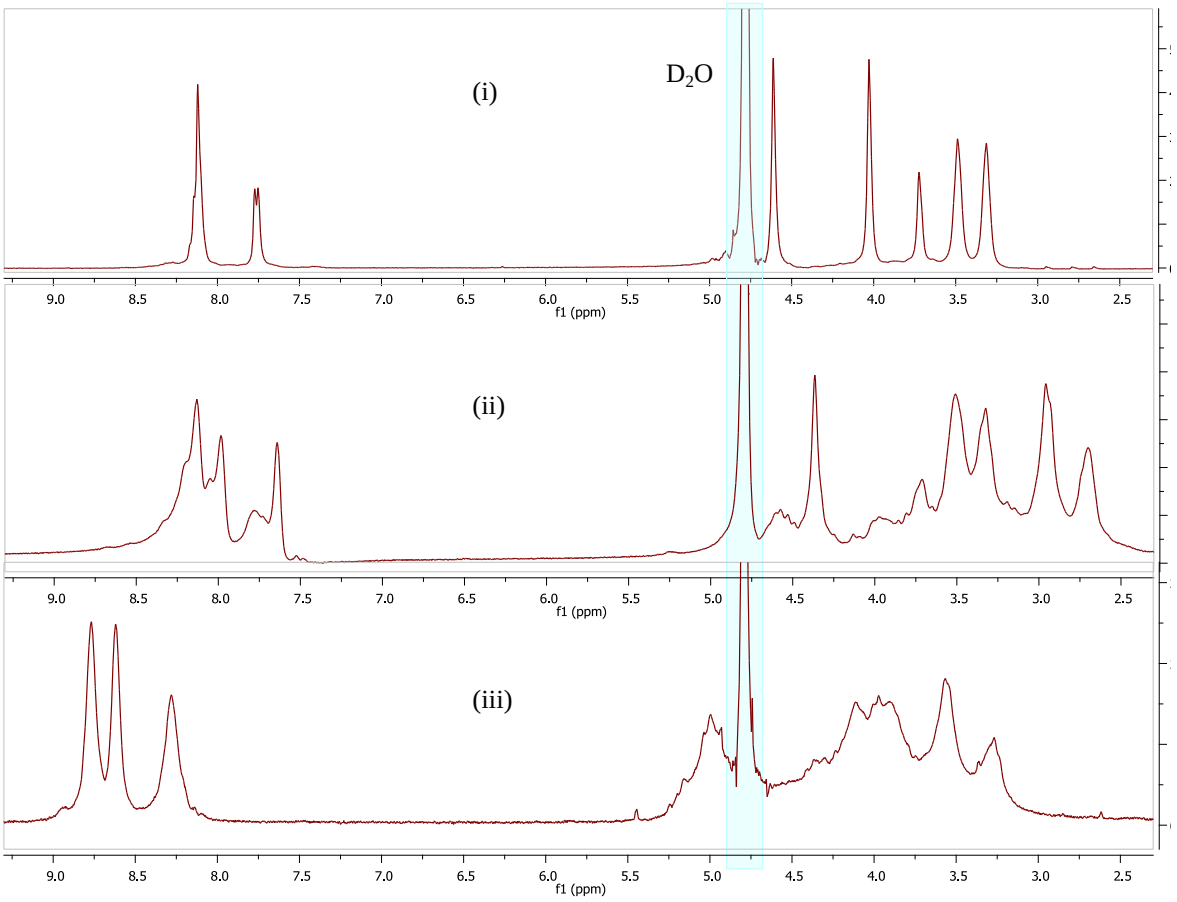


**Figure 2.2. $^{1}$H NMR spectra of (i) $H_5$decapa (300 MHz) at ambient temperature, (ii) $[Y(decapa)]^{2-}$ at 25°C (400 MHz) and (iii) $[Y(decapa)]^{2-}$ at 85°C (400 MHz), showing the formation of multiple fluxional isomers upon $Y^{3+}$ chelation in $D_2O$.**

Generally, metal-chelate complexes that exhibit minimal isomerization in solution are preferred as this is thought to imply higher stabilities,[34] although no definitive proof of this trend has been established yet. Comparing the $^{1}$H-NMR spectrum of $H_5$decapa to $[Y(decapa)]^{2-}$ (Figure 2.2), very large broad peaks can be observed upon metal complexation, suggesting that there are multiple fluxional isomers existing in solution. Because $Y^{3+}$ prefers a coordination sphere of 8-9, and $H_5$decapa has 10 available coordination sites, it is possible that one of the acetate arms is not strongly bound and this structure may fluctuate in solution. This is different in comparison to the $[Y(octapa)]^{-}$ $^{1}$H-NMR spectra, where sharp, distinct peaks were seen, presumably representing multiple, well-defined, static isomers in solution.[2]

To further probe the coordination structure and isomerization of $[Y(decapa)]^{2-}$, variable-temperature NMR (VT-NMR) and 2D-COSY/HSQC experiments were performed. As the temperature of the NMR sample (in $D_2O$) was increased from 25°C to 85°C, the peaks began to coalesce, most notably in the aromatic region, where the resonances of the picolinate moieties resemble those of the metal-free ligand, potentially alluding to a single major isomer (Figure 2.2). The VT-NMR experiments suggest that multiple fluxional isomers are present under aqueous conditions at ambient temperature. The fluctuation between isomers of $[Y(decapa)]^{2-}$ is originally on the order of the NMR timescale (relatively slow), which is why the $^1H$ spectrum contains such broad peaks as the signals are all being averaged out. As the temperature is increased, the rate of these fluctuations increases, and the signals of the different isomers coalesce into sharper peaks. This can especially be observed in the aromatic region at 85°C, where the original broad peaks have coalesced into three sharp peaks, a result of the weighted average of all the individual conformations.

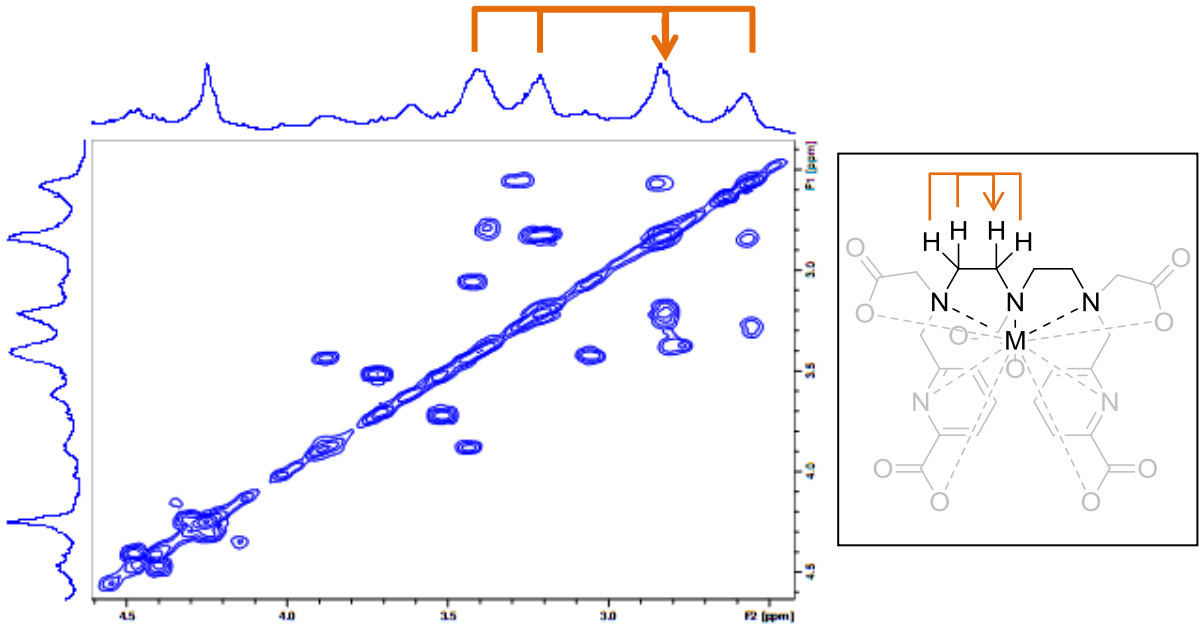


**Figure 2.3. $^1H$-$^1H$ COSY NMR spectrum of $[Y(decapa)]^{2-}$ alkyl region (600 MHz, $D_2O$, 25°C), red arrows mark diastereotopic splitting of dien backbone, pictured right.**

A 2D-COSY experiment was performed to probe the $^1H$-$^1H$ through-bond correlations and to help determine if distinct isomers could be observed at ambient temperature, supplementing the VT-NMR

results (Figure 2.3). The many off-diagonal correlation peaks displayed in the spectrum suggest that there are many different isomers present in solution. Although the exact number of isomers cannot be ascertained, certain other pieces of information can be extracted from this spectrum. When $H_5$decapa coordinates with a metal, a chiral complex most likely is formed; the complex can either be symmetric or asymmetric, and in this case, 2D NMR spectroscopy can provide a better understanding of the complex behaviour in solution. Although the resonances are poorly defined and are very broad, implying that conformations are changing in solution, there appears to be a $^1$H signal (at ~2.81 ppm) that correlates to three other $^1$H signals (2.57 ppm, 3.22 ppm, 3.38 ppm) (red brackets in Figure 2.3). This pattern would be expected for an asymmetric, chiral complex where the hydrogen atoms on the ethylene backbone are diastereotopic, confirming that the ligand is indeed bound to the metal. The other correlations seen in the COSY spectrum may correspond to other conformational isomers present in solution.

Further investigation of the aromatic region (Figure 2.4) of the $[Y(decapa)]^{2-}$ 2D COSY spectra appears to provide additional support towards the suspected appearance of one major conformational isomer. Off-diagonal correlations of the red indicated signals corroborate these suspicions, while blue highlighted peaks appear to be a less abundant fluxional isomer (Figure 2.4).

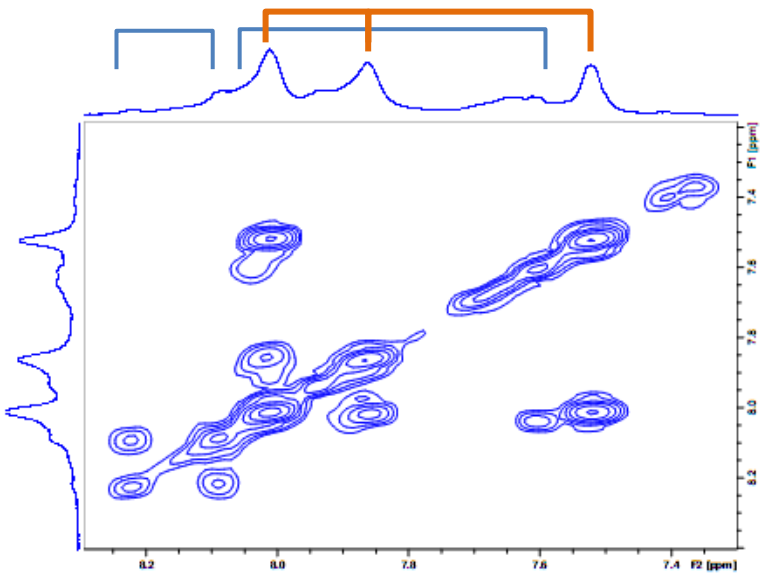


**Figure 2.4. $^1$H-$^1$H COSY NMR spectrum of $[Y(decapa)]^{2-}$ aromatic region (600 MHz, $D_2O$, 25°C).**

The highly fluxional nature of the metal-ligand complex $[Y(decapa)]^{2-}$ resulted in no observable signal in $^{13}C$ NMR experiment after 12 hours at 151 MHz. A 2D HSQC ($^{1}H$-$^{13}C$) correlation NMR was performed to help elucidate some of the $^{13}C$ NMR signals. Four peaks were observed in the aromatic region (Figure 2.5), supporting that an asymmetric complex is formed as only three aromatic peaks would be expected for a symmetric isomer. However, not many other correlations could be observed, once again indicating that the $[Y(decapa)]^{2-}$ complex is very fluxional in solution, which foreshadows the weakness in stability of this metal-ligand complex.

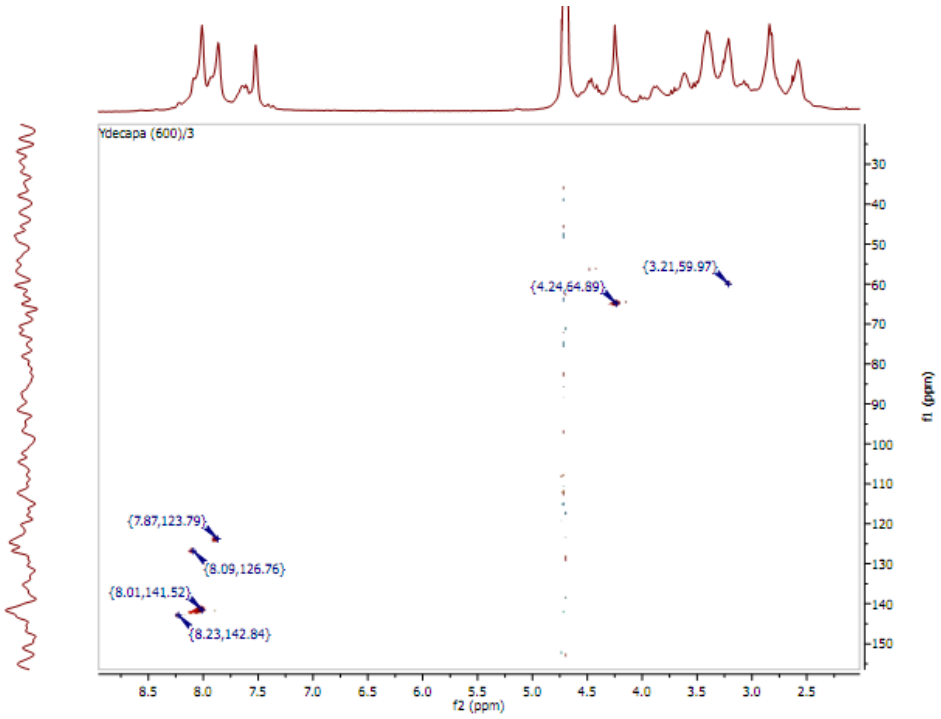


**Figure 2.5. $^{1}H$-$^{13}C$ HSQC NMR spectrum of $[Y(decapa)]^{2-}$ (600 MHz, $D_2O$, 25°C).**

The $[Lu(decapa)]^{2-}$ complex was synthesized as above, whereby the lutetium nitrate $[Lu(NO_3)_3 \cdot 6H_2O]$ salt was mixed with $H_5$decapa to form the desired coordination complex (quantitative). Comparing the $^{1}H$-NMR spectrum of $H_5$decapa to $[Lu(decapa)]^{2-}$, upon complexation many distinct sharp peaks are observed, suggesting that multiple static isomers are formed in solution (Figure 2.6). This is in stark contrast to what was previously described for the $[Y(decapa)]^{2-}$ complex, where many broad,

undefined peaks were seen. The appearance of multiple, static isomers was similarly observed for the $[Lu(octapa)]^-$ complex, which demonstrated high kinetic inertness *in vivo*.[1]

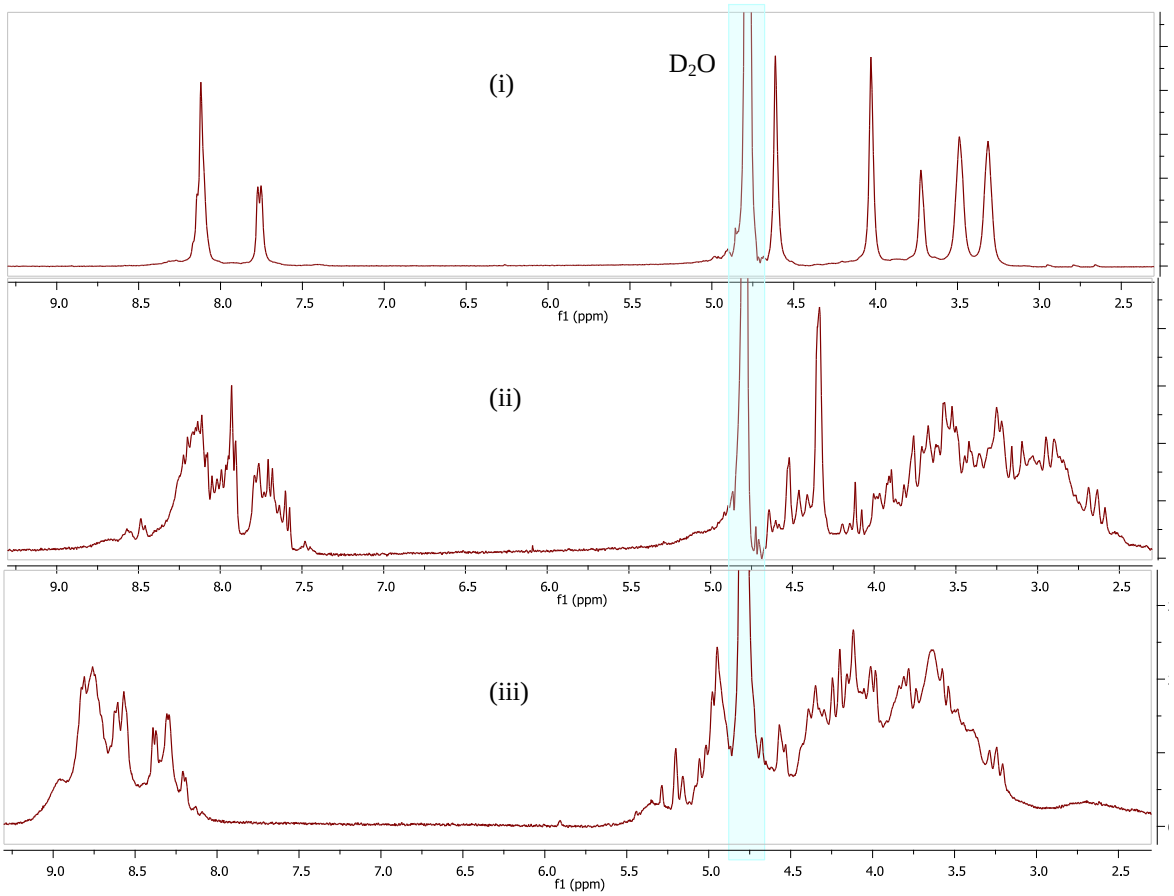


**Figure 2.6. $^1$H NMR spectra in $D_2O$ of (i) $H_5$decapa (300 MHz) at ambient temperature, (ii) $[Lu(decapa)]^{2-}$ at 25°C (400 MHz) and (iii) $[Lu(decapa)]^{2-}$ at 85°C (400 MHz), showing the formation of multiple static isomers upon $Lu^{3+}$ chelation.**

In order to gain more insight into the type of isomerization occurring, 2D COSY NMR was performed to assess the $^1$H-$^1$H correlations (Figure 2.7). Although there are quite a few correlations, it can be noted that there appears to be a doublet of doublets (~2.59 - 2.79 ppm) which most likely corresponds to the hydrogens on the diethylenetriamine backbone, as this is the splitting pattern you would expect for a symmetric chiral molecule (red bracket, Figure 2.7).

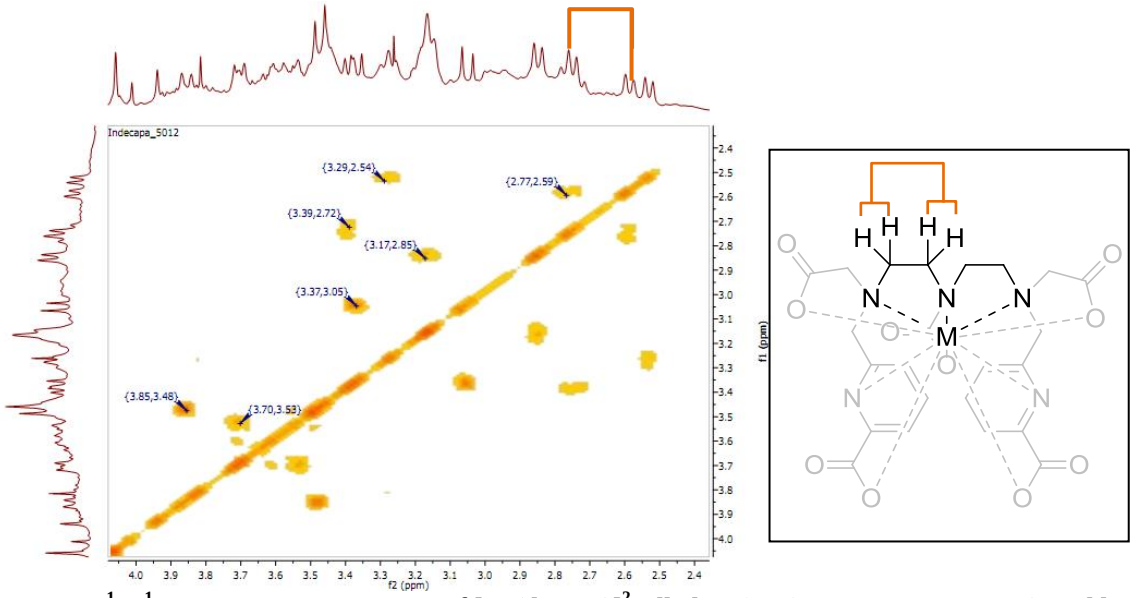


**Figure 2.7. $^{1}$H-$^{1}$H COSY NMR spectrum of [Lu(decapa)]$^{2-}$ alkyl region (600 MHz, $D_2O$, 25°C); red bracket depicting doublet of doublets of dien backbone, pictured right.**

The aromatic region of the COSY is less informative since many correlations were observed (Appendix, Figure A.1), and is similar to the HSQC spectrum (Figure 2.8) where there are multiple static isomers all showing their own individual correlations. This is in contrast to the [Y(decapa)]$^{2-}$ spectrum, where the isomers are not static and result in very few $^{13}$C NMR correlations. The [Lu(decapa)]$^{2-}$ spectrum has many broad HSQC correlations due to multiple isomer signals overlapping with each other. As seen in the HSQC [Lu(decapa)]$^{2-}$ spectrum, there are a few sharp peaks in the $^{13}$C NMR spectrum that correlate to many different peaks in the $^{1}$H NMR spectrum (see inset in Figure 2.8). This implies that the many isomers present in the $^{1}$H NMR spectrum represent very similar structures, as their corresponding carbon signals are at the same frequency. The fact that there are static isomers in solution gives promise that the metal-chelate complex will exhibit stronger thermodynamic stability.

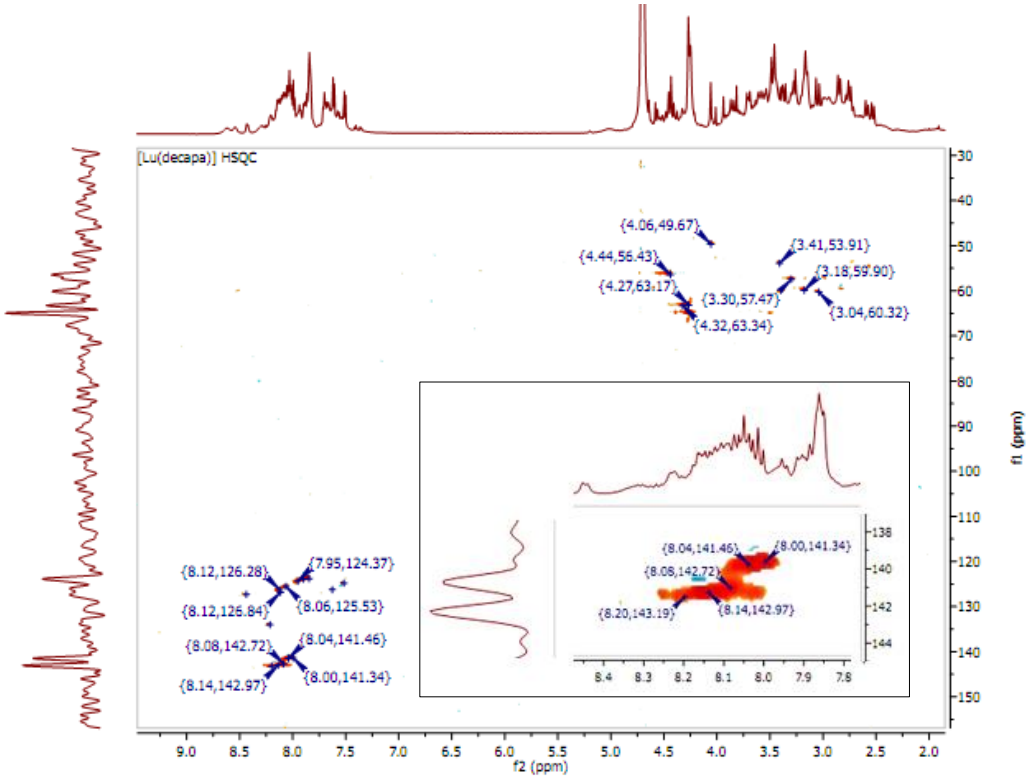


**Figure 2.8. $^{1}H$-$^{13}C$ HSQC NMR spectrum of $[Lu(decapa)]^{2-}$, inset: zoom in on aromatic region (600 MHz, $D_2O$, 25°C).**

Finally, to gain more insight into the solution chemistry of the $[Lu(decapa)]^{2-}$ complex, VT $^{1}H$ NMR experiments were performed. At 85 ºC, the maximum temperature available for $D_2O$ solutions, only slight coalescence and peak broadening can be observed (Figure 2.6). This implies that for the $[Lu(decapa)]^{2-}$ complex while it forms many isomers, these isomers are relatively static and not exchanging in solution, even at high temperatures.

$H_5$decapa was also complexed with Zr(IV), despite the fact that the ligand was not specifically designed for Zr chemistry. Zr(IV) ions tend to precipitate quickly, forming aggregates and polynuclear hydroxo species, especially in mildly acidic or neutral environments. Due to its appropriate denticity and binding cavity size, the Zr-decapa complex was synthesized and subsequently analysed. $H_5$decapa was mixed with $ZrCl_4$ and complexation was confirmed by mass spectrometry. The $^{1}H$ NMR of $[Zr(decapa)]^{-}$ is very different than those of the previous M-decapa complexes, showing sharp well defined resonances

(Figure 2.9). The splitting pattern of the $^{1}H$ signals depict an asymmetric complex and interrogating the aromatic region, one can see clear splitting of the two picolinic acid moieties, which was subsequently confirmed by 2D COSY NMR (Appendix, Figure A.2).

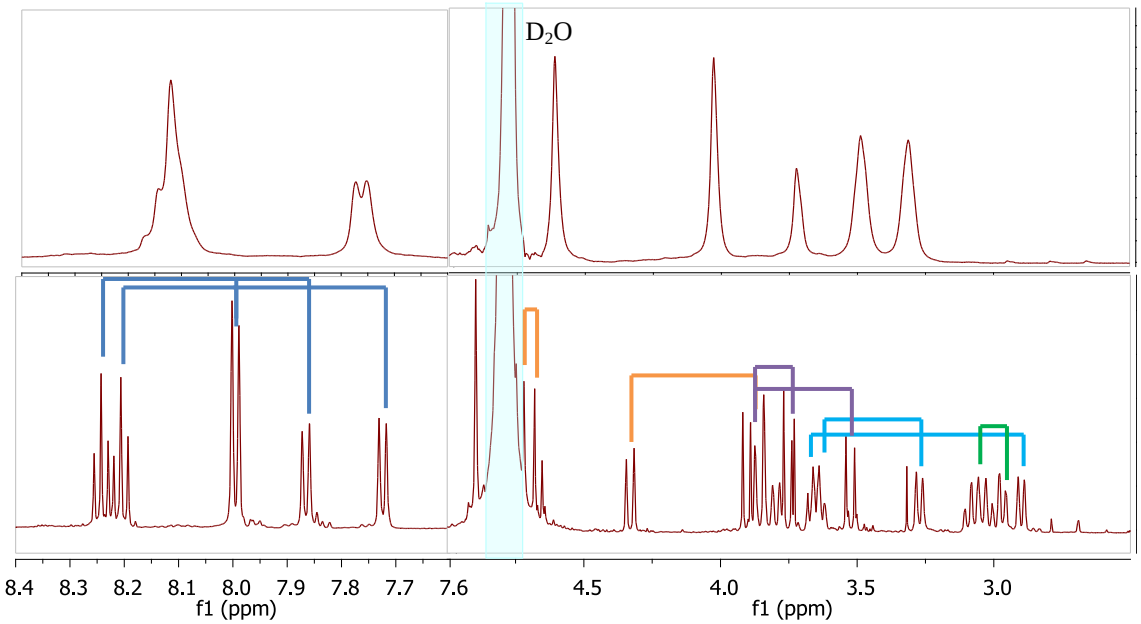


**Figure 2.9. $^{1}H$ NMR spectra at ambient temperature in $D_2O$ of (top) $H_5$decapa (300 MHz) and (bottom) $[Zr(decapa)]^-$ (400 MHz) in $D_2O$, showing the formation of one static isomer upon $Zr^{4+}$ chelation. Correlation peaks determined from 2D COSY NMR (Appendix, Figure A.2).**

Due to the static nature of this metal-ligand complex, a clear $^{13}C$ NMR could be obtained and shows 24 distinct peaks compared to the 12 peaks in the free ligand spectra (Figure 2.10). These results confirm that $[Zr(decapa)]^-$ forms one asymmetric isomer in solution. This could mean that the stable complex that forms causes each binding arm of $H_5$decapa to be in a different conformation. It is also possible that one of the picolinic arms is not bound to the Zr ion, as $Zr^{4+}$ can bind with a CN of 8. While it is very promising that the NMR experiments show one static isomer for $[Zr(decapa)]^-$, if one of the arms is not bound to the metal center this could provide instability *in vivo*. Not only would it provide undistributed charge on the complex, as was seen in the $[In(decapa)]^{2-}$ DFT studies,[1] but it would also provide an unwanted available site for *in vivo* serum proteins to bind to the Zr(IV).

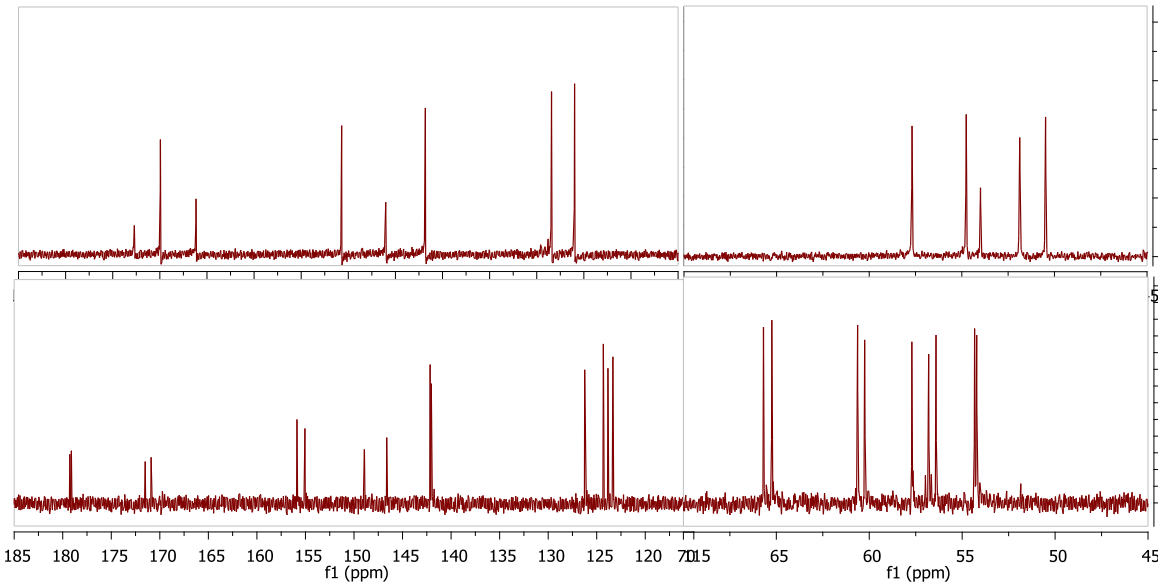


**Figure 2.10. $^{13}$C NMR spectra at ambient temperature of (top) $H_5$decapa (400 MHz) and (bottom) [Zr(decapa)]$^-$ (400 MHz) in $D_2O$, showing the formation of one static, asymmetric isomer upon $Zr^{4+}$ chelation.**

### 2.2.2 Radiolabeling Experiments

To determine the ability of $H_5$decapa to label lutetium and yttrium isotopes, and to evaluate the metal-chelate kinetic inertness, radiolabeling and competition experiments using blood serum were performed. Initial radiolabeling experiments with $H_5$decapa showed less than promising results with $^{86/90}$Y and $^{177}$Lu. Due to the lack of availability of many radiometals, the majority of the radiolabeling experiments were conducted in collaboration with Dr. Eric Price at the Memorial Sloan Kettering Cancer Center (MSKCC) in New York. However, initial $^{86}$Y radiolabeling experiments were performed at TRIUMF using the salty target purification method. This involves the irradiation of a $Sr(NO)_3$ solution on the target (13 MeV TR13 cyclotron). This solution was then purified with a DGA resin that selectively retains Y(III) while the remaining Sr(II) is eluted under acidic conditions.[35] Successive washes with nitric and hydrochloric acids remove the residual cold Sr(II), followed by elution of the desired radioactive $^{86}$Y collected in 1 mL fractions of water.

These aliquots were then used to immediately radiolabel both $H_5$decapa and DOTA, which is used as a control as it is a 'gold standard' chelator for Y(III). Incubation of purified $^{86}$Y with $H_5$decapa for 10 minutes at room temperature and subsequently 40 minutes at 80°C failed to yield any detectable

metal-ligand complex. In contrast, mixing of DOTA with $^{86}$Y at 80ºC resulted in a single sharp peak on the HPLC radiotrace at $t_R$ = 5.4 min, compared to the free $^{86}$Y peak at $t_R$ = 3.1 min. The poor $^{86}$Y labeling efficiency with $H_5$decapa was further corroborated by studies done at MSKCC, that also found no radiolabeling under various incubation conditions with $H_5$decapa, yet DOTA showed quantitative labeling with $^{86}$Y, as has been previously reported.[34] One potential explanation for the low observed results may be due to the production method of $^{86}$Y. Even following purification, there is often excess cold strontium remaining in the $^{86}$Y solution, which may interfere with the binding of $H_5$decapa, if the ligand shows similar or stronger affinity for Sr(II) versus Y(III). Radiolabeling with $^{90}$Y, that can be produced without other side products by Perkin Elmer's patented process was also tested. These binding experiments were conducted with $H_5$decapa, DOTA and DTPA in ammonium acetate buffer and were each heated to 70°C for 30 minutes, to promote quantitative binding. Radiolabeling experiments with $^{177}$Lu, also obtained from Perkin Elmer, were performed following the same method. Radiochemical yield measurements were attempted via instant thin-layer chromatography using acidified silica-embedded paper strips (iTLC-SA) and by HPLC. Unfortunately, useful data could not be obtained by iTLC as the metal-complexes $[^{177}$Lu(decapa)$]^{2-}$ and $[^{90}$Y(decapa)$]^{2-}$ could not be separated from the free-metal ($^{177}$Lu and $^{90}$Y), both eluting with the solvent front. Due to the high polar nature of the metal-ligand complexes, HPLC separation was not useful either as the free metal solutions along with the metal-chelate solutions all eluted in the void-volume of the column (< 4 min). No method was found to completely separate the metal-complexes from the free-metal, preventing the quantification of binding. Serum stability studies were performed to help gauge the stability as well as the percent binding of these complexes as separation of large serum proteins (60-100 kDa) from small chelates is typically efficient.

Radiolabeling $^{89}$Zr using synthetic chelators has proven to be very challenging over the past several years and few complexes have achieved similar results to the gold standard DFO. Our group has searched extensively for a potential ligand that would show strong binding with $^{89}$Zr. Although $H_4$octapa was seen to be an excellent ligand for both $^{111}$In and $^{177}$Lu radiometals, no measurable quantity of its $^{89}$Zr complex could be detected under a vast array of conditions.[36] To that end, $H_6$phospa was designed, where

the carboxylic acids of $H_4$octapa were substituted with methylene phosphonates to better suit zirconium's oxophilic preferences. The new ligand, $H_6$phospa was seen to incorporate $^{89}$Zr with a maximum yield of 12 % (18 hours, 37°C).[31] Due to the well resolved NMR data of [Zr(decapa)]$^-$, appearing as a single static isomer, there was hope that $H_5$decapa may be even more successful. After incubation of $^{89}$Zr with $H_5$decapa for 30 minutes at 37°C, quantitative binding (>99%) was shown by a single sharp peak in the radiotrace on the HPLC, $t_R$ = 6.3 min, (Appendix, Figure A.4) compared to the absence of signal corresponding to free $^{89}$Zr ($t_R$ = 3.8 min); this was further confirmed via iTLC-SA strips (Appendix, Figure A.5). These results were compared with $^{89}$Zr(DFO) which also demonstrated quantitative binding, as seen by both methods (Appendix, Figure A.6).

### 2.2.3 Serum Stability Studies

*In vivo,* kinetic inertness is an imperative parameter in determining the stability of a complex; likewise, competition experiments using native biological ligands such as *apo*-transferrin and albumin are useful methods of predicting the *in vivo* stability and kinetic inertness of radiometal ion complexes. Competition experiments using [$^{90}$Y(decapa)]$^{2-}$ against human blood serum were conducted over a span of 5 days (Figure 2.11). Serum stability was assessed by precipitation with $CH_3CN$, where the addition of cold $CH_3CN$ causes the serum proteins to precipitate out of solution, allowing for the separation and quantification of supernatant (ligand + metal) versus precipitate (protein + metal). Measurement of the radioactivity for each, in comparison to control experiments with free $^{90}$Y, provided percentages of intact metal-chelate complex after 1, 3 and 5 days. The caveat to this method of serum stability analysis is that the metal-ligand complex must be soluble in a mixture of water and acetonitrile, as precipitation of the metal-ligand complex along with serum proteins would provide inaccurate data. Additionally, this method cannot distinguish between radiometal that has been transchelated from chelator to serum proteins and intact chelate-radiometal complexes that are merely adsorbed or occluded with the precipitated serum proteins. The $^{90}$Y serum stability experiments were tested with three ligands, to compare $H_5$decapa with

the well-characterized ligands DOTA and DTPA, the gold standards in the field of $^{90}$Y chelation. The serum stability results for $H_5$decapa show less than 30% of the $H_5$decapa-$^{90}$Y complex remained intact after 24 hours. However, this result may reflect the poor radiolabeling yield for $[^{90}Y(decapa)]^{2-}$, as the bound metal-ligand levels remain relatively constant over the 5 day period. This implies that the $^{90}$Y that is bound to $H_5$decapa remains chelated, however much of the radiometal is left unbound. A low radiolabeling yield could also explain why no labeling was seen during the $^{86}$Y experiments, especially if the solution also had some Sr(II) contaminations. The serum stability experiment supports previously reported data that DOTA is a stable ligand for $^{90}$Y whereas DTPA suffers from stability issues *in vivo*.[37] Furthermore, this supports the obtained NMR data that showed the $[Y(decapa)]^{2-}$ complex to be fluxional in solution, ultimately determining that $H_5$decapa is not an ideal ligand for Y(III) chelation.

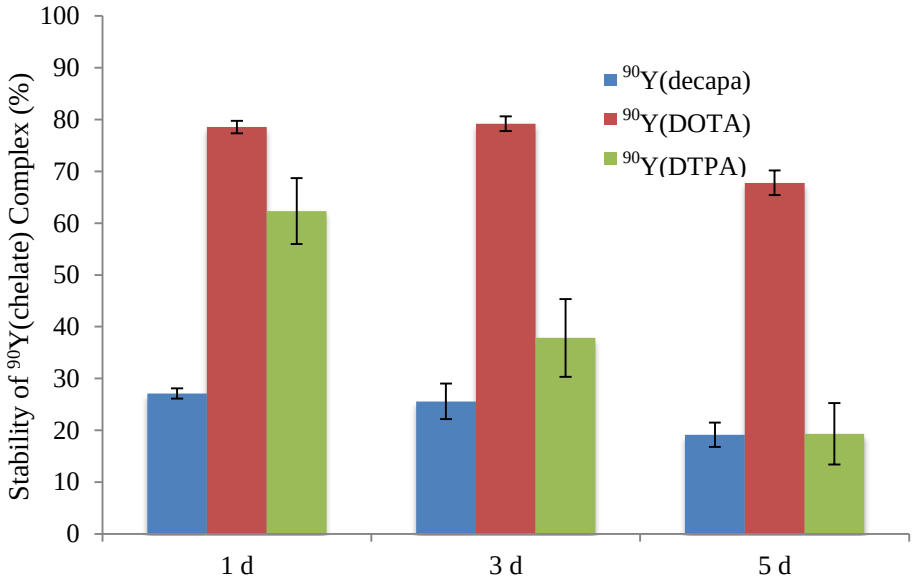


**Figure 2.11. $^{90}$Y stability of transchelation by human serum proteins via $CH_3CN$ precipitation at 37°C with $H_5$decapa and DOTA over 5 days.**

Analogous metal-ligand serum stability tests were performed with $[^{177}Lu(decapa)]^{2-}$ yielding more promising results than were observed with $^{90}$Y (Figure 2.12). $[^{177}Lu(decapa)]^{2-}$ showed comparable binding abilities to $^{177}$Lu(DOTA) and $^{177}$Lu(DTPA) after 24 hours (69.5 ± 1.7%, 76.9 ± 1.3% and 74.7 ± 1.0% respectively). However, $[^{177}Lu(decapa)]^{2-}$ demonstrated improved kinetic inertness over the 5 day

period, showing a minimal change in stability (3%), whereas $^{177}$Lu(DTPA) decreased stability 15% over the same time frame. These findings are comparable to previous results obtained via PD10 column stability experiments, where [$^{177}$Lu(decapa)]$^{2-}$ showed improved stability over $^{177}$Lu(DTPA), but slightly lower values compared to $^{177}$Lu(DOTA) and [$^{177}$Lu(octapa)]$^{-}$ (Appendix, Table A.1*)*. While DOTA remains the best known chelator for $^{177}$Lu, $H_5$decapa demonstrates comparable results and promising kinetic inertness. These results also confirm that $^{177}$Lu was effectively bound by $H_5$decapa, despite iTLC and HPLC methods being unable to confirm radiochemical yields.

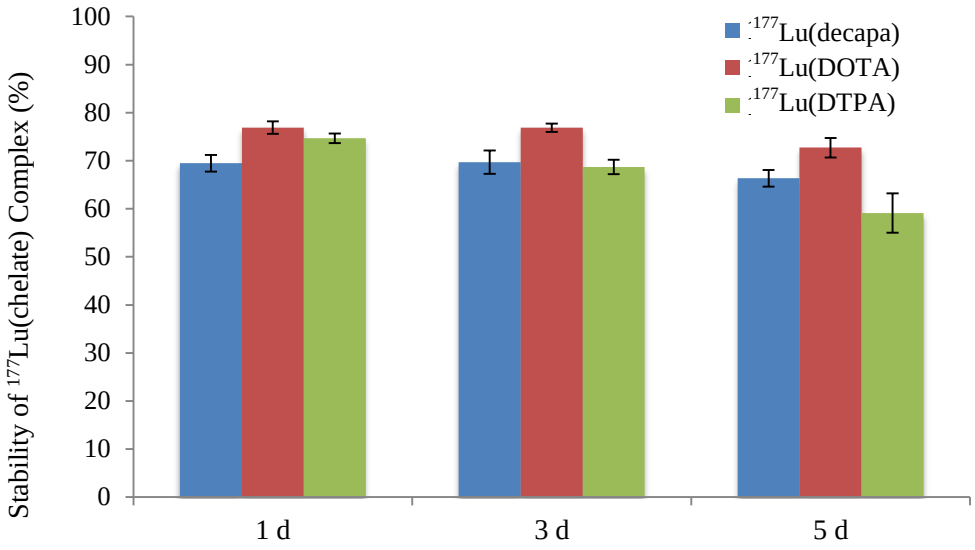


**Figure 2.12. $^{177}$Lu stability of transchelation by human serum proteins via $CH_3CN$ precipitation at 37°C with $H_5$decapa, DOTA, and DTPA over 5 days.**

Serum stability experiments were also performed with human blood serum and both the $^{89}$Zr(DFO) and $^{89}$Zr(decapa) complexes compared to a control of neutralized free $^{89}$Zr (Figure 2.13). The results from the serum stability tests were analysed by the $CH_3CN$ precipitation method, described previously for $^{90}$Y and $^{177}$Lu, as well as by iTLC-SA. Unfortunately, the [$^{89}$Zr(decapa)]$^{-}$ complex was found to be unstable in serum, and shows almost complete transchelation to serum proteins after just 1 day. Nevertheless, the difficulty of labeling $^{89}$Zr in any quantity, as seen for most ligands, makes these preliminary results very promising. In light of the extreme preference of Zr(IV) for hard oxygen donor atoms, it was very surprising that the ligand $H_5$decapa could achieve such high radiochemical yields with

$^{89}$Zr. These results will inspire potential modifications to the $H_5$decapa scaffold which can be explored in an attempt to further stabilize the Zr-chelate complex.

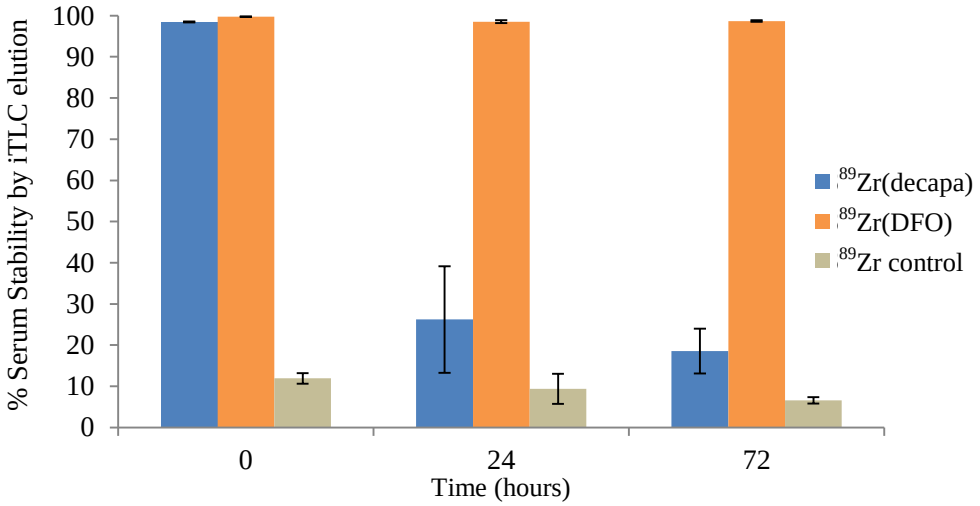


**Figure 2.13. $^{89}$Zr stability of transchelation by human serum proteins via iTLC (50 mM EDTA) at 37°C with $H_5$decapa, DFO and free $^{89}$Zr control over 3 days.**

### 2.2.4 Thermodynamic Stability

Stability constants (log $K_{ML}$) are well-established methods for determining and comparing relative thermodynamic stabilities for metal-ligand complexes; however, a more accurate measurement is the pM value (-log[$M^{n+}_{free}$]), which indicates the metal-scavenging ability of the ligand, and simultaneously provides a more accurate figure for predicting the *in vivo* thermodynamic stability of metal-ligand chelates under relevant physiological conditions. pM values are calculated under specific conditions (usually 10 μM total ligand, 1 μM total [$M^{3+}$], pH 7.4, 25°C) that account for ligand basicity (ligand p$K_a$ values), free metal concentration, ligand-to-metal ratios, pH, variable denticity, and metal hydroxide formation. The thermodynamic stability of [Y(decapa)]$^{2-}$ was determined by potentiometric titrations to be log $K_{ML}$ = 24.5 (1) (pM = 20.0), which is slightly higher, and therefore better, than the other 'gold standard' ligands tested with $Y^{3+}$. This aptly illustrates how thermodynamic stability does not always predict the stability of the metal-chelate complex *in vivo*. While [Y(decapa)]$^{2-}$ has a comparable log $K_{ML}$

value in comparison to DOTA, the Y(DOTA) complex is significantly more kinetically inert than the $H_5$decapa complex. This was also seen with $In^{3+}$ and $H_5$decapa, which has a high log $K_{ML}$ value, but is shown not to label with very high yields.[1] Conversely, $[Lu(decapa)]^{2-}$ was found to have much lower thermodynamic stability values, log $K_{ML}$ = 20.4 (pM = 16.2), compared to $[Y(decapa)]^{2-}$ and $[In(decapa)]^{2-}$; however, the $[Lu(decapa)]^{2-}$ complex obtained the highest radiolabeling yields and serum stability over the 5 day experiment between the three compounds.

**Table 2.1. Thermodynamic stability values (log $K_{ML}$ and pM) for $H_4$octapa, $H_5$decapa, DTPA and DOTA with $In^{3+}$, $Y^{3+}$, and $Lu^{3+}$.**[1–3]

| | Ligand | log $K_{ML}$ | pM[a] |
|---|---|---|---|
| **$In^{3+}$** | $octapa^{4-}$ | 26.8(1) | 26.5 |
| | $decapa^{5-}$ | 27.56(5) | 23.1 |
| | $DTPA^{4-}$ | 29.0 | 25.7 |
| | $DOTA^{4-}$ | 23.9(1) | 18.8 |
| **$Y^{3+}$** | $octapa^{4-}$ | 18.3(1) | 18.1 |
| | $decapa^{5-}$ | 24.5(1) | 20.0 |
| | $DTPA^{4-}$ | 21.2-22.5 | 17.6-18.3 |
| | $DOTA^{4-}$ | 24.3-24.9 | 19.3-19.8 |
| **$Lu^{3+}$** | $octapa^{4-}$ | 20.08(9) | 19.8 |
| | $decapa^{5-}$ | 20.4(1) | 16.2 |
| | $DTPA^{4-}$ | 22.6 | 19.1 |
| | $DOTA^{4-}$ | 21.6(1) | 17.1 |

[a] Calculated for 10 μM total ligand and 1 μM total $[M^{3+}]$ at pH 7.4 and 25°C.

While thermodynamic stability values (log $K_{ML}$ and pM) can provide a good gauge of stability of a metal-chelate complex, facilitating comparisons to other known ligands, discrepancies between predicted and actual stabilities *in vivo* have been clearly shown.[38] Therefore, this serves to demonstrate that thermodynamic parameters are not the only factors contributing to the biological stability of the metal-ligand complexes: kinetic parameters such as ligand-metal on/off rates are far more important in determining biological stability.

### 2.2.5 Circular Dichroism

Circular dichroism (CD) measures the difference in absorption of left and right circularly polarized light, which makes it a good probe for chiral molecules such as proteins. The CD spectrum provides information regarding the bonds and structures that lead to this chirality in the solution phase.[39] CD is extensively used to help elucidate protein secondary structure; the number of α-helices, β-sheets and random coils can all be deduced from the difference in absorption in the UV range (250-350 nm) of the CD spectra.[40] Moreover, it can be used to study changes in structural formation during the binding of metals, ligands or to probe protein-protein interactions.

While the synthetic chelator may efficiently bind a desired metal isotope that can be confirmed and characterized by NMR studies and thermodynamic stability constants, it does not provide a measure of how the anticipated complex will behave when exposed to other metal-seeking chelators, which are omnipresent *in vivo*. Human serum albumin (HSA) is the constitutive protein of blood plasma and is essential in distribution and transport of transition metals in the body.[41] HSA has four distinct metal binding sites and can bind a plethora of metal ions including $Cu^{2+}$, $Zn^{2+}$, $Fe^{3+}$ and $VO^{4+}$.[41] Another widely distributed metal-binding protein, *apo*-transferrin, serves principally to transport $Fe^{3+}$ ions in the body, yet it can also bind a number of other metal ions *in vivo*.[42] Previously it has been shown that $Lu^{3+}$ can bind both *apo*-transferrin and albumin,[43,44] and that $Y^{3+}$ can also bind albumin, through various spectroscopic methods.[45] UV-vis spectroscopy and CD were used in an attempt to assess the stability of $[Lu(decapa)]^{2-}$ upon exposure to *apo*-transferrin. For the UV-vis experiments, *apo*-transferrin solutions were made up in phosphate buffer (pH 7.4, 10 mM) and their spectra were recorded. Upon the addition of 1 and 2 equivalents of $Lu^{3+}$, one can see the decrease in the absorbance at the 280 nm peak, along with the increase in the peak around 230 nm, (Figure 2.14) which have been previously characterized.[44]

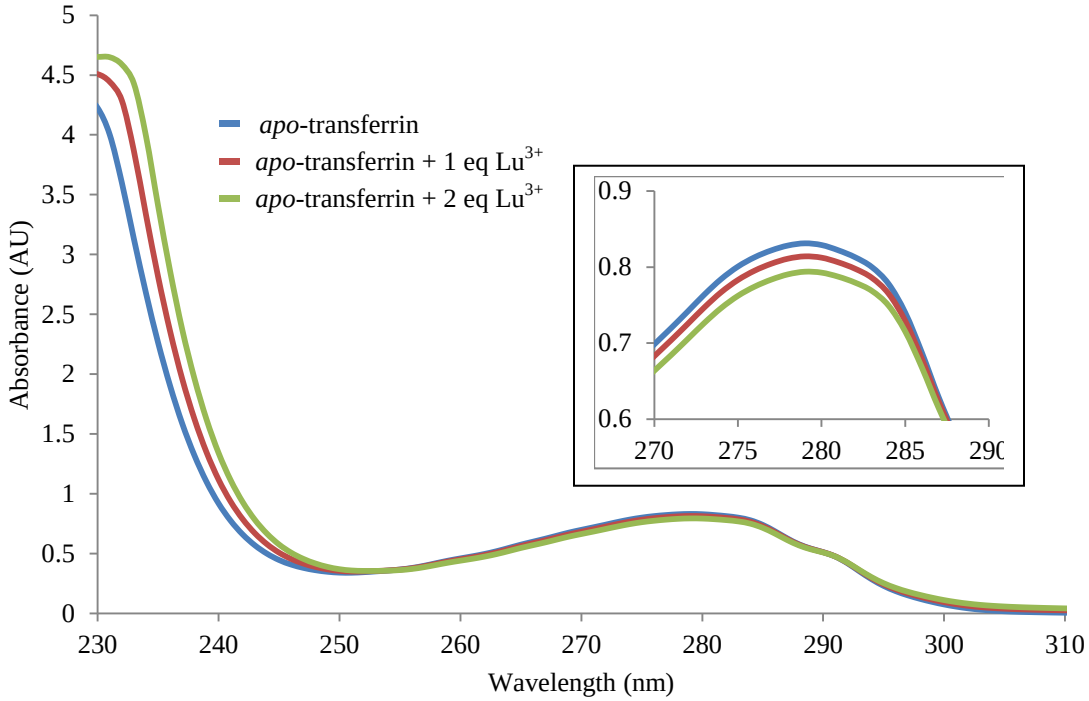


**Figure 2.14. UV-vis spectrum of *apo*-transferrin with the addition of 1 and 2 equivalents of $Lu^{3+}$.**

A set of experiments were designed using CD to evaluate the stability of the preformed metal-chelate complex upon exposure to human metal binding proteins. Initial experiments were performed with $Lu^{3+}$ and *apo*-transferrin as the protein has been proven to bind the metal isotope, and $Lu^{3+}$ has been demonstrated to form a stable complex with $H_5$decapa. Circular dichroism spectra can be measured over a large range of wavelengths. The intrinsic region, in the far UV region (190-245 nm), depicts major changes in the secondary structure of the protein, and would only cause a change in the CD spectrum if the binding of the metal isotope caused significant conformational changes to the α-helices and β-pleated sheets.[46,47] The aromatic region, in the near-UV region (245-320 nm), probes the absorption of the aromatic amino acids residues (Trp, Phe, Tyr), and is the region where native *apo*-transferrin has a characteristic absorbance spectrum. The aromatic region will report changes to the tertiary folding of the polypeptide chain that induces alterations to the chiral environment of the aromatic side group chromophores.[48] The final region is the visible region (320-600 nm), where there is no notable absorption

for *apo*-transferrin. Induced CD spectra can be observed in this region if the whole metal-ligand complex binds the transferrin together, due to d → d electronic transitions.[49,50]

The CD spectrum of *apo*-transferrin was recorded in phosphate buffer (pH 7.4, 10 mM) in the aromatic region, and then subsequently monitored upon incubation with $[Lu(decapa)]^{2-}$ over 2 hours (Figure 2.15). As only slight spectral changes were observed over the 2 hours from the initial *apo*-transferrin curve, it appears as if the $Lu^{3+}$ is remaining bound to the ligand and is not being released to the *apo*-transferrin.

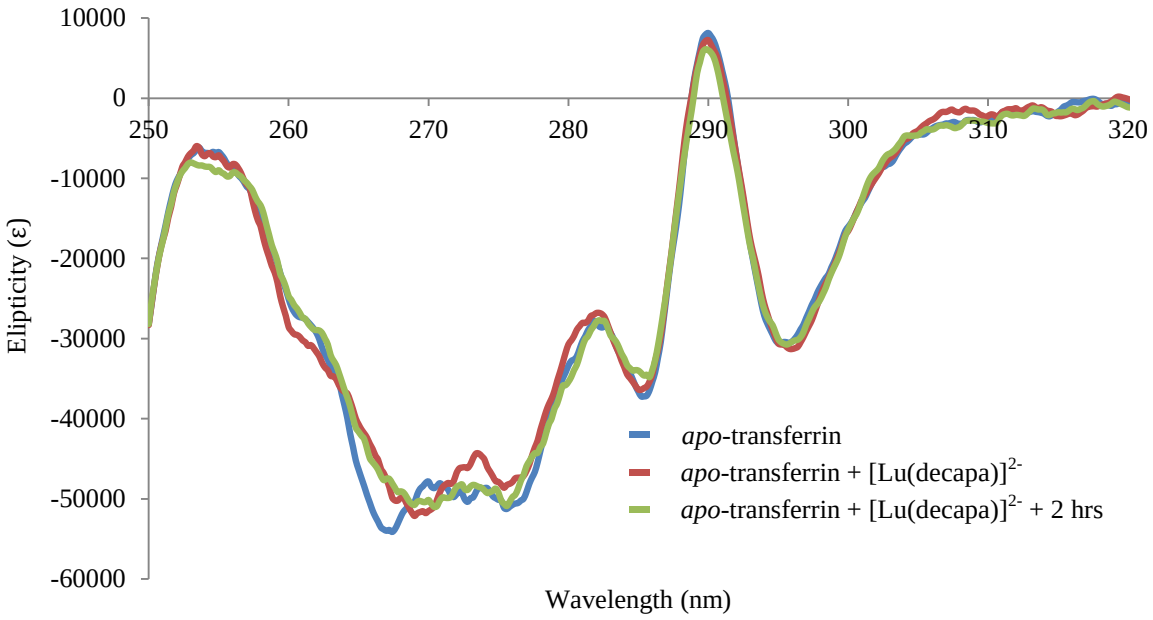


**Figure 2.15. CD spectra of *apo*-transferrin upon addition of metal-ligand complex $[Lu(decapa)]^{2-}$.**

Next, *apo*-transferrin was exposed to equimolar amounts of Lu(III) (Figure 2.16). Larger changes were observed between the 2 spectra, suggesting that $Lu^{3+}$ is bound to *apo*-transferrin. It is known that $Fe^{3+}$ interacts with two tyrosine residues within the *apo*-transferrin binding site and that coordination induces conformational changes that can be observed via CD.[48] If $Lu^{3+}$ is binding in the $Fe^{3+}$ binding sites, similar conformational changes to the aromatic amino acid residues should be observed. The local minimum at 288 nm is characteristic of tyrosine (Tyr) and tryptophan (Trp) absorption, and changes in intensity on binding $Lu^{3+}$ would indicate that these amino acids are involved.[46] The Lu-transferrin

solution was subsequently exposed to free ligand ($H_5$decapa) to observe potential conformational changes towards the original *apo*-transferrin spectrum; such results would indicate that $H_5$decapa preferentially binds $Lu^{3+}$ in the presence of *apo*-transferrin. Although, many slight changes can be observed that are similar to the native protein, the most notable region is at 288 nm where the two spectra (green & blue) overlap, suggesting that the tyrosine and tryptophan residues have returned to their original orientation.

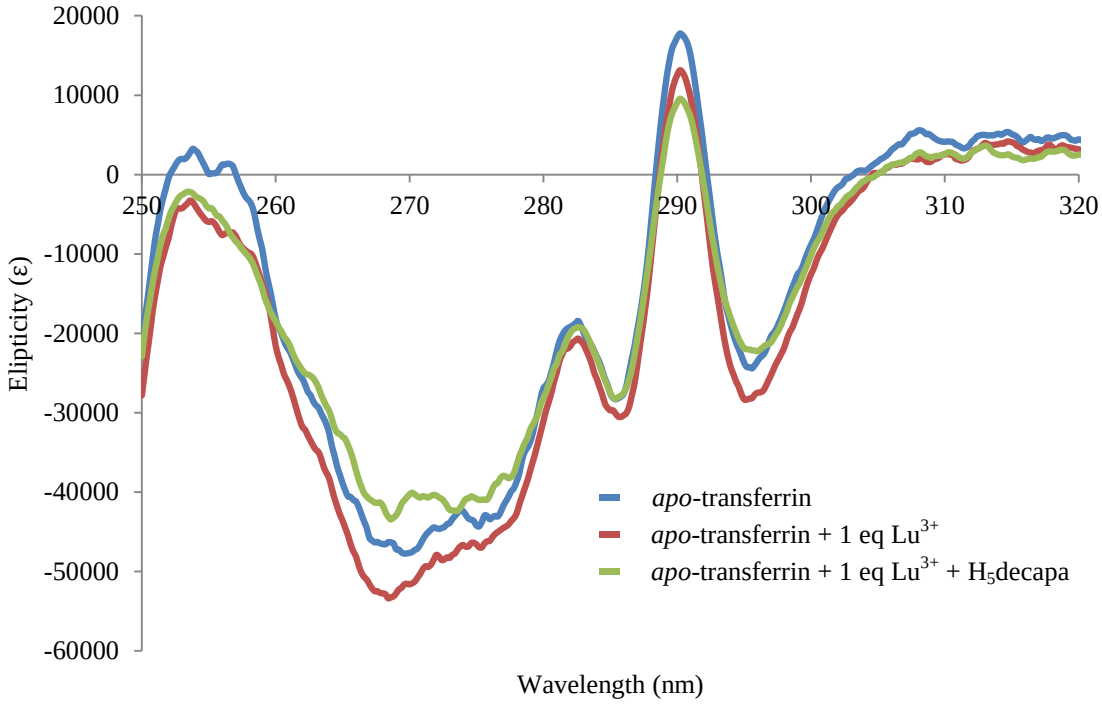


**Figure 2.16. CD spectra of *apo*-transferrin upon addition of metal ($Lu^{3+}$) and ligand ($H_5$decapa).**

Although a more exhaustive set of experiments are required to draw any conclusive results from these experiments, the initial findings provide insight into a potentially unique method of measuring competitive metal binding between ligand and human serum proteins. Classically, these experiments are conducted with radioactive isotopes so that the metal isotope can be easily traced. However, experiments based on UV-vis and CD would allow for some preliminary *in vitro* competition assays to be performed using the 'cold' metal complexes, avoiding the cost and safety considerations that encumber the use of radioisotopes.

### 2.2.6 Europium Fluorescence Studies

There are major differences between nuclear imaging and optical imaging; however, each mode provides unique attributes that can be combined together to provide a wider breadth of application. Optical imaging provides resolution down to the micrometer scale with real time imaging, but is limited by its penetration depth in tissue, which is only a few millimeters; however, there are a variety of situations where optical imaging is critical. Coupling nuclear imaging with optical imaging can help narrow the gap between the vast depth but poor detail of the former, compared with the poor depth but great detailing of the later. One potential widespread need could be for tumor imaging and removal, for instance, a patient could be injected with a BFC radiolabeled with an isotope for SPECT or PET imaging. Once the tumour has been localized, a fluorescent BFC could be injected to assist clinicians with removing the cancerous cells by illuminating the tagged cells using fluorescence techniques. Even before the clinical stages, where fluorescent BFCs could be of great use, they could also be used to help understand and elucidate pathways in many preclinical assessments. Often, little is known about antigen-biomolecule interactions, especially whether or not they are uptaken into the cell. Fluorescent techniques allow for real-time imaging and are also widely used in luminescent assays to evaluate receptor ligand interactions, critical to the field of drug discovery and development.

Previously, organic fluorescent reagents had been widely used as tags or labels; unfortunately, the high cellular auto-fluorescence decreased the signal-to-noise ratio, reducing the dynamic range and sensitivity of the tags.[51] Lanthanide complexes, on the other hand, are efficient fluorescent labels due to their unique properties such as excitation in the UV region (310 - 340 nm) and long lifetimes (100 μs - 1 ms). These characteristics led to lanthanide detection by time-resolved fluorescence (TRF) which yields a specific signal with very low background.[51] The luminescent properties of lanthanides are dominated by their low extinction coefficients; however, unbound in solution, they tend to lack significant fluorescent properties and often require a covalently attached organic chromophore (antenna effect). Europium is a luminescent lanthanide which prefers the oxidation state of 3+ and has an ionic radius of 95-112 pm (CN 6-10).[52] Since water molecules quench the lanthanide fluorescence, an ideal chelator would saturate the

coordination sphere of the ion. Because of its large binding cavity, $H_5$decapa was projected as a potential chelator for $Eu^{3+}$ to be used for TRF in cell studies.

To form the metal-ligand complex, $H_5$decapa was mixed with $Eu(NO_3)_3{\cdot}6H_2O$ and the product was detected by mass spectrometry, confirming the synthesis of the cold metal complex as $Na_2$[Eu(decapa)]. The $^1$H NMR spectrum of $[Eu(decapa)]^{2-}$ is very different than the previous metal complexes due to europium being a paramagnetic isotope (Figure 2.17). While integrations, peak splitting and chemical shifts do not unambiguously show the coordination chemistry of the metal-chelate complex, the fact that clear peaks can be detected indicates that one isomer is formed in solution. Fifteen peaks can be distinguished in the spectrum, corresponding to the number of protons expected for $H_5$decapa if an asymmetric complex is formed. This suggests that $[Eu(decapa)]^{2-}$ forms a stable complex in solution and could be suitable for *in vivo* experiments.

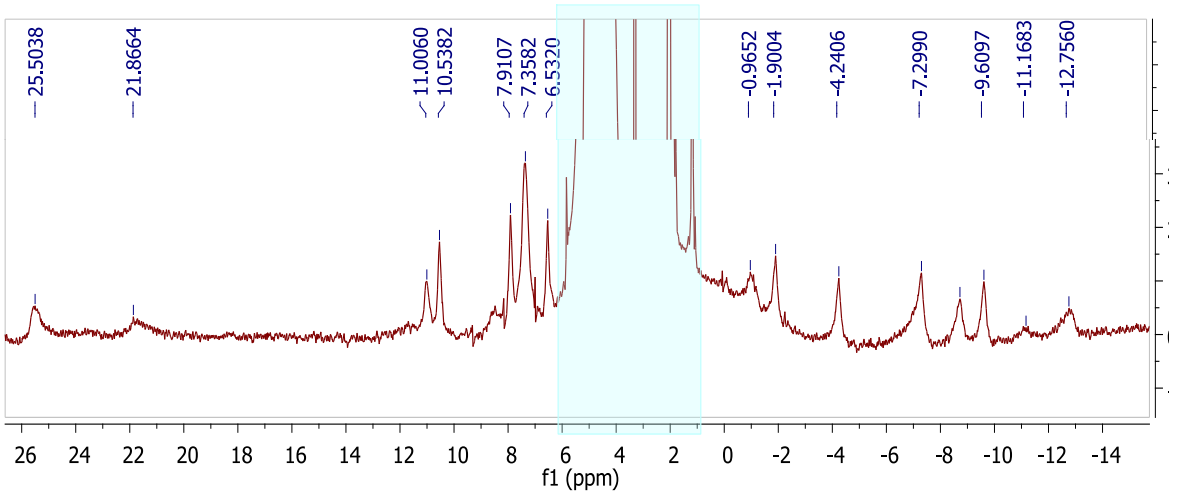


**Figure 2.17. $^1$H NMR spectra at ambient temperature of $[Eu(decapa)]^{2-}$ (400 MHz) in $D_2O$, showing the effect of binding the paramagnetic $Eu^{3+}$ ion.**

The major benefit of lanthanide-based labels is the characteristically long lifetime of the excited state, which allows for separation of the specific signal from the surrounding non-specific signals. The typical cellular background fluorescence is emitted on the order of picoseconds, a cell can be excited and the emission signal recorded until the background signals have completely decayed, leaving only the lanthanide fluorescence. Europium, when bound to a chelator, exhibits a strong, sharp emission at 615

nm (when excited at 340 nm), which can be seen in Figure 2.18. This provides confirmatory evidence that $Eu^{3+}$ forms a stable chelate with $H_5$decapa, as no quenching is observed, and the known shift in fluorescent emission from the free-metal to the bound-metal is observed.

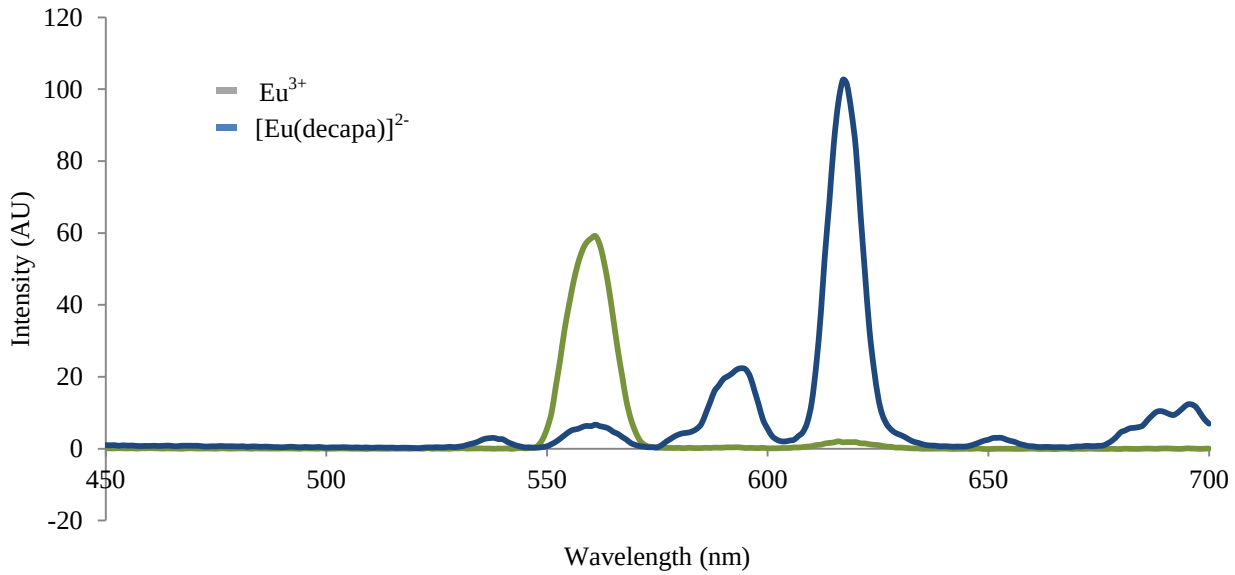


**Figure 2.18. $Eu^{3+}$ and $[Eu(decapa)]^{2-}$ emission spectrum (excitation wavelength = 280 nm).**

Multicellular spheroids, which are 3-dimensional structures of cancerous cells that act as *in vitro* tumor models, were grown to measure the uptake of the $[Eu(decapa)]^{2-}$ complex. Unfortunately, access to a time-resolved fluorescence microscope prevented this experiment from being completed. The emission spectrum shown in Figure 2.18 suggests that the $[Eu(decapa)]^{2-}$ complex should be further investigated in the future when access to an appropriate microscope is obtained.

### 2.2.7 Synthesis and Characterization of Bifunctional Decapa

While it is important to first assess the metal-ligand stability and binding characteristics of a ligand scaffold before increasing the synthetic complexity, until the system is bifunctional no truly informative *in vivo* experiments can be done. Furthermore, it is critical that once a metal-ligand system shows promise, the bifunctional derivative must retain the radiometal complex stability and properties

upon the addition of a linking moiety. Previous attempts to synthesize a bifunctional version of $H_5$decapa stemming from the diethylenetriamine backbone, in a similar manner to what was accomplished for $H_2$dedpa and $H_4$octapa,[1,27] proved to be unsuccessful. The larger backbone of $H_5$decapa led to greater asymmetry and instability when one of the bridging ethyl moieties was functionalized, rendering the complex unstable. The synthesis of a linker moiety from the central nitrogen in exchange for an acetate arm was attempted. This maintained the symmetry of the compound, while removing a single potential binding group. Because $H_5$decapa is decadentate and many of the metal isotopes in consideration do not require all 10 binding sites, changing one arm may not affect the binding of the ligand too much. The chosen linker used in this case was an ethyl-nitrobenzene sidechain. The ethyl linkage should provide distance and flexibility from the metal binding atoms in the chelate so that it does not sterically hinder their binding properties. The nitrobenzene group has been the linker of choice for most of the bifunctional 'pa' family ligands as it is a stable functional group that can be chemically modified to the phenyl-isothiocyanate, and this isothiocyanate can subsequently be coupled to a suitable primary amine on a chosen biomolecule, forming a thiourea linkage under mildly basic conditions.

The synthesis of the bifunctional complex (BF-decapa) followed a similar synthesis to the original ligand, differing only in the addition of the linking arm. BF-decapa was synthesized beginning with *N*-nosyl protection (**2.10**), then *N*-alkylation with ethyl-nitrobenzene (**2.11**), *N*-alkylation with an alkyl halide (**2.12**), nosyl deprotection via thiophenol (**2.13**), a second alkyl halide *N*-alkylation (**2.14**), and finally deprotection using boiling HCl (**2.15**) (Scheme 2.3). The nosyl protection was performed under milder conditions then was done for the synthesis of $H_5$decapa to prevent the protection of the more hindered central nitrogen. Since the bromo-nitrobenzene was quite unreactive, there was no major concern of over alkylating the other nitrogens as they were more sterically hindered. This allowed for the subsequent alkylation to occur with the methyl-picolinate before deprotecting with thiophenol.

**Scheme 2.3. Synthesis of BF-decapa (2.10 – 2.15).**

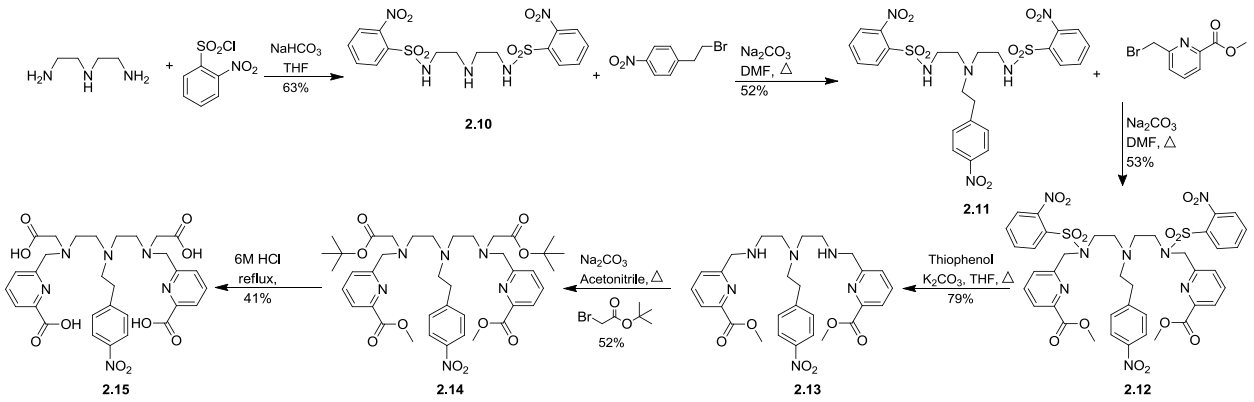


The $Zr^{4+}$ complex of BF-decapa, Zr(BF-decapa), was synthesized by mixing the BF-decapa salt (**2.15**) with $ZrCl_4$ in deionized water, adjusting the pH with NaOH (0.1M) to ~4-5 and stirring at room temperature for 1 hour. The formation of the coordination complex was confirmed by mass spectroscopy and the product was studied by NMR spectroscopy. The resulting metal complex was highly insoluble, most likely due to the neutral charge of the resulting complex compared to $[Zr(decapa)]^-$, which led to difficulties in studying the NMR spectra. The $^1$H-NMR spectrum of Zr(BF-decapa) in DMSO-$d_6$ was analyzed on the 600 Hz spectrometer using a suppressed water measurement (Figure 2.19).

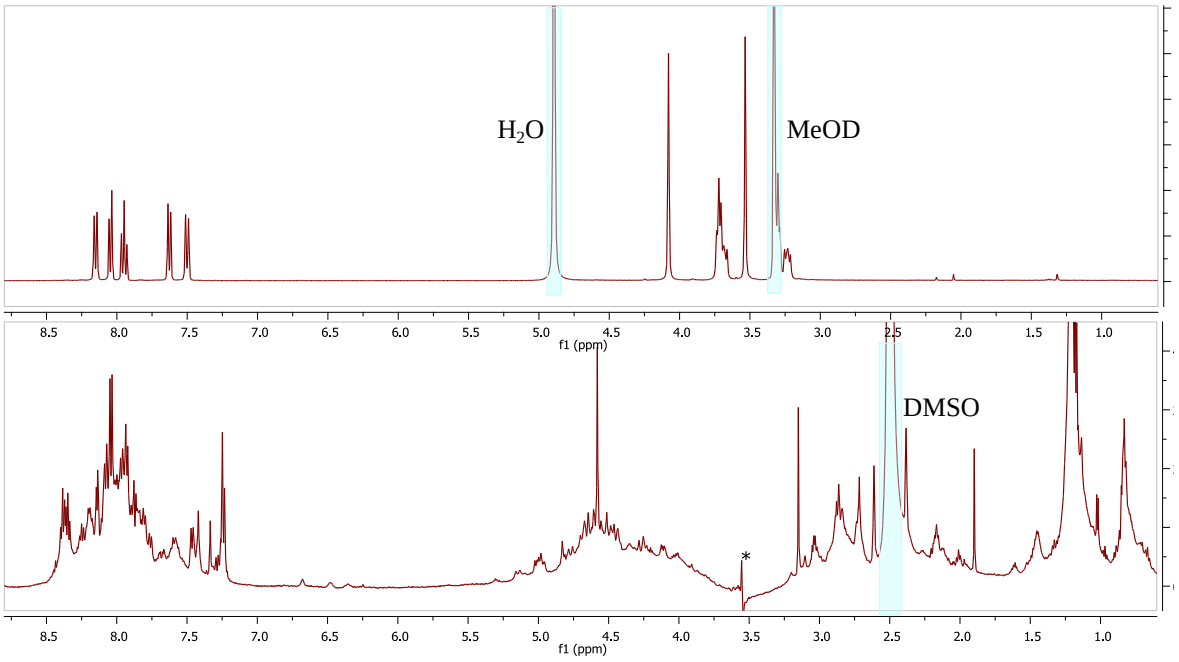


**Figure 2.19. $^{1}$H NMR spectra, 400 MHz at ambient temperature of (top) BF-decapa in $D_2O$, (bottom) [Zr(BF-decapa)] in DMSO-$d_6$, * - water suppression signal.**

The $^{1}$H NMR spectrum of Zr(BF-decapa) appears to depict multiple isomers in solution upon complexation, when compared to the bare ligand spectrum. However, there are sharp peaks which perhaps imply that there is at least one static isomer along with some broader peaks, which could be depicting a fluxional isomer. The 2D COSY spectrum (Appendix, Figure A.3*)* has six correlation peaks in the aromatic region, which hints that the major isomer is asymmetric, as only three correlations would be observed for a symmetric isomer. Nonetheless, further NMR studies, along with thermodynamic testing, radiolabeling and serum stability experiments, are required in order to gain more insight and understanding on the binding abilities and stabilities between BF-decapa and select radioisotopes.

## 2.3 Conclusion

Preliminary investigations into the decadentate ligand $H_5$decapa and its bifunctional derivative BF-decapa show this ligand scaffold to be a promising candidate for radiopharmaceutical applications. While $H_5$decapa did not show promising radiolabeling kinetics with $^{86}$Y/$^{90}$Y, the radiolabeling results with

$^{177}$Lu and thermodynamic stability values obtained for $Lu^{3+}$ demonstrate that $H_5$decapa is a suitable candidate for further testing of the metal-chelate complex. These experiments also demonstrate how finely tuned a chelate must be designed, as even though $Y^{3+}$ and $Lu^{3+}$ bear similar coordination preferences, a ligand may not bind each in a stable manor. Quantitative radiolabeling was observed for $^{89}$Zr with $H_5$decapa, and although the complex was not stable over time, the quick labeling at room temperature was unique for a non-hydroxamate ligand, and provides a basis from which to build future $Zr^{4+}$ chelates.

Initial investigation into alternative methods for *in vitro* testing of the metal-chelate stability via spectroscopic experiments was performed. CD shows promise as a technique to monitor competition experiments between endogenous metal binding proteins found in the body with the 'cold' metal-chelate complex. A preliminary investigation on the use of $Eu^{3+}$ with a radioisotope chelator to expand the scope for clinical use in imaging and removing tumours was explored. Cell studies would give a better understanding of the chelate *in vivo* and would also benefit from the fluorescent chelate.

Following the synthesis of the bifunctional derivative of $H_5$decapa, which can now be bound to an appropriate biomolecule, the metal-ligand binding properties must be reassessed. These tests will help determine whether the newly added ethyl nitrobenzyl moiety modifies the binding properties relative to the native ligand.

## 2.4 EXPERIMENTAL METHODS

### 2.4.1 Materials and Methods

All solvents and reagents were purchased from commercial suppliers (Sigma Aldrich, TCI America, Fischer Scientific, Alfa Aesar) and were used as received. DOTA/DTPA was purchased from Macrocyclics, STREM chemicals, Acros Organics. The analytical thin-layer chromatography (TLC) plates used were aluminum-baked ultra-pure silica gel 60 Å, 250 μm thickness. $^{1}H$ and $^{13}C$ NMR spectra were recorded at ambient temperature unless otherwise noted on Bruker AV300, AV400, or AV600 instruments; the NMR spectra are expressed on the δ scale and were referenced to residual solvent peaks. Low-resolution mass spectrometry was performed using a Waters ZG spectrometer with an ESCI electrospray/chemical-ionization source, and high-resolution electrospray-ionization mass spectrometry (HR-ESI-MS) was performed on a Micromass LCT time-of-flight instrument at the Department of Chemistry, University of British Columbia. Microanalysis for C, H, and N was performed by UBC MS staff on a Carlo Erba Elemental Analyzer EA 1108. The HPLC system used for analysis and purification of cold compounds consisted of a Waters 600 controller, Waters 2487 dual wavelength absorbance detector, and a Waters delta 600 pump. Phenomenex Synergi Hydro-RP 80 Å columns (250 x 4.6 mm analytical and 250 x 21.2 mm semi-preparative) were used for purification of the deprotected ligands. Analysis of radiolabeled complexes was carried out on a Phenomenex Synergi Hydro-RP 80 Å analytical column (250 x 4.6 mm) using a Waters Alliance HT 2795 separation module equipped with a Raytest Gabi Star NaI (Tl) detector and a Waters 996 photodiode array (PDA). DGA (N,N,N',N',-tetra-n-octyl-diglycolamide) resin (Eichrom) was used for the purification of $^{86}Y$.

DMSO used for chelator stock solutions was of molecular biology grade (>99.9%: Sigma, D8418). Desferrioxamine mesylate (DFO) was purchased from Sigma Aldrich (>92.5%). Water used was ultrapure (18.2 MΩ $cm^{-1}$ at 25°C, Milli-Q, Millipore). $^{90}Y$ and $^{177}Lu$ radiolabeling reactions were performed in ammonium acetate buffer (pH 4.5, 200 mM, made from ammonium acetate >99.9995% TraceSELECT®, Fluka), and $^{89}Zr$ radiolabeling was performed in phosphate buffered saline (PBS,

Sigma). $^{177}$Lu-(chelate) and $^{90}$Y-(chelate) analysis was performed using an HPLC system comprised of a Shimadzu SPD-20A prominence UV−vis, LC-20AB prominence LC, a Bioscan flow-count radiation detector, and a C18 reverse phase column (Phenomenex Luna Analytical 250 × 4.6 mm). $^{177}$Lu was procured from Perkin-Elmer (Perkin-Elmer Life and Analytical Sciences, carrier free) as $^{177}LuCl_3$ in 0.05 M HCl. $^{90}$Y was procured from Perkin-Elmer (Perkin-Elmer Life and Analytical Sciences, carrier free) as $^{90}YCl_3$ in 0.05 M HCl. $^{89}$Zr was produced at Memorial Sloan-Kettering Cancer Center on an EBCO TR19/9 variable-beam energy cyclotron (Ebco Industries Inc.) via the $^{89}Y(p,n)^{89}Zr$ reaction and purified in accordance with previously reported methods to yield $^{89}$Zr with a specific activity of 5.28-13.43 mCi/μg (195-497 MBq/μg).[53] Labeling reactions were monitored using acidic silica-gel impregnated glass-microfiber instant thin layer chromatography paper (iTLC-SA, Varian) and analyzed on a Bioscan AR-2000 radio-TLC plate reader using Winscan Radio- TLC software (Bioscan Inc.). All radio-labeling chemistry was performed with ultrapure water (>18.2 MΩ $cm^{-1}$ at 25°C, Milli-Q, Millipore) that had been treated by stirring with Chelex resin (~1.5 g per liter of water for 24 hours, BioRad Laboratories) for 24 hours, followed by filtration with a 0.22 μm nylon media filter (Nalgene). Human blood serum (Sigma, Sera, human, aseptically filled, S7023−100 mL) competition solutions were agitated at 550 rpm and held at 37°C using an Eppendorf Thermomixer. Radioactivity in samples was measured using a Capintec CRC-15R dose calibrator (Capintec). Centrifugation of small Eppendorf tubes was performed with an Eppendorf 5424 centrifuge, and large samples with an Eppendorf 5810R centrifuge.

The UV-vis system used was a Cary 5000 UV-Vis-NIR spectrophotometer. The CD system was a Jasco J-815 CD spectrophotometer operated with Spectra Manager software. The fluorescence spectra were recorded on the Agilent Cary Eclipse Fluorescence Spectrophotometer.

### 2.4.2 2-Nitro-N,N-bis(2-(2-nitrophenylsulfonamido)ethyl)benzenesulfonamide (2.1)

Diethylenetriamine (0.76 mL, 7.00 mmol) was dissolved in dichloromethane (DCM) (50 mL) with trimethylamine (TEA) (1.65 mL, 11.82 mmol, 1.7 equiv). 2-Nitrobenzene sulfonyl chloride (5.00 g, 22.56 mmol, 3.2 equiv) was dissolved in DCM (50 mL) and slowly added to the first solution, which was

allowed to stir overnight at room temperature. The solvent was then removed *in vacuo* and the orange solution was redissolved in DCM (100 mL). The organic layer was washed with saturated $NaHCO_3$, and washed with $H_2O$ (3 x 50 mL). The organic layer was then dried with $MgSO_4$ and the solvent was removed under reduced pressure to yield an orange fluffy solid. This solution was dissolved in a minimal amount of DCM/$CDCl_3$ (9:1) and recrystalized to give an off white solid (83%, 3.80 g). $^1$H NMR (300 MHz, Acetone-$d_6$, 25$^o$C) δ: 8.16-8.08 (m, 3H) 7.98-7.88 (m, 6H), 3.63-3.58 (m, 4H), 3.39-3.35 (m, 4H). $^{13}$C NMR (101 MHz, Acetone-$d_6$, 25$^o$C) δ: 149.45, 149.37, 135.76, 135.41, 134.26, 134.13, 133.55, 133.14, 131.78, 131.66, 126.27, 125.69, 49.79, 43.32. HR-ESI-MS calcd. for $[C_{22}H_{22}N_6O_{12}S_3+Na]^+$: 681.0356; found: 681.0349 $[M+Na]^+$, PPM = -1.0.

### 2.4.3 Dimethyl 6,6'-((((((2-nitrophenyl)sulfonyl)azanediyl)bis(ethane-2,1-diyl))bis(((2-nitrophenyl)sulfonyl)azanediyl))bis(methylene))dipicolinate (2.2)

To a solution of **2.1** (1.05 g, 1.59 mmol) in dimethylformamide (DMF) (10 mL, dried over molecular sieves 4 Å) was added methyl-6-bromomethyl picolinate[1] (0.84 g, 3.66 mmol, 2.3 equiv) and $Na_2CO_3$ (0.96 g, 9.11 mmol, 6.0 equiv). The faint yellow reaction mixture was stirred at 60$^o$C overnight, filtered to remove sodium carbonate, and concentrated *in vacuo*. The crude product was purified by silica chromatography (CombiFlash $R_f$ automated column system; 80 g HP silica; A: Hexanes, B: Ethyl Acetate, 100% A to 100% B gradient) to yield the product **2.2** as a yellow/white fluffy solid (65%, 0.99 g) ($R_f$ : 0.6, TLC in ethyl acetate). $^1$H NMR (300 MHz, Acetone-$d_6$, 25$^o$C) δ: 8.21 (d, *J* = 7.7 Hz, 2H), 8.02 (d, *J* = 7.7 Hz, 1H), 7.93-7.79 (m, 13 H), 7.57 (t, *J* = 5.1 Hz, 2H), 4.80 (s, 4H), 3.85 (s, 6H), 3.74 (s, 8H). $^{13}$C NMR (75 MHz, Acetone-$d_6$, 25$^o$C) δ: 165.86, 157.42, 149.13, 149.01, 148.46, 139.00, 135.36, 135.09, 132.78, 131.51, 131.33, 126.71, 125.34, 125.14, 124.72, 53.87, 52.81, 48.57, 48.08. HR-ESI-MS calcd. for $[C_{38}H_{37}N_8O_{16}S_3]^+$: 957.1490; found: 957.1511, $[M+H]^+$, PPM = 2.2.

### 2.4.4 Dimethyl 6,6'-(((azanediylbis(ethane-2,1-diyl))bis(azanediyl))bis(methylene))dipicolinate (2.3)

To a solution of **2.2** (0.62 g, 0.65 mmol) in tetrahydrofuran (THF) (~8 mL) was added thiophenol (0.22 mL, 2.14 mmol, 3.3 equiv) and potassium carbonate (excess, ~1 g). The reaction mixture was stirred at 50°C for 48 hours, during which time the solution turned a bright yellow colour. The solution was filtered through a medium frit glass filter funnel and evaporated *in vacuo*. The resulting crude yellow oil was purified by neutral alumina chromatography (CombiFlash $R_f$ automated column system; 2 x 24 g neutral alumina; A: dichloromethane, B: methanol, 100% A to 20% B gradient) to yield the product **2.3** as a yellow oil (79%, 0.20 g). $^1$H NMR (300 MHz, $CDCl_3$, 25°C) δ: 7.97 (d, *J* = 7.7 Hz, 2H), 7.61 (t, *J* = 7.7 Hz, 2H), 7.56 (d, *J* = 7.6 Hz, 2H), 4.80 (s, 4H), 3.99 (s, 4H), 3.96 (s, 6H), 2.76 (s, 8H). $^{13}$C NMR (75 MHz, $CDCl_3$, 25°C) δ: 165.82, 160.93, 147.46, 137.44, 125.64, 123.51, 55.13, 52.87, 49.36, 49.09. HR-ESI-MS calcd. for $[C_{20}H_{27}N_5O_4+H]^+$: 402.2141; found: 402.2141, $[M+H]^+$, PPM = -2.0.

### 2.4.5 N,N''-[[6-(Methoxycarbonyl)pyridin-2-yl]methylamino]-N,N',N''-[(tert-butoxycarbonyl)methyl]]diethylenetriamine (2.4)

To a solution of **2.3** (0.17 g, 0.43 mmol) in acetonitrile (10 mL) was added *tert*-butylbromoacetate (0.21 mL, 1.41 mmol, 3.3 equiv) and sodium carbonate (0.15 g, 1.37 mmol, 3.3 equiv). The reaction mixture was stirred at 60°C overnight, filtered to remove sodium carbonate, and concentrated *in vacuo*. The crude product was purified by silica chromatography (CombiFlash $R_f$ automated column system; 40 g HP silica; A: dichloromethane, B: methanol, 100% A to 20% B gradient) to yield the product **2.4** as an off-white solid (52%, ~0.18 g). $^1$H NMR (300 MHz, $CDCl_3$, 25°C) δ: 7.94-7.91 (m, 2H), 7.80-7.71 (m, 4H), 3.95 (s, 4H), 3.83 (s, 6H), 3.26 (s, 6H), 2.69 (s, 8H), 1.38 (s, 27H). $^{13}$C NMR (75 MHz, $CDCl_3$, 25°C) δ: 170.66, 166.02, 161.17, 147.28, 137.51, 123.23, 123.67, 27.04, 60.74, 56.57, 52.94, 52.90, 28.28). HR-ESI-MS calcd. for $[C_{38}H_{57}N_5O_{10}{}^+ H]^+$: 744.4184; found: 744.4174, $[M+H]^+$, PPM = -1.3.

### 2.4.6 $H_5$decapa·6HCl·3$H_2O$ (2.5)

Compound **2.4** (0.14 g, 0.18 mmol) was dissolved in 3:1 THF/d$H_2O$ (15 mL), lithium hydroxide (0.026 g, 1.09 mmol, 6.0 equiv) was added, and the mixture stirred for one hour at room temperature. The reaction was then concentrated *in vacuo* and redissolved in HCl (15 mL, 6M) and heated with a heat gun for 5-10 minutes. The reaction mixture was again concentrated *in vacuo* and then purified via semi-prep reverse-phase HPLC (10 mL/min, gradient A: 0.1% TFA (trifluoroacetic acid) in deionized water, B: $CH_3CN$. 0 to 95% B linear gradient 30 min. $t_R$ = 12.3 min, broad). Product fractions were pooled, concentrated *in vacuo*, dissolved in 6 M HCl, and concentrated *in vacuo*. The HCl salt $H_5$decapa·6HCl·3$H_2O$ (**2.5**) was obtained as an off-white powder (49% yield, 0.079 g, using the molecular weight of the HCl salt as determined by elemental analysis). $^1$H NMR (300 MHz, $D_2O$) δ: 8.25-8.13 (m, 4H), 7.78-7.76 (m, 2H), 4.62 (s, 4H), 4.04 (s, 4H), 3.73 (s, 2H), 3.50 (s, 4H), 3.32 (s, 4H). $^{13}$C NMR (75 MHz, $D_2O$) δ: 172.71, 169.94, 166.16, 150.71, 146.03, 141.82, 128.44, 125.99, 57.68, 54.76, 53.99, 51.87, 50.48. Elemental analysis: calcd. for $H_5$decapa·6HCl·3$H_2O$ ($C_{24}H_{29}N_5O_{10}$ ·6HCl·3$H_2O$ = 820.3279): C 35.14, H 5.04, N 8.53; found: C 35.01, H 5.09, N 8.29. HR-ESI-MS calcd. for [$C_{24}H_{29}N_5O_{10}$ + H]$^+$: 548.1993; found: 548.1989, [M+H]$^+$, PPM = -0.7.

### 2.4.7 $Na_2$[Y(decapa)] (2.6)

$H_5$decapa·6HCl·3$H_2O$ (**2.5**) (15.00 mg, 0.019 mmol) was dissolved in deionized water (1 mL) and $YCl_3$·6$H_2O$ (7.44 mg, 0.025 mmol, 1.3 equiv) was added. The pH was adjusted to 4-4.5 using 0.1 M NaOH and the solution was stirred at 60°C overnight. After confirmation of the product via mass spectrometry, the solvent was removed *in vacuo* to yield detectable $Na_2$[Y(decapa)] (**2.6)** and excess salts. HR-ESI-MS calcd. for [$C_{24}H_{24}N_5O_{10}{}^{89}Y$ + H]$^-$: 632.0660; found: 632.0660, [M+H]$^-$, PPM = 0.0. Multiple isomers in solution were observed; NMR spectra can be found in Figure 2.2.

### 2.4.8 $Na_2$[Lu(decapa)] (2.7)

$H_5$decapa·6HCl·3$H_2O$ (**2.5**) (15.00 mg, 0.019 mmol) was dissolved in deionized water (1 mL) and Lu($NO_3$)$_3$·6$H_2O$ (11.50 mg, 0.025 mmol, 1.3 eq.) was added. The pH was adjusted to 4-4.5 using 0.1 M NaOH and the solution was stirred at 60°C for 3 hours and then left stirring at room temperature for 72 hours. After confirmation of the product via mass spectrometry, the solvent was removed *in vacuo* to yield detectable $Na_2$[Lu(decapa)] and excess salts. HR-ESI-MS calcd. for [$C_{24}H_{24}N_5O_{10}{}^{175}$Lu + H]$^-$: 718.1009; found: 718.1011, [M+H]$^-$, PPM = 0.3. Multiple isomers in solution were observed; NMR spectra can be found in Figure 2.6.

### 2.4.9 Na[Zr(decapa)] (2.8)

$H_5$decapa·6HCl·3$H_2O$ (**2.5**) (3.00 mg, 0.005 mmol) was dissolved in deionized water (1 mL) and $ZrCl_4$ (1.66 mg, 0.0071 mmol, 1.3 equiv) was added. The pH was adjusted to 4 using 0.1 M NaOH and the solution was heated to 60°C and left stirring overnight. After confirmation of the product via mass spectrometry, the solvent was removed *in vacuo* to yield detectable Na[Zr(decapa)] (**2.8**) and excess salts. $^1$H NMR (600 Hz, $D_2O$, 25$^o$C) δ: 8.25 (t, *J* = 7.8 Hz, 1H), 8.21 (t, *J* = 7.8 Hz, 1H), 8.00 (d, *J* = 7.6 Hz, 2H), 7.86 (d, *J* = 7.9 Hz, 1H), 7.72 (d, *J* = 7.9 Hz, 1H), 4.67 (m, 2H), 4.33 (d, *J* = 17.0 Hz, 1H), 3.92-3.73(m, 6H), 3.65 (q, *J* = 13.4, 2H), 3.27 (d, *J* = 13.7 Hz, 1H), 3.08-3.02 (quin, 2H), 2.97 (d, *J* = 12.3 Hz, 1H), 2.90 (d, *J* = 13.5 Hz, 1H). $^{13}$C NMR (151 Hz, $D_2O$, 25$^o$C) δ: 179.26, 179.11, 171.50, 171.48, 170.90, 155.87, 155.05, 148.93, 146.63, 142.16, 142.04, 126.24, 126.20, 124.31, 123.84, 123.37, 123.33, 65.69, 65.24, 60.63, 60.24, 57.71, 56.80, 56.41, 54.33, 54.22. HR-ESI-MS calcd. for [$C_{24}H_{25}N_5O_{10}{}^{90}$Zr + H]$^+$: 634.0727; found: 634.0721, [M+H]$^+$, PPM = -0.9.

### 2.4.10 $Na_2$[Eu(decapa)] (2.9)

$H_5$decapa·6HCl·3$H_2O$ (**2.5**) (3.00 mg, 0.005 mmol) was dissolved in deionized water (1 mL) and Eu($NO_3$)$_3$·6$H_2O$ (3.18 mg, 0.0071 mmol, 1.3 equiv) was added. The pH was adjusted to 4 using 0.1 M

NaOH and the solution was left stirring overnight at room temperature. After confirmation of the product via mass spectrometry, the solvent was removed *in vacuo* to yield detectable $Na_2$[Eu(decapa)] (**2.9**) and excess salts. $^1$H NMR (400 Hz, $D_2O$, 25$^o$C) δ: 25.50, 21.87, 11.01, 10.54, 7.91, 7.36, 6.53, -0.97, -1.90, -4.24, -7.30, -8.73, -9.61, -11.17, -12.76. HR-ESI-MS calcd. for $[C_{24}H_{25}N_5O_{10}\ ^{151}Eu + H]^+$: 694.0800; found: 694.0797, $[M+H]^+$, PPM = -0.4.

### 2.4.11 N,N"-(2-Nitrobenzensulfonamide)-1,2- triaminodiethane (2.10)

Diethylenetriamine (0.50 mL, 4.60 mmol) was dissolved in THF (30 mL) in a round bottom flask (50 ml) that was placed in an ice bath. Sodium bicarbonate (1.17 g, 11.05 mmol, 2.4 equiv) was then added, followed by slow addition of 2-nitrobenzensulfonyl chloride (2.45 g, 11.05 mmol, 2.4 equiv), causing the reaction mixture to turn a pale yellow. The reaction mixture was allowed to warm to ambient temperature and stirred overnight. The off-white mixture was filtered to remove sodium bicarbonate and rotary evaporated. The crude product was purified by silica chromatography (CombiFlash $R_f$ automated column system 80 g HP silica; A: hexanes, B: ethyl acetate, 100% A to 100% B gradient) to yield the product **2.10** as an orange solid (63%, 1.37 g). $^1$H NMR (300 MHz, Acetone**,** 25$^o$C) δ: 8.14-8.11 (m, 2H), 7.97-7.88 (m, 6H), 3.11 (t, *J* = 4.5 Hz, 4H), 2.79 (d, *J* = 10.2 Hz, 4H), 2.68 (t, *J* = 4.4 Hz, 4H). $^{13}$C NMR (75 MHz, Acetone, 25$^o$C) δ: 148.42, 134.17, 133.24, 132.83, 130.73, 125.10, 47.88, 42.75. HR-ESI-MS calcd. for $[C_{16}H_{19}N_5O_8S_2+H]^+$: 474.0753; found: 474.0749, $[M+H]^+$, PPM = -0.8.

### 2.4.12 N,N'-(((4-Nitrophenethyl)azanediyl)bis(ethane-2,1-diyl))bis(2 nitrobenzenesulfonamide) (2.11)

To a solution of **2.10** (1.00 g, 2.11 mmol) in DMF (5 mL) was added $Na_2CO_3$ (0.38 g, 2.75 mmol, 1.3 equiv) and 4-(2-bromoethyl)nitrobenzene (0.63 g, 2.75 mmol, 1.3 equiv). The reaction mixture was heated to reflux and left stirring for 4 days. After 4 days the reaction mixture was cooled to room temperature, filtered, and dried *in vacuo*. The crude product was purified by silica chromatography

(CombiFlash $R_f$ automated column system; 40 g HP silica; A: hexanes, B: ethyl acetate, 100% A to 100% B gradient) to yield the product **2.11** as a dark orange oil (52%, 0.18 g). $^1$H NMR (400 MHz, $CDCl_3$**,** 25$^o$C) δ: 8.07-8.01 (m, 2H), 7.74-7.72 (m, 4H), 7.29 (d, *J* = 8.6 Hz, 2H), 3.04-3.03 (m, 4H), 2.81 (m, 2H), 2.71 (d, *J* = 7.8 Hz, 2H), 2.67 (t, *J* = 6.0 Hz, 4H). $^{13}$C NMR (101 MHz, $CDCl_3$, 25$^o$C) δ: 158.01, 157.64, 147.47, 146.81, 129.57, 129.52, 123.99, 117.30, 114.44, 54.96, 52.53, 37.55, 33.53. HR-ESI-MS calcd. for $[C_{24}H_{26}N_6O_{10}S_2 + H]^+$: 623.1230; found: 623.1237, $[M+H]^+$, PPM = 1.1.

### 2.4.13 Dimethyl 6,6'-(((((4-Nitrophenethyl)azanediyl)bis(ethane-2,1-diyl))bis(((2-nitrophenyl)sulfonyl)azanediyl))bis(methylene))dipicolinate (2.12)

To a solution of **2.11** (0.35 g, 0.56 mmol) in DMF (8 mL, dried over molecular sieves 4 Å) was added methyl-6-bromomethyl picolinate (0.30 g, 1.29 mmol, 2.3 equiv) and sodium carbonate (0.14 g, 1.29 mmol, 2.3 equiv). The bright orange reaction mixture was stirred at 60$^o$C overnight, filtered to remove sodium carbonate, and concentrated *in vacuo*. The crude product was purified by silica chromatography (CombiFlash $R_f$ automated column system; 80 g HP silica; A: Hexanes, B: Ethyl Acetate, 100% A to 100% B gradient) to yield the product **2.12** as an orange/brown oil (53%, 0.28 g). $^1$H NMR (300 MHz, $CDCl_3$**,** 25$^o$C) δ: 8.02-8.00 (m, 4H), 7.96 (d, *J* = 7.7 Hz, 2H), 7.78 (t, *J* = 7.8 Hz, 2H), 7.67-7.60 (m, 6H), 7.54 (d, *J* = 7.8 Hz, 2H), 7.18 (d, *J* = 8.4 Hz, 2H), 4.67 (s, 4H), 3.89 (s, 6H), 3.29 (t, *J* = 6.8 Hz, 4H), 2.58-2.51 (m, 8H). $^{13}$C NMR (101 MHz, $CDCl_3$, 25$^o$C) δ: 165.28, 156.98, 148.13, 147.55, 146.43, 138.14, 132.05, 129.74, 125.97, 125.93, 124.39, 124.38, 123.53, 55.31, 53.90, 52.91, 52.73, 46.87, 33.37. HR-ESI-MS calcd. for $[C_{40}H_{40}N_8O_{14}S_2 + H]^+$: 921.2184; found: 921.2184, $[M+H]^+$, PPM = 0.

### 2.4.14 Dimethyl 6,6'-(((((4-Nitrophenethyl)azanediyl)bis(ethane-2,1-diyl))bis(azanediyl))bis(methylene))dipicolinate (2.13)

To a solution of **2.12** (0.28 g, 0.30 mmol) in THF (~8 mL) was added thiophenol (0.070 mL, 0.68 mmol, 2.3 equiv) and potassium carbonate (0.14 g, 0.98 mmol, 3.3 equiv). The reaction mixture was stirred at 50°C for 48 hours, becoming a dark orange colour. The excess salts were removed by centrifugation (5 min, 4000 rpm) and the filtrate was concentrated *in vacuo*. The resulting crude orange oil was purified by neutral alumina chromatography (CombiFlash $R_f$ automated column system; 2 x 24 g neutral alumina; A: dichloromethane, B: methanol, 100% A to 20% B gradient) to yield the product **2.13** as a yellow/orange oil (79%, 0.20 g). $^1$H NMR (400 MHz, $CDCl_3$, 25°C) δ: 8.01 (d, *J* = 8.6 Hz, 2H), 7.90 (d, *J* = 7.6 Hz, 2H), 7.73 (t, *J* = 7.8 Hz, 2 H), 7.45 (d, *J* = 7.7 Hz, 2H), 7.28 (d, *J* = 8.6 Hz, 2H), 3.99 (s, 4H), 3.91 (s, 6H), 2.79-2.72 (m, 12H). $^{13}$C NMR (101 MHz, $CDCl_3$, 25°C) δ: 165.62, 158.88, 148.61, 147.39, 164.44, 137.76, 129.68, 126.00, 123.87, 123.67, 55.94, 54.02, 52.96, 52.69, 46.99, 33.27. HR-ESI-MS calcd. for $[C_{28}H_{34}N_6O_6+H]^+$: 551.2618; found: 551.2617, $[M+H]^+$, PPM = -0.2.

### 2.4.15 N,N',N"-[(tert-Butoxycarbonyl)methyl-N.N"–[6-(methoxycarbonyl)pyridin-2-yl]methyl]-1,2,3-triaminodiethane (2.14)

To a solution of **2.3** (0.04 g, 0.07 mmol) in acetonitrile (5 mL) was added *tert*-butylbromoacetate (0.025 μL, 0.17 mmol, 2.3 equiv) and sodium carbonate (0.02 g, 0.17 mmol, 2.3 equiv). The reaction mixture was stirred at 60°C overnight, filtered to remove sodium carbonate, and concentrated *in vacuo*. The crude product was purified by silica chromatography (CombiFlash $R_f$ automated column system; 24 g HP silica; A: dichloromethane, B: methanol, 100% A to 20% B gradient) to yield the product **2.14** as an orange oil (52%, 0.18 g). $^1$H NMR (400 MHz, $CDCl_3$, 25°C) δ: 8.11 (d, *J* = 8.5 Hz, 2H), 8.03 (d, *J* = 7.7 Hz, 2H), 7.89 (t, *J* = 7.7 Hz, 2H), 7.52 (d, *J* = 7.6 Hz, 2H), 7.43 (d, *J* = 8.5 Hz, 2H), 4.18 (s, 4H), 3.96 (s, 6H), 3.90 (s, 4H), 3.73 (m, 2H), 3.54 (s, 4H), 3.45 (br s, 4H), 3.24 (m, 2H), 1.38 (s, 18H). $^{13}$C NMR (75 MHz, $CDCl_3$, 25°C) δ: 168.74, 165.14, 156.74, 147.32, 147.25, 143.78, 139.10, 130.05, 127.49, 124.95,

124.02, 83.20, 57.47, 55.99, 54.47, 53.26, 50.42, 48.83, 29.83, 28.01. HR-ESI-MS calcd. for $[C_{40}H_{54}N_6O_{10} + H]^+$: 779.3980; found: 779.3973, $[M+H]^+$, PPM = -0.9.

### 2.4.16 BF·decapa (2.15)

Compound **2.14** (0.009 g, 0.01 mmol) was dissolved in 6 M HCl (2.5 mL), heated to reflux and left stirring overnight. The reaction mixture was concentrated *in vacuo* and then purified via semi-prep reverse-phase HPLC (10 mL/min, gradient A: 0.1% TFA (trifluoroacetic acid) in deionized water, B: $CH_3CN$. 5 to 100% B linear gradient 25 min. $t_R$ = 15.4 min, broad). Product fractions were pooled and then concentrated *in vacuo*. BF·decapa (**2.15**) was obtained as an off white powder (41% yield, 0.003 g). $^1$H NMR (400 MHz, $CDCl_3$**,** 25$^o$C) δ: 8.13 (d, *J* = 7.6 Hz, 2H), 8.02 (d, *J* = 7.0 Hz, 2H), 7.93 (t, *J* = 7.7 Hz, 2H), 7.60 (d, *J* = 7.7 Hz, 2H), 7.48 (d, *J* = 8.0 Hz, 2H), 4.06 (s, 4H), 3.70-3.65 (m, 6H), 3.51 (s, 4H), 3.51 (s, 4H), 3.24-3.17 (m, 2H). $^{13}$C NMR (101 MHz, MeOD-$d_4$, 25ºC) δ: 30.93, 50.21, 52.55, 55.93, 56.01, 59.09, 124.91, 125.51, 128.33, 131.32, 140.09, 145.89, 148.70, 149.03, 160.20, 167.59, 174.30. HR-ESI-MS calcd. for $[C_{30}H_{34}N_6O_{10} + H]^+$: 639.2415; found: 639.2417, $[M+H]^+$, PPM = 0.3.

### 2.4.17 Zr(BF-decapa) (2.16)

BF-decapa (**2.15**) (5.00 mg, 0.005 mmol) was dissolved in deionized water (1 mL) and $ZrCl_4$ (2.17 mg, 0.0093 mmol, 1.3 equiv) was added. The pH was adjusted to 4 using 0.1 M NaOH and the solution was left stirring at room temperature for 4 hours. After confirmation of the product via mass spectrometry, the solvent was removed *in vacuo* to yield detectable Zr(BF-decapa) and excess salts. HR-ESI-MS calcd. for $[C_{30}H_{30}N_6O_{10}\,^{90}Zr + Na]^+$: 747.0968; found: 747.0987, $[M+Na]^+$, PPM = 2.5. Multiple isomers in solution were observed; NMR spectra can be found in Figure 2.19.

### 2.4.18 Solution Thermodynamics

As a result of the strength of the binding of $Y^{3+}$ and $Lu^{3+}$ to $H_5$decapa, the complex formation constants with this ligand could not be determined directly and the ligand-ligand competition method using the known competitor $Na_2H_2EDTA$ was used by me. Potentiometric titrations were performed using a Metrohm Titrando 809 equipped with a Ross combination pH electrode and a Metrohm Dosino 800. Data was collected in triplicate using PC Control (Version 6.0.91, Metrohm). The titration apparatus consisted of a water-jacketed glass vessel maintained at 25.0 (± 0.1°C, Julabo water bath). Prior to and during the course of the titration, a blanket of nitrogen (passed through 10% NaOH to exclude any $CO_2$) was maintained over the sample solution. Lutetium and yttrium ion solutions were prepared by dilution of the appropriate atomic absorption standard (AAS) solution. The precise amount of acid present in each metal standard was determined by titration of an equimolar solution of $Y^{3+}/Lu^{3+}$ and $Na_2H_2EDTA$. The amount of acid present in the metal standard solutions was determined by Gran's method.[54] Calibration of the electrode was performed prior to each measurement by titrating a known amount of HCl with 0.1 M NaOH. Calibration data was analyzed by standard computer treatment provided within the program *GLEE*[55] to obtain the calibration parameters $E_0$ and $pK_w$. Equilibration times for titrations were 10 minutes for p$K_a$ and 15 minutes for metal complex titrations. Concentrations of ligand and metal were in the range of 0.75-1.0 mM for potentiometric titrations. The data were analysed by Dr. Jacqueline Cawthray using the program Hyperquad2008.[56] The proton dissociation constants corresponding to the hydrolysis of $Y^{3+}_{(aq)}/Lu^{3+}_{(aq)}$ ions were taken from Baes and Mesmer.[57] The $K_{ML}$ value for yttrium-EDTA and lutetium-EDTA complexes were taken from Martell.[38] All values and errors represent the average of at least two independent experiments.

### 2.4.19 Purification of $^{86}$Y

Purification of $^{86}$Y followed the procedure by E. Oehlke *et al*.[35] The liquid target solution was prepared by dissolving $Sr(NO_3)_2$ (14 g) in $H_2O$ (22.7 mL ) and adding concentrated $HNO_3$ (4 M, 2.3 mL).

The solution was irradiated on TRIUMF's TR13 cyclotron, a 13 MeV self-shielded, negative hydrogen ion cyclotron. The irradiated solution was diluted with ultrapure $H_2O$ (8 mL) and conc. $HNO_3$ (4 M, 4 mL). This solution was loaded onto a 50 mg prewashed (5 mL $H_2O$ and 5 mL of 4 M $HNO_3$) DGA resin column. The column was then washed with $HNO_3$ (4 M, 5 mL), $HNO_3$ (3 M, 5 mL), and HCl (6M, 5 mL). This was followed by aliquots of $H_2O$ (1 mL) that were collected individually and measured for radioactivity. The $^{86}Y$ was collected in1 mL vials between 4-8 mL of $H_2O$ (1.59 mCi). The pH of the $^{86}Y$ solutions were adjusted to 3 with NaOH (s) before radiolabeling experiments.

### 2.4.20 $^{86}$Y Radiolabeling Studies

The ligands $H_5$decapa (10 mg/mL, ~$10^{-2}$ M) and DOTA (1 mg/mL, ~$10^{-3}$ M) were made up as stock solutions in pH 5.5 NaOAc (100 mM). A 10 μL ($H_5$decapa) or 100 μL (DOTA) aliquot of stock solution was transferred to a screw-cap mass spectrometry vial and diluted with pH 5.5 NaOAc (100 mM) and $^{86}Y$ (~0.3-0.5 mCi) was added to the vials containing the ligand and heated to 70°C for 40 minutes to allow for radiolabeling. The complexes were then analyzed by RP-HPLC to confirm radiolabeling and to calculate yields. Areas under the peaks observed in the HPLC radiotrace were integrated to determine radiolabeling yields. Elution conditions used for RP-HPLC analysis were gradient: A: 0.1% TFA in $H_2O$, B: $CH_3CN$; 0 to 100% B linear gradient 20 min, 1mL/min). Free $^{86}Y$ ($t_R$ = 3.073), [$^{86}$Y(DOTA)] ($t_R$ = 5.420).

### 2.4.21 Ligand Stock Solutions and Radiolabeling Solutions

The following radiolabeling and serum stability experiments were performed by Dr. Eric Price at the Memorial Sloan Kettering Cancer Center, Department of Radiology. The chelators DTPA, DOTA, and $H_5$decapa were dissolved in DMSO (>99.9%, molecular biology grade) to make stock solutions at concentrations of 10 mM. For radiolabeling reactions, 5 μL of these stock solutions (10 mM, DMSO) were transferred to 495 μL of labeling buffer (ammonium acetate, 200 mM, pH 4.5 for $^{90}Y$ and $^{177}Lu$, and

PBS pH 7.4 for $^{89}$Zr) to make 100 μM ligand solutions for radiolabeling (50 nmol total ligand each sample).

### 2.4.22 $^{89}$Zr Radiolabeling and Serum Stability[53]

Radiolabeling solutions (500 μL, 100 μM, 50 nmol ligand, PBS pH 7.4) were mixed with ~300 μCi of $^{89}$Zr (neutralized to pH ~7 with $Na_2CO_3$, 1 M) and reacted for 30 minutes (550 rpm agitation, 37°C, thermomixer). Radiolabeling reactions were evaluated by iTLC–SA (regular non-acidic iTLC-SG did not separate free from bound radiometal) using an EDTA mobile phase (50 mM, pH 5), and by HPLC (5%-100% $CH_3CN$ (B) in 25 minutes, A = $H_2O$ with 0.1% TFA). "Free" radiometal eluted to the solvent front of the iTLC-SA strips, where $^{89}$Zr(decapa) and $^{89}$Zr(DFO) remained near the baseline. iTLC-SA strips were scanned using a Bioscan AR-2000 iTLC plate reader, and the area under the peaks was used to determine radiolabeling yields. After 30 minutes, both $H_5$decapa and DFO achieve >99% radiochemical yields with $^{89}$Zr. Using RP-HPLC the $^{89}$Zr(decapa) complex had a retention time of 6.3 minutes by radiotrace, where "free" neutralized $^{89}$Zr had a retention time of 3.8 minutes. $^{89}$Zr(decapa) showed no free $^{89}$Zr at 3.8 minutes on the radiotrace. These methods of analysis confirmed quantitative $^{89}$Zr radiolabeling with both DFO and $H_5$decapa after 30 minutes at 37°C.

Aliquots (~100 μCi, ~150 μL, n = 3) of $^{89}$Zr(DFO), $^{89}$Zr(decapa), and neutralized "free" $^{89}$Zr (control) were added to human blood serum (750 μL), and placed on a thermomixer (550 rpm, 37°C). Serum stability was evaluated by iTLC-SA as described above, or by precipitation with $CH_3CN$. For the precipitation method, 300 μL aliquots of the serum competition mixture were transferred to Eppendorf tubes (1.5 mL) and 700 μL of cold $CH_3CN$ was added to precipitate serum proteins. Precipitated serum mixtures were centrifuged for 10 minutes (10,000 rpm), and the supernatant was decanted to a new Eppendorf tube. The radioactivity present in the serum protein tube (serum protein bound $^{89}$Zr) and the radioactivity present in the supernatant (ligand bound) were counted with a dose calibrator, and the percentage of radioactivity in the supernatant was calculated to be the percentage intact radiometal

complex at each time point, [(μCi supernatant) / ((μCi supernatant) + (μCi serum proteins))] X 100 %. Control experiments with "free" $^{89}$Zr showed 99.5 ± 0.1% to be serum protein bound after 24 hours by the precipitation method, and 88.1 ± 1.3 % by iTLC-SA, suggesting the $CH_3CN$ precipitation method was most accurate.

### 2.4.23 $^{177}$Lu and $^{90}$Y Radiolabeling and Serum Stability

$^{177}LuCl_3$ (0.05 M HCl) and $^{90}YCl_3$ (0.05 M HCl) were transferred (~300-500 μCi, ~2-5 μL) to separate DOTA, DTPA, and $H_5$decapa radiolabeling solutions (50 nmol ligand each as described above, ammonium acetate buffer, 200 mM, pH 4.5), and heated at 70°C for 30 minutes to ensure quantitative radiolabeling (550 rpm agitation, thermomixer). Radiolabeling reactions were evaluated by iTLC–SA using an EDTA mobile phase (50 mM, pH 5), and by HPLC (5%-100% $CH_3CN$ (B) in 25 minutes, A = 0.1% TFA in $H_2O$) as described above in the $^{89}$Zr section. iTLC-SA elution was not successful for these samples, as $^{177}$Lu(decapa) and $^{90}$Y(decapa) could not be separated from free $^{177}$Lu/$^{90}$Y (both eluted near the solvent front). Standard aluminum-backed silica TLC plates and RP-TLC (C18) (eluted with 50:50 methanol:water) also could not separate free from bound radiometal. Due to the high polarity of these radiometal-ligand complexes, HPLC was also not ideal for evaluation, as the $^{177}$Lu/$^{90}$Y(chelate) complexes as well as the free $^{177}$Lu/$^{90}$Y radiometal eluted at the same retention time at the void-volume of the column (~3.9-4.0 minutes). The retention times for $^{177}$Lu/$^{90}$Y (free), $^{177}$Lu/$^{90}$Y(decapa), and $^{177}$Lu/$^{90}$Y(DOTA) were all 3.9-4.0 minutes; however, the $^{177}$Lu/$^{90}$Y(decapa) samples had more intense UV absorption at 254 nm than the free $^{177}$Lu/$^{90}$Y injections due to the presence of the picolinic acid rings in decapa. The free $^{177}$Lu/$^{90}$Y injections had UV absorption values at 254 nm of ~4-5 mAU, where $^{177}$Lu/$^{90}$Y(decapa) had absorption values of ~80 mAU. Although not ideal for accurate radiochemical yield determination, no method could be found to provide a clean separation between free $^{177}$Lu/$^{90}$Y and the $H_5$decapa radiolabeled radiometals. Serum stability results for $^{177}$Lu(decapa) (*vide infra*) suggest that $^{177}$Lu was indeed bound by $H_5$decapa as it showed resistance to binding by serum proteins. In contrast to

the serum stability of $^{177}$Lu(decapa), control samples of free $^{177}$Lu showed complete binding to serum proteins after 24 h.

Aliquots (~100 μCi, 150 μL, n = 3) of $^{177}$Lu/$^{90}$Y (free, control), $^{177}$Lu/$^{90}$Y(decapa), $^{177}$Lu/$^{90}$Y(DOTA), and $^{177}$Lu/$^{90}$Y(DTPA) were added to human blood serum (750 μL), and placed on a thermomixer (550 rpm, 37°C). Serum stability could not be evaluated by iTLC-SA as described above for $^{89}$Zr, due to poor separation between free and chelate bound radiometal. Precipitation of serum proteins with cold $CH_3CN$ was performed as described above in the $^{89}$Zr section, by transfer of 300 μL aliquots of the serum competition mixture to Eppendorf tubes (1.5 mL) and addition of 700 μL of cold $CH_3CN$. $^{90}$Y samples were also counted in a dose calibrator using the $^{90}$Y calibration setting, and were not counted using scintillation fluid on a scintillation counter. The readings for $^{90}$Y using the dose calibrator were approximate, as this method produces a lot of drift in the reading and is very sensitive to geometry. In order to minimize inaccuracy from sensitivity to geometry in the dose calibrator, each sample was affixed to the same physical location in the dose calibrator well by using a piece of sticky tape, and readings were allowed to stabilize for several minutes. The percent stability was determined in the same manner as described for $^{89}$Zr above, and control samples of free $^{90}$Y and $^{177}$Lu were 98.1 ± 0.1 % and 99.6 ± 0.1 % serum protein bound after 24 hours, respectively.

### 2.4.24 UV-vis and Circular Dichroism Experiments

The following stock solutions were prepared in phosphate buffer (pH 7.4, 10 mM): $NaHCO_3$ (0.17 g in 5 mL, 0.4 M), human *apo*-transferrin (4 mg in 5 mL, $10^{-5}$ M), lutetium atomic absorption standard solution (350 μL in 2 mL, $10^{-3}$ M), $H_5$decapa (0.80 mg in 1 mL, $10^{-3}$ M). Aliquots of $H_5$decapa (500 μL) and $Lu^{3+}$ (500 μL) buffered solutions were mixed together and the pH was adjusted to 7.4. Baselines on both the UV-vis and CD spectrometers were taken of phosphate buffer (2.5 mL) and $NaHCO_3$ (25 μL). UV-vis spectra were taken of *apo*-transferrin (2.5 mL) and $NaHCO_3$ (25 μL) in a quartz cuvette to measure the exact concentration of protein (at 278 nm, ε = 93, 000) using Beer's Law ($A = \varepsilon c \ell$).[39] Both UV-vis and CD spectra were recorded after the addition of $[Lu(decapa)]^{2-}$ (50 μL, 1 equiv)

and measured over time (until 2 hours) to monitor changes. UV-vis and CD spectra were also recorded after the addition $Lu^{3+}$ (25 μL, 1 equiv) followed by the addition of $H_5$decapa (25 μL, 1 equiv). The CD spectra were converted from mdeg to ellipticity using the concentration of protein obtained from the UV-vis spectrum.

### 2.4.25 Europium Fluorescence Study

The following stock solutions were prepared in acetate buffer (pH 5, 50 mM): $H_5$decapa (3.97 mg in 5 mL, $10^{-3}$ M) and $Eu^{3+}$ AAS (3 μL in 5 mL, $10^{-3}$ M). $H_5$decapa solution (5 μL) was combined with $Eu^{3+}$ solution (5 μL) in buffer (5 mL). Each solution was measured by UV-vis initially to record absorption wavelengths; $H_5$decapa solution absorbs at 280 nm. Fluorescence spectra were measured for each, recording the emission profiles for $Eu^{3+}$, $H_5$decapa and $[Eu(decapa)]^{2-}$ solutions individually excited at 280 nm.

# Chapter 3 : ATTEMPTED SYNTHESIS: $^{89}$ZR-LIGAND

## 3.1 INTRODUCTION

The positron-emitting radiometal zirconium-89 ($^{89}$Zr) has recently garnered a lot of attention for its use in PET imaging. Unlike the current, commonly used PET imaging agents (see Chapter 1), $^{89}$Zr boasts a long half-life of 78.41 hours (3.27 days). This is much longer than most $\beta^+$ emitting radionuclides, whose half-lives are rarely longer than 1 or 2 hours. The longer half-life allows for a radioimmunoconjugate to circulate throughout the body and accumulate at the target site, while any unbound tracer is cleared through the normal pathways, greatly improving the image contrast and tumor-to-background activity.[22] Furthermore, the lengthier half-life perfectly matches the biological lifetime of antibodies, subsequently expanding the scope of PET imaging's capabilities. In addition to its ideal half-life, $^{89}$Zr also exhibits low-energy positron decay which yields high resolution images, while ultimately being relatively simple and low cost in its production.[58]

Although $^{89}$Zr exhibits many ideal properties for improved PET imaging, one major factor has limited its extensive use: zirconium's coordination properties. Unlike most radiometals, where chelators are designed to accommodate the unique size and coordination preferences of the desired metal, additional factors need to be deliberated when considering $Zr^{4+}$ chelation. The $Zr^{4+}$ cation is a highly charged Lewis acid, that has a relatively large radius (84 pm) and prefers to form complexes with a high coordination number (8-9).[21] Under acidic to neutral conditions, $Zr^{4+}$ tends to form polynuclear hydroxo-species, subsequently precipitating out of solution, making it a difficult ion to chelate. Due to its hard acid characteristics, it prefers hard anionic donors, like oxygen, which should therefore be incorporated into any potential ligand scaffolds.[31]

The current gold standard (and it is a poor one) for $^{89}$Zr chelation is DFO, desferrioxamine B, an acyclic bacterial siderophore (see Chapter 1). DFO contains three hydroxamate groups that provide six oxygen donors for coordination of the metal, as well as a pendent amine that allows for derivatization

towards creating bifunctional conjugates to desired biomolecules. While DFO has been shown to radiolabel $^{89}$Zr under mild conditions (30-60 minutes, room temperature), *in vivo* studies have shown that the complex lacks kinetic inertness, as significant uptake of $^{89}$Zr can be seen in the bones, due to the osteophilic nature of the free metal ion.[22] This major shortcoming in the clinical potential of $^{89}$Zr has increased the urgency to design and characterize a more suitable chelator for this hard metal ion $Zr^{4+}$.

Subsequently, these factors all contributed to the design of a novel chelator with potential for Zr(IV) chelation, for use as a radiopharmaceutical. This design amalgamates aspects of the 'pa' ligand family with the functional binding groups of DFO. The 'pa' family of ligands has shown promise with a variety of radioisotopes and has a relatively robust synthesis. Due to the large ionic radius of $Zr^{4+}$, $H_5$decapa appears to be the logical chelate size, and this was proven in Chapter 2. Therefore, the scaffold of the new ligand is based on $H_5$decapa's dien backbone; however, to make a kinetically inert zirconium chelator, specific atoms should be used to cater to its hard acid preferences. Hydroxamic acids are bidentate ligands that are known to have a high binding affinity to a range of transition metals, including $Zr^{4+}$.[58,59] Because of DFO's success as a zirconium chelator, many new ligands have attempted to incorporate the hydroxamate functionality, the metal-binding moiety of DFO.[58,60] Herein, the synthesis of a zirconium ligand was attempted, combining facets of the $H_5$decapa binding scaffold with the DFO hydroxamate binding moiety.

## 3.2 Results and Discussion

### 3.2.1 Synthesis and Characterization

The synthesis of this new chelator was deconstructed into two goals, the synthesis of the backbone and the synthesis of the binding arms. To increase efficiency, the synthetic design of the backbone revolved around incorporating a bifunctional handle right from the start. To do this, the central nitrogen of the dien was selected to be the site of attaching the linker, as was done in the case of BF-decapa. To allow for functionalization on the secondary nitrogen of the diethylenetriamine, the two outer

primary amines need first be protected. The trifluoroacetyl (TFA) moiety was chosen as a protecting group (Scheme 3.1) as it offers selective primary amine acylation in the presence of secondary amines, due to the difference in steric hindrance of primary and secondary amines during the aminolysis of esters.[61] Although several synthetic procedures have been reported,[61,62,63] the reaction that was the most successful was carried out in cold diethyl ether, and the desired product precipitated from solution (**3.1**).[64]

**Scheme 3.1. Synthesis of precursors 3.1, 3.2 and 3.3.**

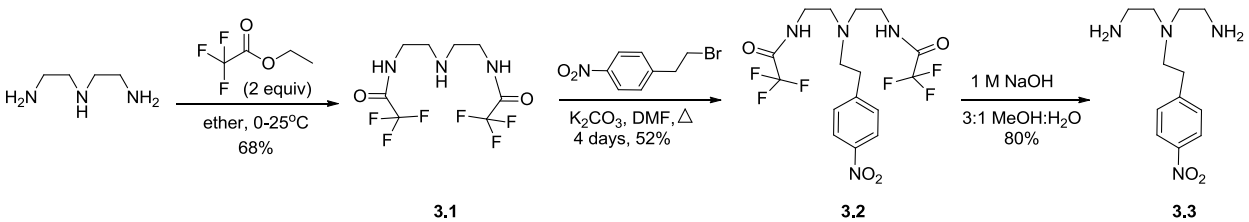


A nitro-benzene group was chosen as the linker moiety, as it can later be transformed to an isothiocyanate that would provide a site for conjugation to biomolecules. The addition of the ethyl nitrobenzene proved to be challenging due to the steric hindrance surrounding the central nitrogen and the electron withdrawing characteristics of the para-nitro group. Following the procedure by Ramaswamy *et al.*,[65] the coupling was first attempted in a polar aprotic solvent (acetonitrile) with an inorganic base ($NaHCO_3$). The reaction was carried out both at room temperature and then subjected to heating (60°C) yet mass spectroscopy analysis over the course of three days displayed no change from the starting material. As these conditions failed to produce detectable amounts of the coupled product, reaction optimization was performed as the temperature, solvent and base choices were explored (Table 3.1). Prior to changing solvent, the use of a soluble organic base and a halide salt were tested. *N*, *N*-diisopropylethylamine (DIPEA) was chosen as the base as it has a similar p$K_a$ to sodium bicarbonate (10.7 vs 10.3), but there is no issue of solubility, which increases the reactivity. When this was unsuccessful, the addition of potassium iodide that can act as a nucleophilic catalyst for alkylations with

bromides (Finkelstein reaction) was added; nevertheless, no change to the starting material was observed. Finally, changing solvents to DMF, which has a slightly higher dielectric constant, ultimately helped the reaction proceed. The best results were achieved using DMF and a stronger inorganic base ($K_2CO_3$); however, it still required elevated temperatures and time (**3.2**).

**Table 3.1. Reaction conditions, reagents and solvents tested for Scheme 3.2.**

| | Solvent | Base | Temperature | Duration | Result |
|---|---|---|---|---|---|
| **Trial 1:** | Acetonitrile | $NaHCO_3$ | RT, 60°C | 3 days | SM |
| **Trial 2:** | Acetonitrile | DIPEA | 60°C, 80°C reflux | 4 days | SM |
| **Trial 3:** | Acetonitrile | DIPEA, KI | 80°C, reflux | 4 days | SM |
| **Trial 4:** | DMF | $NaHCO_3$ | 80°C | 4 days | SM + P |
| **Trial 5:** | DMF | $K_2CO_3$ | 80°C | 4 days | P |

DIPEA= N,N-diisopropylethylamine; SM = starting material; P = product

Another benefit of using TFA as a protecting group for the dien backbone is the ease with which it can be removed. The cleavage of the trifluoroacetamide only requires mild basic conditions to deprotect,[66] and was achieved using 1M sodium hydroxide (**3.3**).

Having successfully synthesized the functionalized backbone, the next task was to design pendant arms with suitable chemical properties for binding zirconium. Due to the previous success of the picolinic acid moieties as chelating arms for a range of radioisotopes, this scaffold was thought to be a suitable starting point for terminal amine functionalization. Furthermore, following the binding interactions of DFO, the carboxylates were to be converted to the subsequent hydroxamate, that had been best shown to suit zirconium.[60]

The first approach to this synthesis began with saponification of the 6-(bromomethyl)picolinic acid obtained from dimethyl pyridine-2,6-carboxylate, to yield the desired methylated bromo-picolinic acid (**3.4**) (Scheme 3.2). This acid could then be condensed with the benzyl protected hydroxylamine, via the mixed anhydride, to give the *o*-protected pyridine hydroxamate (**3.5**).[67] This step involved the formation of the activated mixed anhydride intermediate using ethylchloroformate; however, *N*-

methylation in the subsequent step was hindered by the inability to properly purify the desired hydroxamate product from the crude mixture.

**Scheme 3.2 Synthesis of precursors 3.4 and 3.5.**

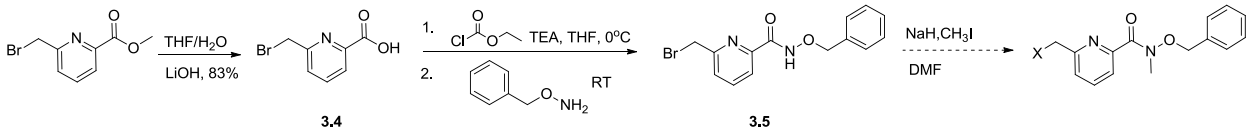


Due to the aforementioned issues during purification and methylation observed in the previous approach, a different method towards creating the desired *o*-protected 6-(bromomethyl)-*N*-hydroxypicolinamide (**3.5**) was attempted (Scheme 3.3). In order to avoid some issues previously observed with the labile terminal bromine, this synthetic scheme began instead with the 6-methylpicolinic acid, which was then similarly transformed into the benzyl-protected hydroxamate product. This reaction occurred without any observable side product formation, which allowed for facile isolation and purification of the *N*-(benzyloxy)-6-methylpicolinamide (**3.6**). In order to perform *N*-methylation on the hydroxamate moiety, relatively harsh conditions were employed.[68] Sodium hydride was chosen as the base, as it is very capable of deprotonating secondary amines, allowing for nucleophilic attack of the alkyl halide. The alkylating agent chosen for this case was methyl iodide, a common reagent used for alkylating a wide variety of compounds, including amines (**3.7**).

**Scheme 3.3. Synthesis of precursors 3.6 and 3.7.**

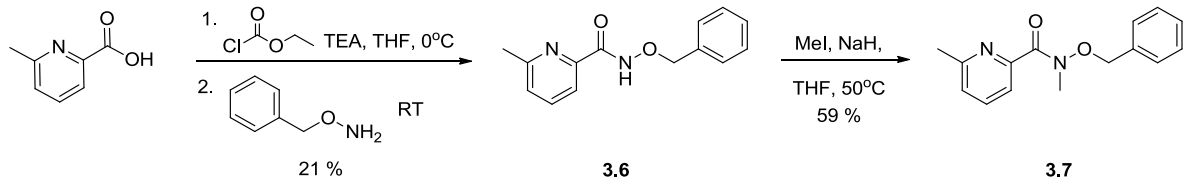

In order to easily alkylate the diethylenetriamine backbone with the 6-methyl-pyridine hydroxamate, a good leaving group was required on the terminal alkane to facilitate coupling. Halogens, such as bromine, are often employed as a suitable leaving group. The most common way to add a bromine to an alkyl chain is via NBS bromination (Scheme 3.4). This radical reaction requires a radical initiator, such as a peroxide, and an external initiator such as heat or light. Although this type of bromination reaction has previously provided an efficient method to brominating the protected 6-methyl picolinic acid,[2] in this case the hydroxamate moiety appears unstable towards radical conditions. Reactions conditions were varied in an attempt to optimize the bromination (Table 3.2); however, fragmentation of the N-O bond was most often observed.

**Scheme 3.4. Attempted reaction to methylate the hydroxamate nitrogen.**

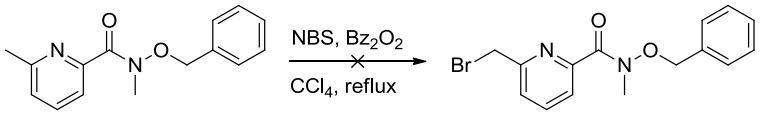


**Table 3.2. Reaction conditions, solvents and reagents tested for Scheme 3.4.**

| Trial | NBS (equiv) | 'Base' | Solvent | Conditions: | Result: |
|---|---|---|---|---|---|
| **1** | 0.7 + (24 hrs) 0.5 | Benzoyl peroxide | $CCl_4$ | -refluxing 60°C,[2] | SM |
| **2** | 0.7 | Benzoyl peroxide | $CCl_4$ | Reflux, IR lamp | fragmented |
| **3** | 1.1[69] | Benzoyl peroxide | $CCl_4$ | Reflux, IR lamp | fragmented |
| **4** | 1.1 (new bottle) | AIBN[69,70] | $CCl_4$ | Reflux, IR lamp | fragmented |

IR lamp = 150 W Halogen lamp, 5 cm from reactor – heat is used to reflux [71]

### 3.2.2 Future Directions

Due to time constraints, the synthetic approaches were not exhaustive towards the synthesis of the potential bifunctional Zr chelator. Many alternative synthetic pathways could be attempted in order to make the activated picolinic hydroxamate. First, a non-radical initiated bromination reaction could be attempted in place of the analogous reaction in Scheme 3.4. To do so, the methyl 6-

(hydroxymethyl)picolinate would serve as the starting material (the first step in the synthesis of the methyl 6-(bromomethyl)picolinate). Once the methylated hydroxamate was formed, the bromination could ensue by substituting the terminal alcohol with bromine, using phosphorous tribromide, a milder reaction. Second, methylation of the *o*-benzylhydroxylamine[68,72] prior to coupling with bromo-picolinic acid would eliminate the aforementioned troublesome methylation step and potentially allow for the final pendant arm to be synthesized. Alternatively, purchasing the *N*,*O*-dimethylhydroxylamine hydrochloride for the coupling reaction with the picolinic acid may prove to be more successful.

**Scheme 3.5. Designed synthetic pathway for Zr-ligand.**

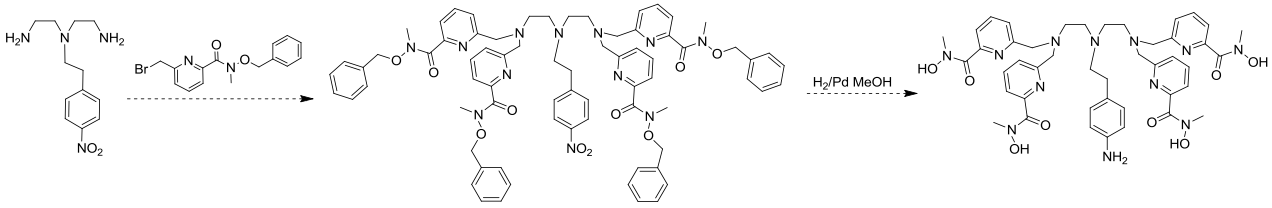


Ideally, once the *o*-protected 6-(bromomethyl)-*N*-hydroxy-*N*-methylpicolinamide is successfully synthesized, coupling to form the desired ligand can be accomplished (Scheme 3.5). To perform the required *N*-alkylation to the previously functionalized backbone, a strong base and aprotic solvent could be used. Reduction with $H_2$/Pd could deprotect the benzylated arms and simultaneously reduce the aromatic nitro group to the corresponding primary amine. The prepared ligand could then be bound with $Zr^{4+}$, characterized and tested rigorously for thermodynamic stability, radiolabeling yield, and serum stability, as was done for $H_5$decapa. The success of the hydroxylamine pendant arm would uncover the possibility of synthesizing a range of new ligands based off the 'pa' family scaffold that could be investigated towards $Zr^{4+}$ chelation (Figure 3.1).

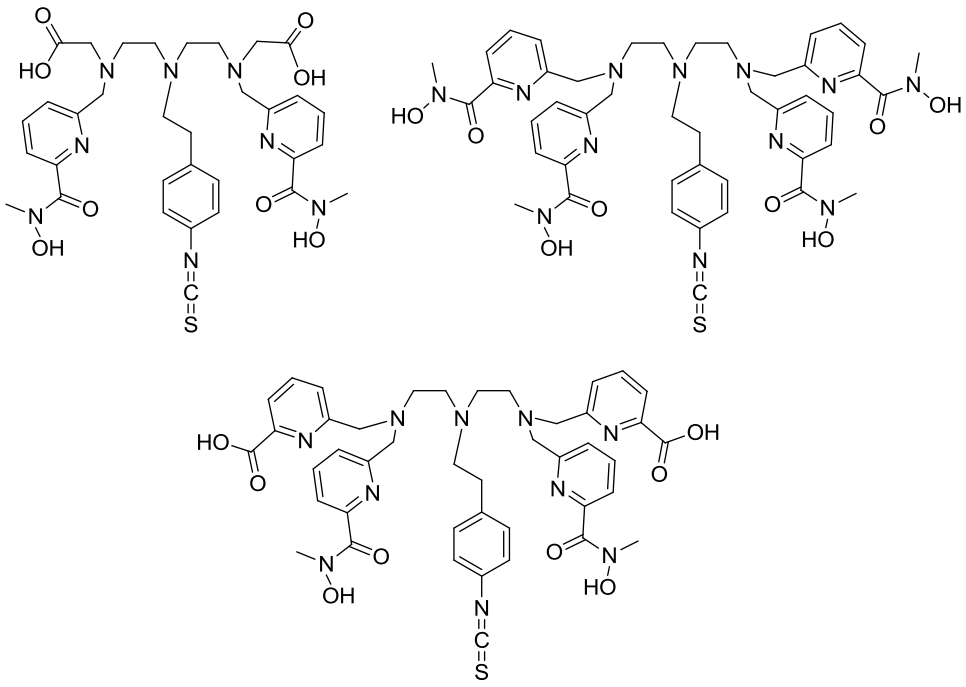

**Figure 3.1. Potential ligands for $Zr^{4+}$ based on the 'pa' family of ligands.**

## 3.3 Experimental Methods

### 3.3.1 Materials and Methods

General materials and methods are the same as those listed in Chapter 2.

### 3.3.2 N,N'-(Trifluoroacetamide)-1,2- triaminodiethane (3.1)

The synthesis was adapted from a literature preparation.[64] To a solution of diethylenetriamine (0.70 ml, 6.45 mmol) in 10 mL of diethyl ether on ice was added ethyl trifluoroacetate (1.76 mL, 14.8 mmol, 2.3 equiv). The reaction mixture was sealed and stirred at room temperature for 6 hours and placed in the freezer overnight. The crude product was rinsed with cold ether and dried *in vacuo* to yield **3.1** as a white solid (68%, 1.3 g). $^{1}$H NMR (400 MHz, $CDCl_3$**,** 25$^{o}$C) δ: 6.97 (br s, 2H), 3.44 (s, 4H), 2.86 (t, *J* = 7.6 Hz, 4H). $^{13}$C NMR (101 MHz, $CDCl_3$, 25$^{o}$C) δ: 158.00, 157.63, 120.28, 117.42, 114.56, 111.70, 47.52, 39.46. $^{19}$F NMR (282 MHz, $CDCl_3$, 25$^{o}$C) δ: 76.44. HR-ESI-MS calcd. for $[C_8H_{11}N_3O_2F_6 + H]^+$: 296.0834; found: 296.0832, $[M+H]^+$, PPM = -0.7.

### 3.3.3 N,N'-(Trifluoroacetamide)-1,2- triaminodiethane (3.2)

The synthesis was adapted from a literature preparation.[65] To a solution of **3.1** (0.50 g, 1.69 mmol) in 5 mL DMF was added $K_2CO_3$ (0.30 g, 2.20 mmol, 1.3 equiv) and 4-(2-bromoethyl)nitrobenzene (0.50 g, 2.20 mmol, 1.3 equiv). The reaction mixture was heated to reflux and left stirring for 4 days. After 4 days it was cooled to room temperature, filtered, and dried *in vacuo*. The crude product was purified by silica chromatography (CombiFlash $R_f$ automated column system; 40 g HP silica; A: hexanes, B: ethyl acetate, 100% A to 100% B gradient) to yield the product **3.2** as a red/orange oil (52%, 0.18 g). $^{1}$H NMR (300 MHz, $CDCl_3$**,** 25$^{o}$C) δ: 8.16 (d, *J* = 8.7 Hz, 2H), 7.33 (d, *J* = 8.7, 2H), 6.67 (br s, 1H), 3.42 (q, *J* = 5.8 Hz, 2H), 2.81-2.80 (m, 2H), 2.74 (t, *J* = 6.1 Hz, 2H). $^{13}$C NMR (101 MHz, $CDCl_3$, 25$^{o}$C) δ: 158.01, 157.64, 147.47, 146.81, 129.57, 129.52, 123.99, 117.30, 114.44, 54.96, 52.53, 37.55, 33.53. $^{19}$F NMR (282 MHz, $CDCl_3$, 25$^{o}$C) δ: 75.90. HR-ESI-MS calcd. for $[C_{16}H_{18}N_4O_4F_6 + H]^+$: 445.1310; found:

445.1309, $[M+H]^+$, PPM = -0.2.

### 3.3.4 N'-(2-Aminoethyl)-N'-(4-nitrophenethyl)ethane-1,2-diamine (3.3)

The synthesis was adapted from a literature preparation.[73] Compound **3.2** (0.20 g, 0.45 mmol) was dissolved in MeOH/$H_2O$ (3:1, 12 mL). 1M NaOH was added drop wise and the reaction progression was monitored by TLC. When the pH reached 10, the product was extracted with DCM (4 x 30 mL). The organic layer was dried with $MgSO_4$ and the solvent was evaporated *in vacuo* to yield **3.3** as a brown oil (80%, 0.090g). $^1$H NMR (300 MHz, MeOD-$d_4$, 25$^o$C) δ: 8.53 (s, 3H), 8.15 (d, *J* = 8.7 Hz, 2H), 7.49 (d, *J* = 8.7 Hz, 2H), 2.90 (d, *J* = 7.4 Hz, 2H), 2.79 (d, *J* = 5.7 Hz, 2H), 2.64 (d, *J* = 5.3 Hz, 2H), 2.59 (d, *J* = 5.5 Hz, 2H). $^{13}$C NMR (75 MHz, MeOD-$d_4$, 25$^o$C) δ: 150.57, 147.66, 131.03, 124.46, 57.40, 56.55, 40.03, 34.20. HR-ESI-MS calcd. for $[C_{12}H_{20}N_4O_2 + H]^+$: 253.1665; found: 253.1666, $[M+H]^+$, PPM = 0.4.

### 3.3.5 6-(Bromomethyl)picolinic acid (3.4)

The synthesis was adapted from a literature preparation.[74] Methyl 6-(bromomethyl)picolinate[1] (1.00 g, 4.35 mmol) was dissolved in THF/$H_2O$ (2:1, 12 mL). LiOH (0.26 g, 10.87 mmol, 2.5 equiv) was added and the reaction mixture was stirred at ambient temperature for 1 hr. The pH was adjusted to 2 with 1M HCl and the aqueous layer was extracted with ethyl acetate (5 x 60 mL). The combined organic phases were dried with $MgSO_4$ and concentrated *in vacuo* yielding **3.4** as a white solid (83%, 0.78 g). $^1$H NMR (300 MHz, $CDCl_3$, 25$^o$C) δ: 8.15 (d, *J* = 7.7 Hz, 1H), 7.95 (t, *J* = 7.7 Hz, 1H), 7.73 (d, *J* = 7.8 Hz, 1H), 4.58 (s, 2H). $^{13}$C NMR (101 MHz, $CDCl_3$, 25$^o$C) δ: 164.01, 156.35, 146.04, 139.77, 127.98, 123.33, 32.02. HR-ESI-MS calcd. for $[C_7H_6NO_2Br + Na]^+$: 237.9480; found: 237.9482, $[M+Na]^+$, PPM = 0.8. HR-ESI-MS calcd. for $[C_7H_6NO_2Cl + Na]^+$: 193.9985; found: 193.9982, $[M+Na]^+$, PPM = -1.5.

### 3.3.6 *N*-(Benzyloxy)-6-(bromomethyl)picolinamide (3.5)

The synthesis was adapted from a literature preparation.[71] Compound **3.4** (0.098 g, 0.45 mmol)

was dissolved in 5 mL of THF at 0°C. TEA (0.19 mL, 1.36 mmol, 3.0 equiv) and ethyl chloroformate (0.064 mL, 0.68 mmol, 1.5 equiv) were added to the vial. After 1 hour the reaction mixture had turned an opaque yellow/white colour and the *o*-benzyl hydroxylamine (0.073 g, 0.45 mmol) was added. After 4 hours the reaction mixture was quenched with saturated sodium bicarbonate, and the organic layer was separated with EtOAc. The organic layer was then separated with 0.1 M HCl, and washed with a brine solution. The organic layer was dried with $MgSO_4$, filtered, and dried *in vacuo.* The crude product was purified by silica chromatography (CombiFlash $R_f$ automated column system; 24 g HP silica; A: hexanes, B: ethyl acetate, 100% A to 100% B gradient) to yield the product **3.5** (16%, 0.018 g). $^1$H NMR (300 MHz, $CDCl_3$, 25$^o$C) δ: 8.15 (d, *J* = 7.7 Hz, 1H), 7.93 (t, *J* = 7.8 Hz, 1H), 7.65 (d, *J* = 7.7 Hz, 1H), 7.41 (m, 2H), 7.44-7.41 (m, 4H), 5.10 (s, 2H), 4.63 (s, 2H). $^{13}$C NMR (75 MHz, $CDCl_3$, 25$^o$C) δ: 161.60, 155.66, 148.78, 135.28, 129.45, 128.98, 128.79, 126.03, 121.87, 78.83, 24.21. HR-ESI-MS calcd. for $[C_{14}H_{13}N_2O_2Cl+H]^+$: 277.0744; found: 277.0752, $[M+Na]^+$, PPM = 2.9.

### 3.3.7 *N*-(Benzyloxy)-6-methylpicolinamide (3.6)

The synthesis was adapted from a literature preparation.[71] 6-Methylpicolinic acid (0.12 g, 0.86 mmol) was dissolved in 5 mL of THF at 0°C. TEA (0.36 ml, 2.59 mmol, 3.0 equiv) and ethyl chloroformate (0.12 mL, 1.30 mmol, 1.5 equiv) was added to the vial. After 1 hour the reaction mixture had turned an opaque yellow/white colour, and the *o*-benzylhydroxylamine (0.14 g, 0.86 mmol, 1.2 equiv) was added. After 4 hours the reaction mixture was quenched with saturated sodium bicarbonate, and the organic layer was separated with EtOAc. The organic layer was then separated with 0.1 M HCl, and washed with a brine solution. The organic layer was dried with $MgSO_4$, filtered, and dried in vacuo. The crude product was purified by silica chromatography (CombiFlash Rf automated column system; 24 g HP silica; A: hexanes, B: ethyl acetate, 100% A to 100% B gradient) to yield the product **3.6** (21%, 0.044 g). $^1$H NMR (300 MHz, $CDCl_3$, 25$^o$C) δ: 8.02 (d, *J* = 7.7 Hz, 1H), 7.74 (t, *J* = 7.7 Hz, 1H), 7.51-7.49 (m, 2H), 7.41-7.30 (m, 3H), 7.30 (d, *J* = 7.7 Hz, 2H), 5.08 (s, 2H), 2.51 (s, 3H). $^{13}$C NMR (75 MHz, $CDCl_3$, 25$^o$C) δ: 162.32, 157.50, 148.50, 137.58, 135.43, 128.79, 126.54, 119.49, 78.67, 24.21. HR-ESI-MS

calcd. for [$C_{14}H_{14}N_2O_2$ + Na]+: 265.0653; found: 265.0952, [M+Na]+, PPM = -0.4.

### 3.3.8 *N*-(Benzyloxy)-*N*,6-dimethylpicolinamide (3.7)

The synthesis was adapted from a literature preparation.[68] Compound **3.6** (0.11 g, 0.45 mmol) was added to a three headed round bottom with NaH (0.042 g, 0.59 mmol, 1.3 equiv) and placed under argon. Dry DMF (5 mL) was added to the solution before adding the MeI (0.042 ml, 0.68 mmol, 1.5 equiv). The reaction mixture was heated to 50°C under reflux and an inert atmosphere and left stirring overnight. The solvent was removed *in vacuo* and redissolved in EtOAc and separated with $H_2O$. The organic layer was dried with $MgSO_4$ and the crude product was purified by silica chromatography (CombiFlash $R_f$ automated column system; 40 g HP silica; A: hexanes, B: ethyl acetate, 100% A to 100% B gradient) to yield the product **3.7** (59%, 0.068 g). $^1$H NMR (300 MHz, $CDCl_3$, 25°C) δ: 10.28 (s, 1H), 8.02 (d, *J* = 7.7 Hz, 1H), 7.73 (t, *J* = 7.7 Hz, 1H), 7.51-7.49 (m, 2H) 7.41-7.39 (m, 3H), 7.30 (d, *J* = 7.7 Hz, 1H), 5.08 (s, 2H), 2.51 (s, 3H). $^{13}$C NMR (75 MHz, $CDCl_3$, 25°C) δ: 157.57, 152.79, 136.85, 134.79, 128.52, 124.46, 120.33, 77.58, 34.13*, 24.44 (*from HSQC data). HR-ESI-MS calcd. for [$C_{15}H_{16}N_2O_2$ +H]$^+$: 257.1290 found: 257.1291, [M+H]$^+$, PPM = 0.4.

# Chapter 4 : CONCLUSIONS AND FUTURE DIRECTIONS

## 4.1 CONCLUSION

The studies performed throughout this thesis focused on designing syntheses of ligands for larger radioisotopes based on the 'pa' family scaffold. The excellent results demonstrated by the original ligand $H_2$dedpa with $^{68}Ga/Ga^{3+}$, as well as the second generation $H_4$octapa with $^{111}In/In^{3+}$, gave promise for matches between other radiometals and future generation ligands. $H_5$decapa had previously been synthesized and tested with $^{111}In$; however, poor matching of the radioisotope and chelate size lead to poor observed coordination stability between the two *in vivo*. The synthetic difficulties of synthesizing $H_5$decapa previously limited the ability of research to test the ligand on other radiometals. A new and improved synthetic strategy was developed to make $H_5$decapa in considerably higher yield than described. This allowed for tests to be performed with other radioisotopes in an attempt to expand the library of available radiopharmaceuticals for PET/SPECT imaging and therapy. Preliminary experiments were performed between $H_5$decapa and $^{90}Y$, $^{177}Lu$ and $^{89}Zr$ to measure the radiolabeling efficiently as well as the serum stability. While $H_5$decapa had overall poor stability with both $^{90}Y$ and $^{89}Zr$, $[^{177}Lu(decapa)]^{2-}$ appeared to be relatively stable upon exposure to serum over the span of 5 days. Other spectroscopic methods to assess various parameters of the 'cold' metal-ligand complexes were undertaken. Although these were very preliminary experiments, there appears to be potential in using CD as a method to determine serum stability of a metal-ligand complex. The potential to use lanthanide fluorescence to perform cell studies and monitor the BFC *in vitro* was also explored, with the europium complex of $H_5$decapa showing promise.

In order for $H_5$decapa to be a viable radiopharmaceutical, a bifunctional derivative had to be designed. Functionalization of the backbone was originally attempted to mimic the previous 'pa' family ligands; however, it proved to be synthetically challenging. Instead, the central nitrogen of the dien was used as a point of functionalization, removing one of the binding arms. Since this could potentially

change the binding preferences compared to $H_5$decapa, many more binding and characterization experiments are required to compare its function to the unfunctionalized $H_5$decapa.

Although $H_5$decapa showed very poor long-term stability over several days with $^{89}Zr$, the fact that it was able to bind $^{89}Zr$ quantitatively after 30 minutes at room temperature is very promising, as this is relatively rare amongst standard chelators. In order to help retain the $Zr^{4+}$ isotope within the chelator, adjustments to the binding arms were designed to cater to zirconium's observed binding preferences. The addition of a hydroxamate moiety to the picolinic acid arms was attempted through various synthetic pathways, but synthesis was incomplete at the time of writing and the desired product has not been obtained to date. Further work, as outlined above, will be done to overcome these synthetic barriers and allow for assessment of the new and improved ligands towards $Zr^{4+}$ chelation.

## 4.2 Future Directions

The new synthesis for $H_5$decapa, along with that of the bifunctional derivative, will help expand the 'pa' family library that has been extensively studied by our group over the past several years. While $H_5$decapa did not show any improvements to current "gold standard" ligands, there is still a great deal of potential that lies ahead. These preliminary results illustrate the complexity required in designing ligands that cater to specific radiometals; while $Y^{3+}$ and $Lu^{3+}$ both share similar chemical properties, ionic radii, coordination numbers and charge, they clearly have differing binding preferences, as demonstrated by the NMR studies and radiolabeling experiments performed. The viability of a potential radiopharmaceutical can only be truly assessed by *in vivo* experiments that can measure the biodistribution and clearance of the radioactivity, although physical and *in vitro* tests aid in directing the choice of ligand to study. The bifunctional derivative of $H_5$decapa will allow for these experiments to be performed by providing a site to couple a biological targeting vector. Although imaging of cancerous tumors is critical to diagnosis, the attraction that these isotopes provide as potential therapeutics is undeniable. The need to harness α-emitting isotopes via a more accessible means is growing, so that their properties can be harnessed for

radiopharmaceutical testing. While there still lie many challenges with the incorporation of an α-emitting isotope into a practicable radiopharmaceutical, once the major challenge of production is overcome, rigorous testing can proceed to find an appropriate match. Due to the large size of many of these potentially accessible α-emitters, $H_5$decapa provides a good basis towards chelation of these larger isotopes.

# REFERENCES


(1) Price, E. W.; Cawthray, J. F.; Bailey, G. A.; Ferreira, C. L.; Boros, E.; Adam, M. J.; Orvig, C. *J. Am. Chem. Soc.* **2012**, *134*, 8670–7683.

(2) Price, E. W.; Cawthray, J. F.; Adam, M. J.; Orvig, C. *Dalton Trans.* **2014**, *43*, 7176–7190.

(3) Price, E. W.; Zeglis, B. M.; Cawthray, J. F.; Ramogida, C. F.; Ramos, N.; Lewis, J. S.; Adam, M. J.; Orvig, C. *J. Am. Chem. Soc.* **2013**, *135*, 12707–12721.

(4) Hoffman, J. M.; Gambhir, S. S.; Kelloff, G. J. *Radiology* **2007**, *245*, 645–660.

(5) Wadas, T. J.; Wong, E. H.; Weisman, G. R.; Anderson, C. J. *Chem. Rev.* **2010**, *110*, 2858–2902.

(6) Green, M. A. *J. Nucl. Med.* **1990**, *31*, 1641–1645.

(7) Kang, C. S.; Sun, X.; Jia, F.; Song, H. A.; Chen, Y.; Lewis, M.; Chong, H. S. *Bioconjug. Chem.* **2012**, *23*, 1775–1782.

(8) Holland, J. P.; Williamson, M. J.; Lewis, J. S. *Mol. Imaging* **2010**, *9*, 1–20.

(9) Volkert, W. A.; Hoffman, T. J. *Chem. Rev.* **1999**, *99*, 2269–2292.

(10) Vaidyanathan, G.; Zalutsky, M. R. *Phys. Med. Biol.* **1996**, *41*, 1915–1931.

(11) Wilbur, S. D. *Curr. Radiopharm.* **2011**, *4*, 214–247.

(12) Ramogida, C. F.; Orvig, C. *Chem. Commun.* **2013**, *49*, 4720–4739.

(13) Cutler, C. S.; Hennkens, H. M.; Sisay, N.; Huclier-Markai, S.; Jurisson, S. S. *Chem. Rev.* **2013**, *113*, 858–883.

(14) O'Donoghue, J. A.; Wheldon, T. E. *Phys. Med. Biol.* **1996**, *41*, 1973–1992.

(15) Donnelly, P. S. *Dalton Trans.* **2011**, *40*, 999–1010.

(16) Chang, A. J.; De Silva, R. A.; Lapi, S. E. *Mol Imaging* **2013**, *12*, 17–27.

(17) Shannon, R. D. *Acta Crystallogr. Sect. A* **1976**, *32*, 751.

(18) Clinical Trials https://clinicaltrials.gov/ct2/show/NCT02236910?term=lutetium-177&rank=1 (accessed Apr 17, 2015).

(19) Price, E. W.; Orvig, C. *Chem. Soc. Rev.* **2014**, *43*, 260–290.

(20) Cardinal Health. FDA-approved radiopharmaceuticals http://www.cardinal.com/us/en/nuclearmedicinecompliance/fdaapproved (accessed Apr 17, 2015).

(21) Deri, M. A.; Zeglis, B. M.; Francesconi, L. C.; Lewis, J. S. *Nucl. Med. Biol.* **2013**, *40*, 3–14.

(22) Deri, M. A.; Ponnala, S.; Zeglis, B. M.; Pohl, G.; Dannenberg, J. J.; Lewis, J. S.; Francesconi, L. C. *J. Med. Chem.* **2014**, *57*, 4849–4860.

(23) Clinical Trials https://clinicaltrials.gov/ct2/show/NCT01565200?term=zirconium-89&rank=4 (accessed Apr 17, 2015).

(24) Hancock, R. D. *J. Chem. Educ.* **1992**, *69*, 615–621.

(25) Cole, W. C.; DeNardo, S. J.; Meares, C. F.; McCall, M. J.; DeNardo, G. L.; Epstein, A. L.; O'Brien, H. A.; Moi, M. K. *J. Nucl. Med.* **1987**, *28*, 83–90.

(26) Byegård, J.; Skarnemark, G.; Skålberg, M. *J. Radioanal. Nucl. Chem.* **1999**, *241*, 281–290.

(27) Boros, E.; Ferreira, C. L.; Cawthray, J. F.; Price, E. W.; Patrick, B. O.; Wester, D. W.; Adam, M. J.; Orvig, C. *J. Am. Chem. Soc.* **2010**, *132*, 15726–15733.

(28) Ramogida, C. F.; Cawthray, J. F.; Boros, E.; Ferreira, C. L.; Patrick, B. O.; Adam, M. J.; Orvig, C. *Inorg. Chem.* **2015**, 2017–2031.

(29) Boros, E.; Ferreira, C. L.; Yapp, D. T. T.; Gill, R. K.; Price, E. W.; Adam, M. J.; Orvig, C. *Nucl. Med. Biol.* **2012**, *39*, 785–794.

(30) Bailey, G. A.; Price, E. W.; Zeglis, B. M.; Ferreira, C. L.; Boros, E.; Lacasse, M. J.; Patrick, B. O.; Lewis, J. S.; Adam, M. J.; Orvig, C. *Inorg. Chem.* **2012**, *51*, 12575–12589.

(31) Price, E. W.; Zeglis, B. M.; Lewis, J. S.; Adam, M. J.; Orvig, C. *Dalton Trans.* **2014**, *43*, 119–131.

(32) Blower, P. J. *Dalton Trans.* **2015**, *44*, 4819–4844.

(33) Garret, T.; Umbenhauer, J.; Romberger, G.; Smith, A.; Goulden, M.; Engle, J.; Harris, M. *J. Undergrad. Chem. Res.* **2008**, *7*, 19.

(34) Liu, S.; Pietryka, J.; Ellars, C. E.; Edwards, D. S. *Bioconjug. Chem.* **2002**, *13*, 902–913.

(35) Oehlke, E.; Hoehr, C.; Hou, X.; Hanemaayer, V.; Zeisler, S.; Adam, M.; Ruth, T. J.; Celler, A.; Buckley, K.; Benard, F.; Schaffer, P. *Nucl. Med. Biol.* **2015**.

(36) Price, E. Synthesis, evaluation and application of new ligands for radiometal based radiopharmaceuticals, University of British Columbia. Phd Thesis, 2014.

(37) Koppe, M. J.; Bleichrodt, R. P.; Soede, A. C.; Verhofstad, A. A.; Goldenberg, D. M.; Oyen, W. J. G.; Boerman, O. C. *J. Nucl. Med.* **2004**, *45*, 1224–1232.

(38) Martell, A. E.; Smith, R. M. *Critical Stability Constants, Vol 1-6*; Plenum Press: New York, 1974.

(39) Rodger, A.; Marrington, R.; Roper, D.; Windsor, S. In *Protein-Ligand Interactions Methods and Applications*; Nienhaus, G. U., Ed.; Springer, 2005; Vol. 305, pp 343–363.

(40) Pessoa, J. C.; Correia, I.; Gonçalves, G. *J Argent Chem Soc* **2009**, *97*, 151–165.

(41) Bal, W.; Sokołowska, M.; Kurowska, E.; Faller, P. *Biochim. Biophys. Acta - Gen. Subj.* **2013**, *1830*, 5444–5455.

(42) Chung, M. C.-M. *Biochem. Educ.* **1984**, *12*, 146–154.

(43) Shahid, F.; Gomez, J. E.; Birnbaum, E. R.; Darnall, D. W. *J. Biol. Chem.* **1982**, *257*, 5618–5622.

(44) Harris, W. R.; Yang, B.; Abdollahi, S.; Hamada, Y. *J. Inorg. Biochem.* **1999**, *76*, 231–242.

(45) Wu, J.; Li, M.; Liu, Z.; Hu, Y.; Wang, M. *Chinese J. Lumin.* **2012**, *33*, 1153–1159.

(46) Tang, S.; MacColl, R.; Parsons, P. J. *J. Inorg. Biochem.* **1995**, *60*, 175–185.

(47) Yao, L.; Chen, Q. Y.; Xu, X. L.; Li, Z.; Wang, X. M. *Spectrochim. Acta - Part A Mol. Biomol. Spectrosc.* **2013**, *105*, 207–212.

(48) Vidaud, C.; Gourion-Arsiquaud, S.; Rollin-Genetet, F.; Torne-Celer, C.; Plantevin, S.; Pible, O.; Berthomieu, C.; Quéméneur, E. *Biochemistry* **2007**, *46*, 2215–2226.

(49) Kiss, T.; Jakusch, T.; Hollender, D.; Dörnyei, Á.; Enyedy, É. A.; Pessoa, J. C.; Sakurai, H.; Sanz-Medel, A. *Coord. Chem. Rev.* **2008**, *252*, 1153–1162.

(50) Jakusch, T.; Hollender, D.; Enyedy, E. A.; González, C. S.; Montes-Bayón, M.; Sanz-Medel, A.; Costa Pessoa, J.; Tomaz, I.; Kiss, T. *Dalton Trans.* **2009**, 2428–2437.

(51) Handl, H. L.; Gillies, R. J. *Life Sci.* **2005**, *77*, 361–371.

(52) Vicentini, G.; Zinner, L. B.; Zukerman-Schpector, J.; Zinner, K. *Coord. Chem. Rev.* **2000**, *196*, 353–382.

(53) Holland, J. P.; Sheh, Y.; Lewis, J. S. *Nucl. Med. Biol.* **2009**, *36*, 729–739.

(54) Gran, G.; Dahlenborg, H.; Laurell, S.; Rottenberg, M. *Acta Chem. Scand.* **1950**, *4*, 559–577.

(55) Gans, P.; O'Sullivan, B. *Talanta* **2000**, *51*, 33–37.

(56) Gans, P.; Sabatini, A.; Vacca, A. *Talanta* **1996**, *43*, 1739–1753.

(57) Baes, C. F. J.; Mesmer, R. E. *The Hydrolysis of Cations*; Wiley-Interscience: New York, 1976.

(58) Guérard, F.; Lee, Y.-S.; Brechbiel, M. W. *Chemistry* **2014**, *20*, 5584–5591.

(59) Codd, R. *Coord. Chem. Rev.* **2008**, *252*, 1387–1408.

(60) Guérard, F.; Lee, Y.-S.; Tripier, R.; Szajek, L. P.; Deschamps, J. R.; Brechbiel, M. W. *Chem. Commun.* **2013**, *49*, 1002–1004.

(61) Xu, D.; Prasad, K.; Repic, O.; Blacklock, T. J. *Tetrahedron Lett.* **1995**, *36*, 7357–7360.

(62) Napolitano, R.; Pariani, G.; Fedeli, F.; Baranyai, Z.; Aswendt, M.; Aime, S.; Gianolio, E. *J. Med. Chem.* **2013**, *56*, 2466–2477.

(63) Asseline, U.; Chassignol, M.; Draus, J.; Durand, M.; Maurizot, J. C. *Bioorganic Med. Chem.* **2003**, *11*, 3499–3511.

(64) Hay, M. P.; Pruijn, F. B.; Gamage, S. A.; Liyanage, H. D. S.; Kovacs, M. S.; Patterson, A. V; Wilson, W. R.; Brown, J. M.; Denny, W. A. *J. Med. Chem.* **2004**, *1*, 475–488.

(65) Ramaswamy, S.; Colony, J. Polyaminocarboxylate Chelators. 5808003, 1998.

(66) Wuts, P. G. M.; Greene, T. W. *Greene's Protective Groups in Organic Synthesis*; Wiley-Interscience: New York, 2007.

(67) Shinji, C.; Maeda, S.; Imai, K.; Yoshida, M.; Hashimoto, Y.; Miyachi, H. *Bioorganic Med. Chem.* **2006**, *14*, 7625–7651.

(68) Classen-Houben, D.; Wolkerstorfer, A.; Szolar, O.; Smith, M. Heteroaryl Hydroxmic Acid Derivatives and Their Use in the Treatment, Amerlioration or Prevention of Viral Disease. 057251, 2013.

(69) Wei, Z.; Xie, X.; Zhao, J.; Huang, L.; Liu, X. *Inorganica Chim. Acta* **2012**, *387*, 277–282.

(70) Yager, K.; Kim, I. C.; Saunder, M.; Gerrish, D.; Kumn, D. V.; Anderson, M. B. Antiviral Compounds and Use Thereof. 127364, 2008.

(71) Ijuin, R.; Umezawa, N.; Higuchi, T. *Bioorg. Med. Chem.* **2006**, *14*, 3563–3570.

(72) Mannion, J.; Dax, S.; Macintyre, Duncan, E.; Golder, Francis, J.; McLeod, James, F. Novel Compounds and Compositions for Treatment of Breathing Control Disorders or Diseases. 181217, 2012.

(73) Blum, A.; Böttcher, J.; Sammet, B.; Luksch, T.; Heine, A.; Klebe, G.; Diederich, W. E. *Bioorg. Med. Chem.* **2008**, *16*, 8574–8586.

(74) Dong Jog, C.; Eun Young, Y.; Gun Bong, L.; Soon Ok, K.; Wan Joo, K. Novel Tricyclic Derivatives and Their Use. 7119229, 2007.

# APPENDIX

## Appendix A Supplementary Figures and Data

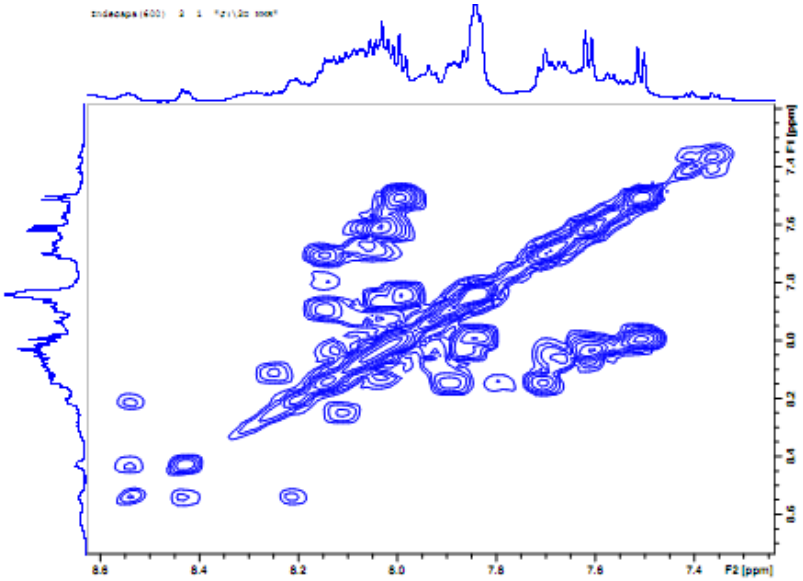


**Figure A.1. [Lu(decapa)]$^{2-}$ 2D COSY NMR spectrum, aromatic region (600 Hz, in $D_2O$).**

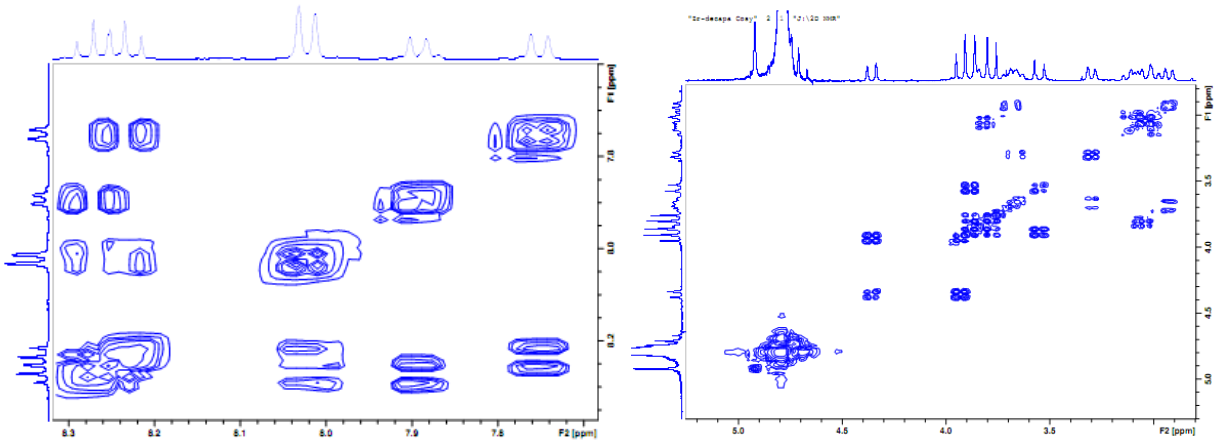


**Figure A.2. [Zr(decapa)]$^{-}$ 2D COSY spectrum, 400 Hz, in $D_2O$, aromatic region (left) alkyl region (right).**

**Table A.1. $^{177}$Lu human serum competition via PD10 column - 1.5 and 24 hours, 37.0 ± 0.1°C at 550 rpm agitation; background activity / mCi = 0.5.**

| Chelator | Radiolabeling conditions | Average % chelate intact 1.5 hr | Average % chelate intact 24 hr |
|---|---|---|---|
| **DTPA** | 10 min, RT | 77.4 ± 1.2% | 81.6 ± 2.3% |
| **DOTA** | 90°C, 1 hour | 87.7 ± 0.7% | 87.4 ± 2.1 % |
| **$H_4$octapa** | 10 min, RT | 88.1 ± 1.2% | 86.2 ± 0.7% |
| **$H_5$decapa** | 10 min, RT | 81.2 ± 1.0% | 79.7 ± 1.9% |

Experiments performed by Dr. Eric Price at MSKCC.[1]

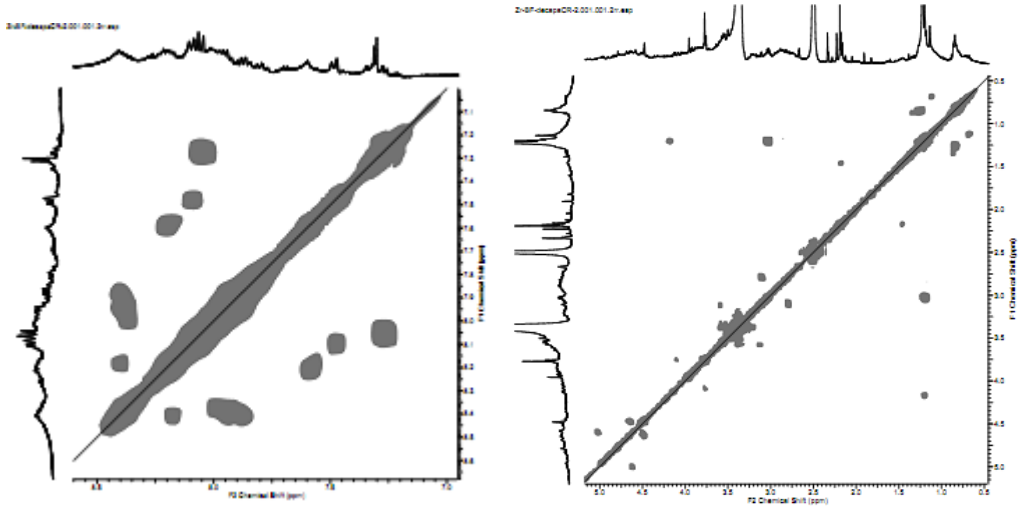

**Figure A.3. Zr(BF-decapa) 2D COSY spectrum, 400 Hz, in DMSO-$d_6$, aromatic region (left) alkyl region (right).**

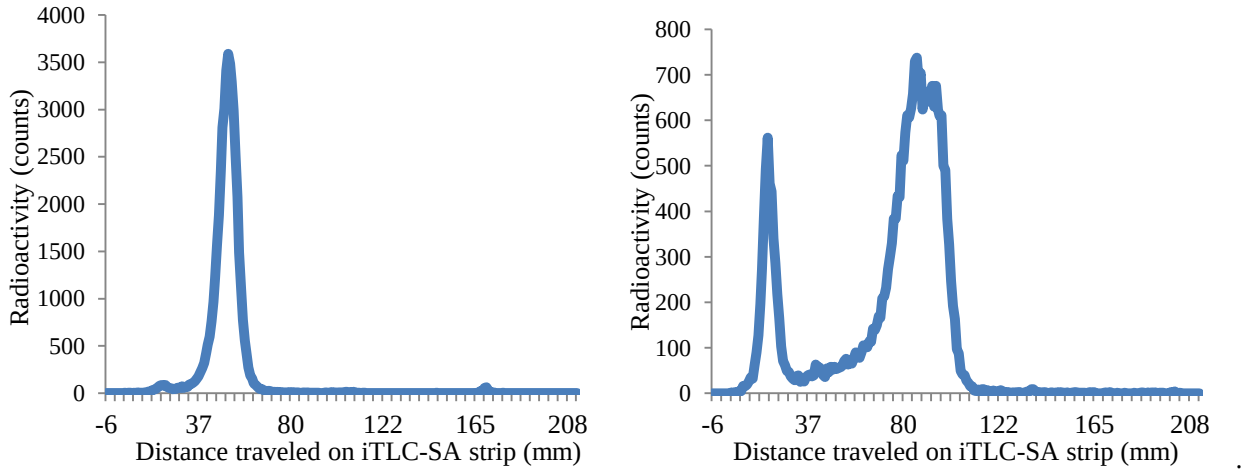


**Figure A.4. iTLC-SA radioactivity distribution of [$^{89}$Zr(decapa)]$^-$ labelled at ambient temperature, 30 minutes reaction time, >99% RCY (left) and after 72 hours, (free/serum bound $^{89}$Zr at ~60-100 mm solvent front) ~17% stable (right).**

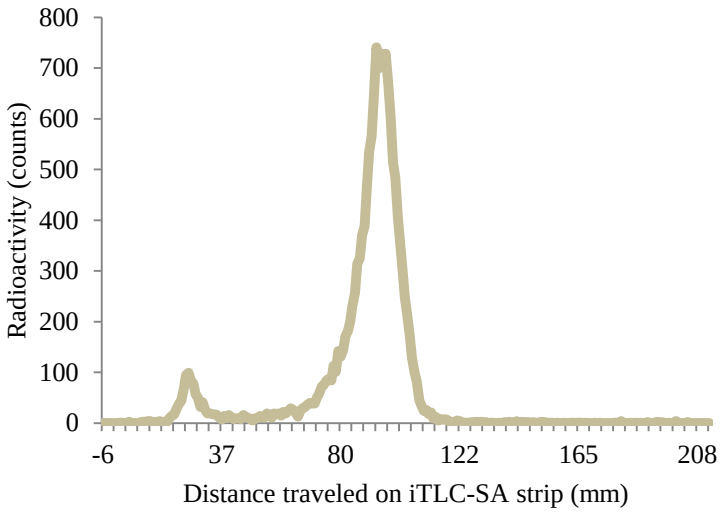


**Figure A.5. iTLC-SA radioactivity distribution of free $^{89}$Zr after 24h (free/serum bound $^{89}$Zr at ~100 mm solvent front), some sticks to baseline (~6%).**

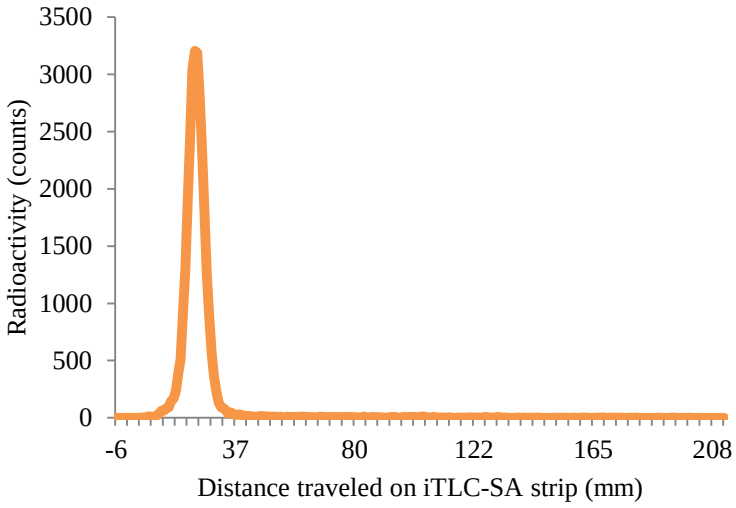


**Figure A.6. iTLC-SA radioactivity distribution of $^{89}$Zr(DFO) in serum after 72 hours, (free/serum bound $^{89}$Zr at ~60-100 mm solvent front) >98% stable.**